pocket provides a hydrophobic environment to accommodate the A24-consensus p2 tyrosine side chain of the NYA peptides. The F pocket is also large enough for the p9 phenylalanine side chain to be buried comfortably. However, the F pocket has a triad of negative charge contributed by aspartic acid at positions 74, 77, and 116, which provide an electrostatic environment that favors the characteristic C-terminal lysine anchor found in HLA-A\*11 binding peptides. The model suggests that to accommodate the p9 phenylalanine from the NYA peptide, aspartic acid 116 may be stabilized via electrostatic interactions with arginine 114. At the same time, the two other negatively charged side chains of aspartic acid 74 and 77 may be repositioned to be neutralized by interaction with the p6 arginine side chain of the NYA peptide buried within C pocket.

One of the key observations made in Dengue over the last two decades is that the most of the severe disease leading to DHF and Dengue shock syndrome is seen in secondarily infected individuals (3, 4). Some of the best such data comes from observations of island populations, where epidemics can occur through the introduction of a single virus serotype. Such an event occurred in Cuba in 1977 when there was an epidemic caused by Den-1, which was introduced to a population that had previously been protected by an effective mosquito control program and was therefore largely Dengue naive (23). DHF was rare in this epidemic, which petered out over the next few years. It was followed in 1981 by an epidemic of Den-2, and on this occasion there were >10,000 cases of DHF representing ~3% of cases and >150 deaths.

In our cohort of 90 patients, 8 were shown by serology to be suffering a primary infection and the rest were reinfections. A number of years ago, Halstead et al. (6) suggested that Ab enhancement could explain the increase in severity of disease seen upon reinfection with Dengue. It is proposed that, following a primary infection, Ab generated to the primary infecting virus may have suboptimal neutralization capabilities against a second viral serotype, whose envelope protein will show considerable differences in sequence. Rather than neutralize the second virus, this partially cross-reactive serum may instead opsonise the virus and potentiate its uptake via FcR-mediated endocytosis into macrophages, a primary site of virus replication. Ab enhancement can be readily demonstrated in vitro (although it often requires several logs of serum dilution) and has also been shown in a primate model (6, 7). Furthermore, Ab-dependent enhancement has also been put forward to explain an excess of DHF in children in the first year of life, who suffer a primary Dengue infection that is proposed to be accentuated by enhancement by passively transferred maternal anti-Dengue Ig (24).

Ab enhancement may well lead to higher viral loads on reinfection, and it has been demonstrated that there is a correlation between the peak viral load and disease severity (25). However, it is now very well established that when the clinical syndrome reaches its peak with shock and hemorrhage, the viral load has fallen precipitously and indeed the virus may be undetectable at this point (26). The coincidence of the severe symptoms with viral control and a storm of proinflammatory cytokine release suggest that the defect in vascular permeability leading to the profound vascular leak may be the result of immune-mediated damage or immunopathology rather than being solely the result of virus-mediated cytopathogenesis. One major source of inflammatory cytokines such as TNF- $\alpha$ , IFN- $\gamma$ , etc. are T cells, meaning that severe disease may be the result of T cell-mediated tissue damage. In addition to the secretion of proinflammatory mediators, cytotoxic CD8<sup>+</sup> T cells may also contribute to the vascular leak by directly lysing infected endothelial cells.

However, one question that is raised is why should the T cell response be more damaging the second time round than it is during the primary infection? First, like Ab responses, boosting or reinfection will lead to a higher amplitude response that is usually generated faster (19). There are a number of animal models of T cell immunopathology in which both CD8<sup>+</sup> and CD4<sup>+</sup> T cells can cause damage when they are produced at high frequencies in the context of a high Ag load, and indeed immunopathology has been recently suggested to play a role in severe acute respiratory syndrome (27). These include models of LCMV immunopathology and also RSV (8, 9). The latter are particularly pertinent in the context of Dengue because they illustrate the potential problems that can be encountered with poorly protective vaccines. In the 1960s, a formalin-inactivated RSV vaccine was tested in children; rather than protecting from infection, this vaccine actually enhanced lung disease when the children became naturally infected (28).

In secondary Dengue infection, there is a further important feature that may contribute to disease; original antigenic sin. Because the viral variants differ by 25–30% in amino acid sequence, most linear 8- to 10-aa<sup>-</sup> long peptide epitopes will contain one or more differences in amino sequence between variants (chance of identical 9-mer assuming 25% variation (0.75)<sup>9</sup> = 0.075). Upon secondary encounter with a variant Ag, the T cell response will frequently select from memory a set of T cells that are capable of recognizing the new epitope rather than selecting a novel response from the naive T cell pool. The reason for this is probably that the frequency of memory cells outnumbers naive cells, and, in addition, memory cells have a lower threshold for stimulation than naive cells (19).

This latter feature may prove to be detrimental because there is a danger that a set of T cells with a lower avidity for the currently infecting virus may be expanded in addition to high-avidity crossreactive cells, and it is also possible that the generation of this population in some way interferes with the kinetics of the response, both delaying the generation of a more avid response from the naive pool and also the generation of truly cross-reactive highavidity T cells. In this study, we have demonstrated that a crossreactive response to the A24-NYA epitope is generated and that the response is made up of three populations of cells: those that show preferential avidity for the primarily encountered virus; a population that is cross-reactive between the primary and secondary viruses (both of these populations have probably been generated by original antigenic sin because they show equal or greater avidity for the virus encountered on the primary occasion); and a third group of cells (which show preference for the secondary infecting virus), which we propose have been newly generated during the secondary response from naive T cells.

When we examined the function of these T cell populations, we did indeed find that nearly 50% of the cells with low avidity for the secondarily infecting virus showed no reactivity to stimulation with this epitope. We believe that these nonresponding T cells are not merely bystanders because they have clearly undergone proliferation during the secondary response. One very interesting feature of the cells produced in the secondary response is differences in their ability to produce inflammatory cytokines and to degranulate. A higher proportion of the cross-reactive T cells show cytokine production but do not degranulate when compared with the cells that show single specificity for the secondary infecting virus. These latter cells more resemble the anti-CMV response, where few cells produce cytokines in the absence of degranulation. We propose that the generation of a response skewed toward cytokine production in the absence of degranulation may be detrimental in Dengue infection, meaning that when the virus is finally controlled it occurs in the context of an expanded T cell response and a cytokine storm.

It is likely that the pathogenesis of DHF is multifactorial, being driven by a variety of host and viral factors. We believe that two of the key drivers are the Ag load and the amplitude and quality of the T cell response. Any factor that leads to the development of a high Ag load concurrent with a high amplitude T cell response may contribute. In this study, we have discussed original antigenic sin in the context of the T cell response but it is perhaps better known for its effects on the Ab response. The effects of original antigenic sin in the Ab response are dramatic and can be seen in the viral neutralization tests that we have shown for the patients analyzed in these studies. Whether original antigenic sin of the Ab response also contributes to disease by steering the secondary response toward low-avidity Ab should also be considered, because this will also be a potential contributor toward a higher Ag load.

Finally, we have discussed cross-reactive T cells in the context of responses to a single pathogen, Dengue. In a series of highly interesting papers, Welsh and colleagues (29, 30) have looked at the potential for cross-reaction in T cell responses between viruses in mouse model. Several examples of cross-reactivity, which in some cases modulate the pattern of disease, have been described between viruses such as LCMV, Pichinde, and vaccinia (29, 30). This leads to the possibility that our response to pathogen challenge may be programmed in part by our previous exposure to diverse infectious agents. To make the situation even more complicated, it seems that in inbred mouse strains there is an idiosyncratic or private specificity to the cross-reactive response (31).

#### Acknowledgments

We thank S. Chunharasas, L. Damrikarnlerd, P. Petpirin, S. Jinatongthai, R. Promson, P. Songprakhon, and the research nurses at Khon Kaen Hospital.

#### **Disclosures**

The authors have no financial conflict of interest.

#### References

- Endy, T. P., S. Chunsuttiwat, A. Nisalak, D. H. Libraty, S. Green, A. L. Rothman, D. W. Vaughn, and F. A. Ennis. 2002. Epidemiology of inapparent and symptomatic acute dengue virus infection: a prospective study of primary school children in Kamphaeng Phet, Thailand. Am. J. Epidemiol. 156: 40–51.
- World Health Organization. 2002. Dengue and dengue haemorrhagic fever. Fact sheet no. 117. World Health Organization, Geneva, Switzerland.
- Sangkawibha, N., S. Rojanasuphot, S. Ahandrik, S. Viriyapongse, S. Jatanasen, V. Salitul, B. Phanthumachinda, and S. B. Halstead. 1984. Risk factors in dengue shock syndrome: a prospective epidemiologic study in Rayong, Thailand. I. The 1980 outbreak. Am. J. Epidemiol. 120: 653–669
- 1980 outbreak. Am. J. Epidemiol. 120: 653–669.
   Guzman, M. G., G. Kouri, L. Valdes, J. Bravo, M. Alvarez, S. Vazques, I. Delgado, and S. B. Halstead. 2000. Epidemiologic studies on Dengue in Santiago de Cuba, 1997. Am. J. Epidemiol. 152: 793–799.
- Halstead, S. B., and E. J. O'Rourke. 1977. Dengue viruses and mononuclear phagocytes. I. Infection enhancement by non-neutralizing antibody. *J. Exp. Med.* 146: 201–217.
- Halstead, S. B., and E. J. O'Rourke. 1977. Antibody-enhanced dengue virus infection in primate leukocytes. *Nature* 265: 739–741.
- Halstead, S. B. 1979. In vivo enhancement of dengue virus infection in rhesus monkeys by passively transferred antibody. J. Infect. Dis. 140: 527–533.
- Cannon, M. J., P. J. Openshaw, and B. A. Askonas. 1988. Cytotoxic T cells clear virus but augment lung pathology in mice infected with respiratory syncytial virus. J. Exp. Med. 168: 1163–1168.
- Aichele, P., K. Brduscha-Riem, S. Oehen, B. Odermatt, R. M. Zinkernagel, H. Hengartner, and H. Pircher. 1997. Peptide antigen treatment of naive and virus-immune mice: antigen- specific tolerance versus immunopathology. *Immunity* 6: 519–529.

 Yenchitsomanus, P. T., P. Sricharoen, I. Jaruthasana, S. N. Pattanakitsakul, S. Nitayaphan, J. Mongkolsapaya, and P. Malasit. 1996. Rapid detection and identification of dengue viruses by polymerase chain reaction (PCR). Southeast Asian J. Trop. Med. Public Health 27: 228–236.

- Innis, B. L., A. Nisalak, S. Nimmannitya, S. Kusalerdchariya, V. Chongswasdi, S. Suntayakorn, P. Puttisri, and C. H. Hoke. 1989. An enzyme-linked immunosorbent assay to characterize dengue infections where dengue and Japanese encephalitis co-circulate. Am. J. Trop. Med. Hyg. 40: 418–427.
- Jirakanjanakit, N., T. Sanohsomneing, S. Yoksan, and N. Bhamarapravati. 1997. The micro-focus reduction neutralization test for determining dengue and Japanese encephalitis neutralizing antibodies in volunteers vaccinated against dengue. Trans. R. Soc. Trop. Med. Hyg. 91: 614–617.
- World Health Organization. 1997. Dengue Haemorrahgic Fever: Diagnostic, Treatment, Prevention and Control. World Health Organization, Geneva, Switzerland.
- Krausa, P., D. Barouch, J. G. Bodmer, and M. J. Browning. 1995. Rapid characterization of HLA class I alleles by gene mapping using ARMS PCR. Eur. J. Immunogenet. 22: 283–287.
- Altman, J. D., P. A. Moss, P. J. Goulder, D. H. Barouch, M. G. McHeyzer-Williams, J. I. Bell, A. J. McMichael, and M. M. Davis. 1996. Phenotypic analysis of antigen-specific T lymphocytes. *Science* 274: 94–96.
- Mongkolsapaya, J., W. Dejnirattisai, X. N. Xu, S. Vasanawathana, N. Tangthawornchaikul, A. Chairunsri, S. Sawasdivorn, T. Duangchinda, T. Dong, S. Rowland-Jones, et al. 2003. Original antigenic sin and apoptosis in the pathogenesis of dengue hemorrhagic fever. *Nat. Med.* 9: 921–927.
- Chandanayingyong, D., H. A. Stephens, R. Klaythong, M. Sirikong, S. Udee, P. Longta, R. Chantangpol, S. Bejrachandra, and E. Rungruang. 1997. HLA-A, -B, -DRB1, -DQA1, and -DQB1 polymorphism in Thais. *Hum. Immunol*. 53: 174–182.
- Klenerman, P., and R. M. Zinkernagel. 1998. Original antigenic sin impairs cytotoxic T lymphocyte responses to viruses bearing variant epitopes. *Nature* 394: 482–485.
- Veiga-Fernandes, H., U. Walter, C. Bourgeois, A. McLean, and B. Rocha. 2000. Response of naive and memory CD8<sup>+</sup> T cells to antigen stimulation in vivo. *Nat. Immunol.* 1: 47–53.
- Alexander-Miller, M. A., G. R. Leggatt, and J. A. Berzofsky. 1996. Selective expansion of high- or low-avidity cytotoxic T lymphocytes and efficacy for adoptive immunotherapy. *Proc. Natl. Acad. Sci. USA* 93: 4102–4107.
- Betts, M. R., J. M. Brenchley, D. A. Price, S. C. De Rosa, D. C. Douek, M. Roederer, and R. A. Koup. 2003. Sensitive and viable identification of antigen-specific CD8<sup>+</sup> T cells by a flow cytometric assay for degranulation. *J. Immunol. Methods* 281: 65–78.
- Li, L., and M. Bouvier. 2004. Structures of HLA-A\*1101 complexed with immunodominant nonamer and decamer HIV-1 epitopes clearly reveal the presence of a middle, secondary anchor residue. *J. Immunol.* 172: 6175–6184.
- Guzman, M. G., G. Kouri, S. Vazques, D. Rosario, J. Bravo, and L. Valdes. 1999.
   DHF epidemics in Cuba, 1981 and 1997: some interesting observations. *Bull. W. H. O.* 23.
- Kliks, S. C., S. Nimmanitya, A. Nisalak, and D. S. Burke. 1988. Evidence that maternal dengue antibodies are important in the development of dengue hemorrhagic fever in infants. Am. J. Trop. Med. Hyg. 38: 411–419.
- Vaughn, D. W., S. Green, S. Kalayanarooj, B. L. Innis, S. Nimmannitya, S. Suntayakorn, T. P. Endy, B. Raengsakulrach, A. L. Rothman, F. A. Ennis, and A. Nisalak. 2000. Dengue viremia titer, antibody response pattern, and virus serotype correlate with disease severity. J. Infect. Dis. 181: 2–9.
- Libraty, D. H., T. P. Endy, H. S. Houng, S. Green, S. Kalayanarooj, S. Suntayakorn, W. Chansiriwongs, D. W. Vaughn, A. Nisalak, F. A. Ennis, and A. L. Rothman. 2002. Differing influences of virus burden and immune activation on disease severity in secondary dengue-3 virus infections. *J. Infect. Dis.* 185: 1213–1221.
- Chen, H., J. Hou, X. Jiang, S. Ma, M. Meng, B. Wang, M. Zhang, M. Zhang, X. Tang, F. Zhang, et al. 2005. Response of memory CD8<sup>+</sup> T cells to severe acute respiratory syndrome (SARS) coronavirus in recovered SARS patients and healthy individuals. *J. Immunol.* 175: 591–598.
- Kim, H. W., J. G. Canchola, C. D. Brandt, G. Pyles, R. M. Chanock, K. Jensen, and R. H. Parrott. 1969. Respiratory syncytial virus disease in infants despite prior administration of antigenic inactivated vaccine. Am. J. Epidemiol. 89: 422-434.
- Selin, L. K., S. M. Varga, I. C. Wong, and R. M. Welsh. 1998. Protective heterologous antiviral immunity and enhanced immunopathogenesis mediated by memory T cell populations. *J. Exp. Med.* 188: 1705–1715.
- Chen, H. D., A. E. Fraire, I. Joris, M. A. Brehm, R. M. Welsh, and L. K. Selin. 2001. Memory CD8<sup>+</sup> T cells in heterologous antiviral immunity and immunopathology in the lung. *Nat. Immunol.* 2: 1067–1076.
- Kim, S. K., M. Cornberg, X. Z. Wang, H. D. Chen, L. K. Selin, and R. M. Welsh. 2005. Private specificities of CD8 T cell responses control patterns of heterologous immunity. *J. Exp. Med.* 201: 523–533.

#### RESEARCH ARTICLE

### Proteomic identification of alterations in metabolic enzymes and signaling proteins in hypokalemic nephropathy

Visith Thongboonkerd<sup>1</sup>, Somchai Chutipongtanate<sup>1</sup>, Rattiyaporn Kanlaya<sup>1</sup>, Napat Songtawee<sup>1</sup>, Supachok Sinchaikul<sup>2</sup>, Paisal Parichatikanond<sup>3</sup>, Shui-Tein Chen<sup>2, 4</sup> and Prida Malasit<sup>1, 5</sup>

- <sup>1</sup> Medical Molecular Biology Unit, Office for Research and Development, Faculty of Medicine Siriraj Hospital, Mahidol University, Bangkok, Thailand
- <sup>2</sup> Institute of Biological Chemistry and Genomic Research Center, Academia Sinica, Taipei, Taiwan
- <sup>3</sup> Department of Pathology, Faculty of Medicine Siriraj Hospital, Mahidol University, Bangkok, Thailand
- <sup>4</sup> Institute of Biochemical Sciences, College of Life Science, National Taiwan University, Taipei, Taiwan
- <sup>5</sup> Medical Biotechnology Unit, National Center for Genetic Engineering and Biotechnology, National Science and Technology Development Agency, Bangkok, Thailand

Hypokalemic nephropathy caused by prolonged K<sup>+</sup> deficiency is associated with metabolic alkalosis, polydipsia, polyuria, growth retardation, hypertension, and progressive tubulointerstitial injury. Its pathophysiology, however, remains unclear. We performed gel-based, differential proteomics analysis of kidneys from BALB/c mice fed with high-normal-K+ (HNK), low-normal-K+ (LNK), or K<sup>+</sup>-depleted diet for 8 wk (n = 6 in each group). Plasma K<sup>+</sup> levels were 4.62  $\pm$  0.35,  $4.46 \pm 0.23$ , and  $1.51 \pm 0.21$  mmol/L for HNK, LNK, and KD mice, respectively (p < 0.0001; KD vs. others). With comparable amounts of food intake, the KD mice drank significantly more water than the other two groups and had polyuria. Additionally, the KD mice had growth retardation, metabolic alkalosis, markedly enlarged kidneys, renal tubular dilation, intratubular deposition of amorphous and laminated hyaline materials, and tubular atrophy. A total of 33 renal proteins were differentially expressed between the KD mice and others, whereas only eight proteins were differentially expressed between the HNK and LNK groups, as determined by quantitative intensity analysis and ANOVA with Tukey's post hoc multiple comparisons. Using MALDI-MS and/or quadrupole-TOF MS/MS, 30 altered proteins induced by K<sup>+</sup>-depletion were identified as metabolic enzymes (e.g., carbonic anhydrase II, aldose reductase, glutathione S-transferase GT41A, etc.), signaling proteins (14–3-3  $\epsilon$ , 14–3-3  $\zeta$ , and cofilin 1), and cytoskeletal proteins (γ-actin and tropomyosin). Some of these altered proteins, particularly metabolic enzymes and signaling proteins, have been demonstrated to be involved in metabolic alkalosis, polyuria, and renal tubular injury. Our findings may lead to a new road map for research on hypokalemic nephropathy and to better understanding of the pathophysiology of this medical disease when the functional and physiological significances of these altered proteins are defined.

Received: July 15, 2005 Revised: September 27, 2005 Accepted: October 13, 2005

#### **Keywords:**

Hypokalemic nephropathy / Kidney / Potassium / Proteome / Urine

Correspondence: Dr. Visith Thongboonkerd, MD, FRCPT, Medical Molecular Biology Unit, Office for Research and Development, 12th Floor Adulyadej Vikrom Building, 2 Prannok Road, Siriraj Hospital, Bangkoknoi, Bangkok 10700, Thailand

E-mail: thongboonkerd@dr.com; vthongbo@yahoo.com Fax: +66-2-4184793

Abbreviations: CAII, carbonic anhydrase isoform II; HNK, highnormal-K+; KD, K+ depletion; LNK+, low-normal-K+; Q-TOF, quadrupole-TOF

#### 1 Introduction

crucial for maintaining the normal homeostasis of living cells, tissues, and organs. The kidney is the main organ responsible for regulation of the normal K<sup>+</sup> balance. However, abnormal K<sup>+</sup> homeostasis may occur when K<sup>+</sup> intake and its output are in imbalance. Inadequate dietary K+ intake, renal K<sup>+</sup> loss (excessive urinary K<sup>+</sup> excretion), and/or

Potassium is one of the most important electrolytes that are



extrarenal  $K^+$  loss (*e.g.*, diarrhea and vomiting) can lead to hypokalemia, which is widely defined as a serum  $K^+$  of less than 3.5 mmol/L. Hypokalemia is one of the most common electrolyte abnormalities encountered in clinical practice and is found in more than 20% of hospitalized patients [1]. For outpatients, it is a particularly prominent problem in those who receive thiazide diuretics for treatment of hypertension, with an incidence of up to 48% [2].

Hypokalemia may be asymptomatic if the deficit is temporary and degree of the deficit is modest to mild (3.0-3.5 mmol/L), but can be a cause of death when degree of the deficit is severe (<3.0 mmol/L) and the dysregulation is left untreated. Prolonged K<sup>+</sup> deficiency can affect several organ systems, especially hemodynamic, cardiovascular, muscular, gastrointestinal, and renal systems [3–5]. Renal involvement of prolonged K+ depletion (KD) has been defined as "hypokalemic nephropathy," a disease known for a half of the century [6-8]. Hypokalemic nephropathy is associated with metabolic alkalosis, growth retardation, hypertension, polydipsia, polyuria, enlarged kidney, progressive tubulointerstitial injury, and ultimately renal failure or end-stage renal disease [9-14]. Even with a long history of the disease, the pathophysiology of hypokalemic nephropathy remains unclear. Although K+ repletion can reverse renal ultrastructural changes occur in acute K+ deficiency state [15], these changes and renal dysfunction remain in some cases of chronic K<sup>+</sup> deficiency, even with the repletion therapy [9, 16].

The present study has applied proteomic technology aiming to discover previously unknown changes in renal protein expression that are associated with hypokalemic nephropathy. Hypokalemia was induced by giving ad libitum K<sup>+</sup>-depleted diet to BALB/c mice for 8 wk, whereas the control mice received high-normal-K+ (HNK) and low-normal-K<sup>+</sup> (LNK) diets. The KD mice displayed many characteristics of human hypokalemic nephropathy, including severe hypokalemia, growth retardation, polydipsia, polyuria, markedly enlarged kidneys, severe tubular dilatation, intratubular deposition of amorphous and laminated hyaline materials, and tubular atrophy. Gel-based, differential proteomics analysis of the kidney revealed alterations in expression of several metabolic enzymes and signaling proteins in the KD mice, as compared to the HNK and LNK animals. These altered proteins have important cellular functions and may be involved in hypokalemia-induced metabolic alkalosis, polyuria, and renal tubular injury.

#### 2 Materials and methods

#### 2.1 Animals and diets

Young male BALB/c mice (n = 6 in each group; total n = 18) were fed with *ad libitum* HNK (1% K<sup>+</sup>; #TD88238; Harland Teklad, Madison, WI), LNK (0.36% K<sup>+</sup>; #TD97214), or KD (<0.001% K<sup>+</sup>; #TD88239) diet and water for 8 wk. Details of dietary compositions are shown in Table 1. Body weight,

Table 1. Dietary compositions

Compositions	Amour	nt, g of nutrient $p$	<i>er</i> kg of diet
	HNK (1% K)	LNK (0.36% K)	KD (<0.001% K)
Organic			
Casein, high protein	200.00	200.00	200.00
DL-methionine	3.00	3.00	3.00
Sucrose	470.26	485.34	493.76
Corn starch	150.00	150.00	150.00
Corn oil	50.00	50.00	50.00
Cellulose	50.00	50.00	50.00
Vitamin mix (Teklad 40060)	10.00	10.00	10.00
Ethoxyquin	0.01	0.01	0.01
Inorganic			
Calcium phosphate, dibasic	20.30	20.30	20.30
Potassium citrate, monohydrate	13.90	4.98	0.00
Calcium carbonate	10.00	10.00	10.00
Potassium chloride	9.60	3.44	0.00
Sodium chloride	7.40	7.40	7.40
Magnesium oxide	2.80	2.80	2.80
Magnesium sulfate	2.00	2.00	2.00
Ferric citrate	0.50	0.50	0.50
Manganese carbonate	0.13	0.13	0.13
Zinc carbonate	0.06	0.06	0.06
Cupric carbonate	0.02	0.02	0.02
Chromium potassium sulfate	0.02	0.02	0.02
Sodium iodate	0.0010	0.0010	0.0010
Sodium selenite	0.0004	0.0004	0.0004

Proteomics 2006, 6, 2273-2285

dietary intake, and water intake were recorded daily. After 8 wk of differential diets, the mice were sacrificed and the kidneys were surgically removed for further proteomic analysis.

#### 2.2 Protein extraction for proteomic analysis

Renal proteins were extracted using a protocol modified from methods described previously [17–19]. Briefly, renal capsule was removed, the kidney was excised into several thin slices, and the contaminated blood was washed with iceProteomics 2006, 6, 2273–2285 Clinical Proteomics 2275

cold PBS. The tissue was then briskly frozen in liquid nitrogen, ground to powder, resuspended in a buffer containing 7 M urea, 2 M thiourea, 40% CHAPS, 2% v/v ampholytes (pH 3-10), 120 mM DTT, and 40 mM Tris-base, and incubated at 4°C for 30 min. After low-speed centrifugation  $(12\,000\times g$  for 5 min), the supernatant was saved and the protein concentration was measured by spectrophotometry using Bio-Rad Protein Assay (Bio-Rad Laboratories, Hercules, CA) based on Bradford's method. Because urea, thiourea, CHAPS, and other compositions in the sample/lysis buffer can interfere with the protein estimation, we generated the standard curve using BSA at the concentrations of 0, 2, 5, 7, and 10  $\mu$ g/ $\mu$ L in the same sample/lysis buffer to make sure that the standards and the samples had the same background that might occur due to chemical interference. Proteins derived from one kidney of each animal were further resolved in individual 2-D gel; (n = 6 gels (from six animals) for each group; total n = 18 gels).

#### 2.3 2-DE and staining

Immobiline<sup>™</sup> DryStrip, linear pH 3–10, 7 cm long (Amersham Biosciences, Uppsala, Sweden) was rehydrated overnight with 200  $\mu g$  total protein (equal loading for each sample) that was premixed with rehydration buffer containing 7 M urea, 2 M thiourea, 2% CHAPS, 2% v/v ampholytes (pH 3-10), 120 mM DTT, 40 mM Tris-base, and bromophenol blue (to make the final volume of 150  $\mu$ L per strip). The first dimensional separation (IEF) was performed in Ettan IPGphor II IEF System (Amersham Biosciences) at 20°C, using stepwise mode to reach 9000 Vh. After completion of the IEF, proteins on the strip were equilibrated in a buffer containing 6 M urea, 130 mM DTT, 30% glycerol, 112 mM Tris-base, 4% SDS, and 0.002% bromophenol blue for 10 min, and then with another buffer containing 6 M urea, 135 mM iodoacetamide, 30% glycerol, 112 mM Tris-base, 4% SDS, and 0.002% bromophenol blue for 10 min. The IPG strip was then transferred onto 12% acrylamide slab gel  $(8 \times 9.5 \text{ cm}^2)$  and the second dimensional separation was performed in SE260 Mini-Vertical Electrophoresis Unit (Amersham Biosciences) with the current 20 μA/gel for 1.5 h. Separated protein spots were then visualized using CBB R-250 stain. We have not preferred using silver stain for differential proteomics study because of its narrow lineardynamic range of the relationship between spot intensity and protein amount (or concentration of protein per spot area).

#### 2.4 Spot analysis and matching

Image Master 2-D Platinum (Amersham Biosciences) software was used for matching and analysis of protein spots on 2-D gels. Parameters used for spot detection were (i) minimal area = 10 pixels; (ii) smooth factor = 2.0; and (iii) saliency = 2.0. A reference gel was created from an artificial gel combining all of the spots presenting in different gels into one image. The reference gel was then used for matching of

corresponding protein spots between gels. Background subtraction was performed and the intensity volume of individual spot was normalized with total intensity volume (summation of the intensity volumes obtained from all spots in the same 2-D gel). Reproducibility of 2-D spot pattern was evaluated by determining the CV of the normalized intensity of corresponding spot across different gels (%CV = SD/mean  $\times$  100%).

#### 2.5 In-gel tryptic protein digestion

Differentially expressed protein spots were excised from the 2-D gels and the gel pieces were washed with 200 μL of 50% ACN/25 mM NH<sub>4</sub>HCO<sub>3</sub> buffer (pH 8.0) for 15 min twice. The gel pieces were then washed once with 200  $\mu L$  of 100% ACN and dried using a Speed Vac concentrator (Savant, Holbrook, NY). Dried gel pieces were swollen with 10 µL of 1% w/v trypsin (Promega, Madison WI) in 25 mM NH<sub>4</sub>HCO<sub>3</sub>. The gel pieces were then crushed with siliconized blue stick and incubated at 37°C for at least 16 h. Peptides were subsequently extracted twice with 50 µL of 50% ACN/5% TFA; the extracted solutions were then combined and dried with the Speed Vac concentrator. The peptide pellets were then resuspended in 10 µL of 0.1% TFA and the resuspended solutions were purified using ZipTip<sub>C18</sub> (Millipore, Bedford, MA). Ten microliters of sample was drawn up and down in the ZipTip for ten times and then washed with  $10\,\mu L$  of 0.1% formic acid by drawing up and expelling the washing solution for three times. The peptides were finally eluted with 5  $\mu$ L of 75% ACN/0.1% formic acid.

#### 2.6 Protein identification by MALDI-MS and MS/MS

For MALDI MS and MS/MS analyses, the samples were premixed 1:1 with the matrix solution (5 mg/mL α-cyano-4hydroxycinnamic acid (CHCA) in 50% ACN, 0.1% v/v TFA, and 2% w/v ammonium citrate) and spotted onto the 96-well MALDI sample stage. The samples were analyzed by the quadrupole-TOF (Q-TOF) Ultima™ MALDI instrument (Micromass, Manchester, UK), which was fully automated with predefined probe motion pattern and the peak intensity threshold for switching over from MS survey scanning to MS/MS, and from one MS/MS to another. Within each sample well, parent ions that met the predefined criteria (any peak within the m/z 800–3000 range with intensity above ten count ± include/exclude list) were selected for CID MS/MS using argon as the collision gas and a mass-dependent  $\pm$  5 V rolling collision energy until the end of the probe pattern was reached (all details are available at http://proteome.sinica. edu.tw).

For PMF, both MASCOT (http://www.matrixscience.com) and ProFound (http://129.85.19.192/profound\_bin/WebProFound.exe) search engines were used. Proteins were identified based on the assumptions that peptides were monoisotopic, oxidized at methionine residues, and carbamidomethylated at cysteine residues. Both NCBI and Swiss-

Prot databases were used and the searches were restricted to mammalians. A mass tolerance of 25 ppm was used and up to one missed trypsin cleavage was allowed. Identities with probability-based MOWSE scores >68 (for MASCOT) and/or Z scores > 1.65 (for ProFound) were considered as "significant hits." In the case of nonsignificant hits with the mass tolerance of 25 ppm, the mass tolerance was changed to 50, 100, and 150, and the searches were again performed. For MS/MS peptide sequence identification, the MASCOT search engine was employed. Search parameters allowed were similar to those for PMF. Peptides with ions scores >44 were considered as "significant hits." Only significant hits from PMF and MS/MS peptide ion search were reported in the Section 3.

#### 2.7 Statistical analysis

Comparisons among three groups were performed using ANOVA with Tukey's post hoc test for multiple comparisons. p values less than 0.05 were considered statistically significant. All data are reported as mean  $\pm$  SEM.

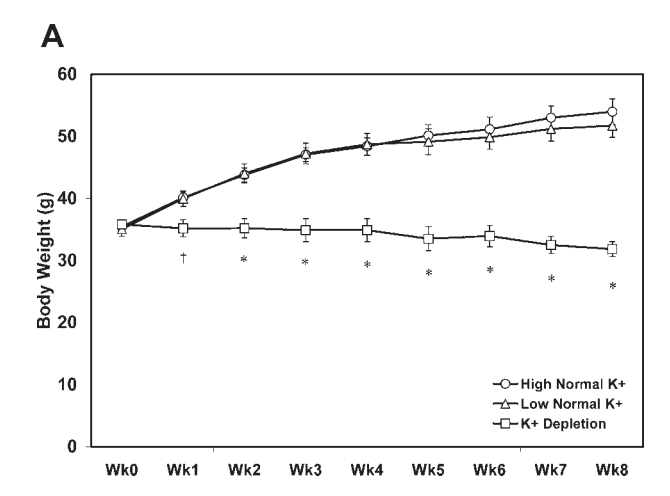
#### 3 Results

#### 3.1 Clinical data and blood chemistry

Initial body weights of the animals were comparable among groups (35.46  $\pm$  0.87, 35.06  $\pm$  1.12, and 35.82  $\pm$  0.68 g for HNK, LNK, and KD mice, respectively; p value was not significant by ANOVA). After only a few days of differential diets through the end of the study, the KD mice had significantly less body weights than the other two groups (Fig. 1A). Body weights of the KD mice had not increased but, indeed, slightly decreased at the end of the study, suggesting that they had growth retardation. All mice had received comparable amounts of ad libitum K+-adjusted diets, except only at weeks 2 and 6 that the KD mice received slightly less amount of diet than the other groups (data not shown). With the comparable amounts of dietary intake, the KD mice drank significantly more water than the other groups throughout the study (Fig. 1B) and, as a result, had polyuria. Figure 2A clearly illustrates that the KD mice had severe hypokalemia whereas the HNK and LNK mice had normokalemia. Plasma K<sup>+</sup> levels were 4.62  $\pm$  0.35, 4.46  $\pm$  0.23, and 1.51  $\pm$ 0.21 mmol/L for HNK, LNK, and KD mice, respectively (p < 0.0001; KD vs. others). Figure 2B shows that the KD mice developed metabolic alkalosis. Plasma HCO<sub>3</sub><sup>-</sup> levels were 25.50  $\pm$  0.47, 25.67  $\pm$  0.38, and 31.90  $\pm$  2.11 mmol/L for HNK, LNK, and KD mice, respectively (p < 0.005; KD  $\nu s$ . others).

#### 3.2 Renal histopathological changes

As expected, kidneys of the KD mice were much larger than the other groups (Fig. 3). Figure 4 shows histopathological changes in the KD murine kidneys, including severe tubular



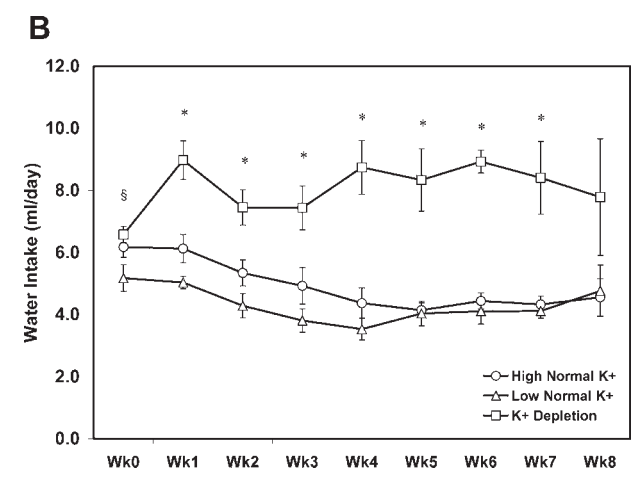


Figure 1. Clinical manifestations of experimental animals. (A) All mice had comparable initial body weights. Body weights of the HNK and LNK mice were gradually increased during the study and were comparable between these two groups. In contrast, body weights of the KD mice were significantly less than those of other two groups and did not increase with the increasing age. (B) KD mice drink significantly more water compared to mice in the other two groups. \* = p < 0.001 KD vs. others; † = p < 0.05 KD vs. others; \$ = p < 0.05 KD vs. tNK.

dilatation, intratubular deposition of amorphous and laminated hyaline materials, intratubular cellular casts, and tubular atrophy. There was no abnormal finding observed in kidneys from the HNK and LNK groups.

#### 3.3 Differentially expressed renal proteins

Using 2-D analysis software and spot detecting parameters as described in Section 2, approximately 250 protein spots were visualized in each 2-D gel. Figure 5 illustrates representative 2-D gels of individual groups. Quantitative intensity analysis and statistical analysis using ANOVA with Tukey's post hoc test for multiple comparisons revealed significantly differential expression of a total of 33 protein spots (Table 2). Of these differentially expressed proteins, all of

 Proteomics 2006, 6, 2273–2285
 Clinical Proteomics
 2277

Table 2. Differentially expressed proteins among groups

Protein <sup>a)</sup>	Spot	NCBI ID	Accession	%Cov	MASCOT	Z score	/ d	MW, N	MS method(s)	LNK v.	LNK vs. HNK	KD vs	KD vs. HNK	ΚDν	KD vs. LNK
					score		ΚΓ	кDа		Ratio (LNK/ HNK)	(p value) <sup>b)</sup>	Ratio (LNK/ HNK)	(p value) <sup>b)</sup>	Ratio (LNK/ HNK)	(p value) <sup>b)</sup>
Metabolic enzymes															
Acetyl-Coenzyme A acetyltrans- ferase 1 precursor [ <i>Mus</i>	138	gi 19354555	AAH24763	47	105	2.43	9.0 4	45.14 N	MS	1.414	(0.004)	0.370	(<0.001)	0.262	(<0.001)
Aldehyde reductase (aldo-keto reductase) (alcohol dehydro-	120	gi 29374169	AA072145	59	206	2.43	6.9 3	36.80 N	MS, MS/MS	1.102	NS	0.537	(0.011)	0.487	(0.002)
Argininosuccinate synthetase 1 [Mus musculus]	148	gi 12805227	AAH02074	33	94	2.43	8.5 4	46.85 N	MS	0.918	NS	0.515	(<0.001)	0.561	(0.001)
Carbonic anhydrase 2 [ <i>Mus</i>	82	gi 33243954	AAH55291	45	26	2.43	6.5	29.14 N	MS	0.954	NS	1.829	(0.003)	1.917	(0.002)
nusculus  Catalase [ <i>Mus musculus</i> ]	185	gi 15488606	AAH13447	47	241	2.43	7.8 6	60.03 N	MS, MS/MS	1.461	NS (0011)	0.637	NS	0.435	(0.008)
Enactate denyariogeniase [ <i>Mus musculus</i> ] Epoxide hydrolase (EC 3.3.2.3) –	188	gi 33333372 qi 477004	A47504	S 14	120	2.43			S S S	1.435	NS NS	0.297	s s	0.207	(0.017)
mouse	} <u></u>			: !		i d					) (				
Glutamate dehydrogenase [ <i>Mus musculus</i> ]	1/5	gi 34785735	AAH5/347	47	201	2.43	8 53 9	61.66 N	MS, MS/MS	0.918	SS	1.796	(<0.001)	1.957	(<0.001)
Glutathione S-transferase GT41A	64	gi 121710	P10648	48	06	1.94	8.9 2	25.63 N	MS, MS/MS	NAc	NS	NAc	(<0.001)	NAc	(<0.001)
(GST class-alpha) [Mus musculus] Ketohexokinase [Mus musculus]	105	gi 15488638	AAH13464	43	108	2.43	5.8		MS	1.138	NS	0.567	(0.001)	0.499	(<0.001)
Lactate dehydrogenase 2, B chain [Mus misculus]	118	gi 28386162	AAH46755	31	79	2.43		36.84 N	MS, MS/MS	1.132	NS	1.405	(0.006)	1.241	NS
Long-chain acyl-CoA dehydro- genase [ <i>Sus scrofa</i> ]	146	gi 47522692	NP_999062	30	77	2.43	7.0 4	48.34 N	MS, MS/MS	1.905	(0.009)	1.197	NS	0.628	(0.039)
Malate dehydrogenase (EC 1.1.1.37), cytosolic –	113	gi 319837	DEMSMC	က	29	NA	6.2 3	36.40 N	MS/MS	1.222	NS	0.377	SN	0.309	(0.013)
Hadhsc protein (medium and short chain L-3-hydroxyacyl- Coenzyme A dehydrogenase)	101	gi 20379935	AAH28833	31	79	2.43	7.2 3	31.97 N	MS, MS/MS	1.094	NS	0.695	(0.035)	0.635	(0.006)
Peroxiredoxin 5 [ <i>Mus musculus</i> ] Phosphoenolpyruvate carboxy- kinase [ <i>Mus musculus</i> ]	35 196	gi 10129957 gi 4102182	AAG13450 AAD01427	85 37	176 174	2.43	7.8 1	N 71.71 70.08 N	MS MS	1.091 0.833	NS NS	0.753 3.626	(0.042) (0.004)	0.690	(0.006)
Pipecolic acid oxidase Pyruvate carboxylase, mitochon- drial precursor (Pc protein) (Pcx protein)	141 223	gi 1548782 gi 1709948	AAH13525 P52873	37 25	315	2.43	7.3 4 6.3 13	44.46 N 130.41 N	MS MS, MS/MS	1.459	S S S	0.820 <b>0.293</b>	NS (< <b>0.001)</b>	0.562	(<0.001)

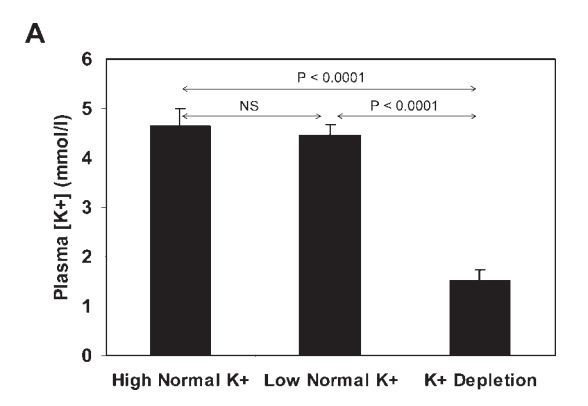
Table 2. Continued

Protein <sup>a)</sup>	Spot	NCBI ID	Accession	%Cov	MASCOT Z score p/	Z score		MS method(s)	LNK v	LNK vs. HNK	KD V:	KD vs. HNK	KD 1	KD vs. LNK
					score		кDа		Ratio (LNK/ HNK)	(p value) <sup>b)</sup>	Ratio (LNK/ HNK)	(p value) <sup>b)</sup>	Ratio (LNK/ HNK)	(p value) <sup>b)</sup>
Sorbitol dehydrogenase (I-iditol 2-dehydrogenase) [ <i>Mus</i>	134	gi 25108890	Q64442	20	138	2.43	6.6 40.64	MS, MS/MS	1.182	NS	0.628	(0.012)	0.532	(<0.001)
Sorbitol dehydrogenase (I-iditol	135 sl	gi 25108890	064442	40	88	2.43	6.6 40.64	MS	1.603	(0.038)	0.717	NS	0.447	(0.003)
Ubiquinol-cytochrome c reductase	162	gi 46593021	NP_079683	48	196	2.43	5.8 53.46	MS	1.278	(0.047)	1.473	(0.001)	1.152	NS
Hypothetical protein <sup>d)</sup> MGC37245 [Mus musculus]	192	gi 21410406	AAH31140	42	196	2.43	8.9 64.76	MS	1.071	NS	0.090	(<0.001)	0.084	(<0.001)
Hypothetical protein <sup>d)</sup> MGC37245 [ <i>Mus misculus</i> ]	193	gi 21410406	AAH31140	47	220	2.43	8.9 64.76	MS	1.486	(0.001)	0.140	(0.039)	0.094	(<0.001)
Unnamed protein product <sup>®</sup> [ <i>Mus musculus</i> ]	106	gi 12832094	BAB21963	=	112	NA	5.4 35.20	MS/MS	1.450	(<0.001)	0.366	(<0.001)	0.252	(<0.001)
Signaling proteins														
14–3-3 protein epsilon isoform [ <i>Mus musculus</i> ]	88	gi 1469948	AAC52676	23	40	2.43	4.6 29.27	MS	1.397	NS	2.436	(0.007)	1.743	(0.050)
14-3-3 zeta [ <i>Mus musculus</i> ] Cofilin 1, nonmuscle [ <i>Mus</i> <i>musculus</i> ]	83	gi 1841387 gi 55777182	BAA11751 AAH46225	33	09	2.43	4.7 27.88 8.2 18.78	MS MS, MS/MS	<b>1.874</b> 2.453	(0.033) NS	2.327 3.439	(0.002)	1.242	NS NS
Cytoskeletal proteins														
Gamma-actin [ <i>Mus musculus</i> ] Tropomyosin isoform 6 [ <i>Rattus</i>	150 92	gi 809561 gi 29336093	CAA31455 NP_775134	46 23	136 44	2.43	5.6 41.34 4.7 29.24	MS, MS/MS MS	1.169	NS NS	1.504	(<0.001) (0.002)	1.287	(0.002)
Miscellaneous CDNA sequence BC021917 [ <i>Mus musculus</i> ]	191	gi 18314540	AAH21917	28	115	1.45	6.4 59.96	MS, MS/MS	1.171	NS	0.583	NS	0.498	(0.014)
Unidentified Unidentified Unidentified	11 16 229								1.038 1.910 0.809	NS NS NS	0.162 6.173 2.885	(<0.001) (0.008) (<0.001)	0.156 3.233 3.565	(<0.001) (0.027) (<0.001)

Proteins were classified based on their major functions appeared in Swiss-Prot and TrEMBL database as well as literature search in the PubMed. Some proteins might have multiple functions but were put into only one functional category in this Table.

<sup>b) Significant p values are in bold.
c) Detected only in the KD group, below the detection limit in the other two groups.
d) 88% Identical to xenobiotic/medium-chain fatty acid:CoA ligase [Rattus norvegicus]. (gi|21426769; NP\_653349)
e) 84% Identical to aspartoacylase-3 (aminoacylase-3) [Rattus norvegicus]. (gi|57526957; NP\_01009603)
NA: Not applicable.
NS: Not significant.</sup> 

Proteomics 2006, 6, 2273–2285 Clinical Proteomics 2279



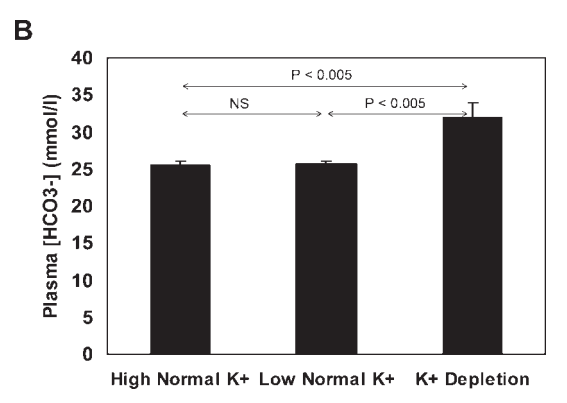


**Figure 2.** Plasma  $K^+$  and  $HCO_3^-$  levels. (A) KD mice developed severe hypokalemia and had significantly less plasma  $[K^+]$  levels than the other two groups. (B) KD mice also developed metabolic alkalosis and had significantly greater plasma  $[HCO_3^-]$  levels than the other two groups.



High Normal K+ Low Normal K+

Figure 3. Hypokalemia-induced renal enlargement. KD mice had larger size of the kidney compared to the HNK and LNK mice at the end of the study.

K\* Depletion

them significantly differed between KD and the other two groups, whereas only eight proteins differed between the HNK and LNK groups. Only these significant differences were subjected to mass spectrometric protein identification. Using MALDI-MS and/or Q-TOF MS/MS, 30 of these differentially expressed proteins were successfully identified. All of the significant hits required a mass tolerance of only 25 ppm. For the three spots with nonsignificant hits using 25-ppm mass tolerance, the peptide mass fingerprint scores as well as MS/MS peptide ion matching scores remain nonsignificant even with modification of the mass tolerance

(up to 150 ppm). These identified proteins were classified based on their major function appeared in the Swiss-Prot and TrEMBL database and literature search in the PubMed; most of them were metabolic enzymes and signaling proteins (Table 2). All protein identities were in the expected size and pI ranges based on their positions in the 2-D gel.

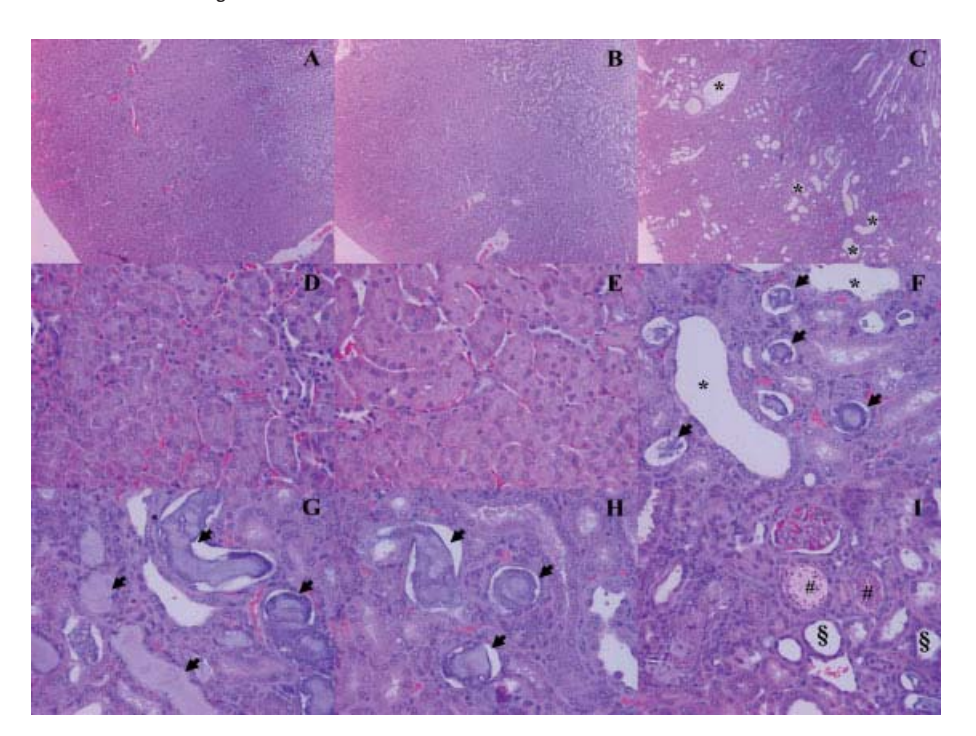
# 3.4 Reproducibility of 2-D spot pattern and comparability of normalized intensity volume of the corresponding spot in different 2-D gels

One of the most critical issues for gel-based proteomic analysis is the reproducibility and comparability of 2-D spot pattern in different 2-D gels. To address this issue in our present study, we evaluated the CV of selected protein spots across 18 different gels. %CV was calculated by dividing the SD by mean of intensity volume of each corresponding spot and multiplying by 100. Figure 6 shows that the pattern of 2-D spots in the zoom-in, cropped area was consistent across 18 different gels obtained from 18 animals. %CV of spots 150, 170, 182, and 183 varied from 9.15 to 25.93% for the analysis within the same group (n = 6) and was 14.43–20.49% for the analysis across 18 gels. We also demonstrated that normalization of spot intensity in our present study was justified for the comparability of intensity volume of each protein spot across different gels, as the summation of normalized intensity volumes of all spots in each 2-D gel was comparable among groups (80.12  $\pm$  1.38, 78.25  $\pm$  1.24, and 79.85  $\pm$  0.97 arbitrary units, in the HKD, LKD, and KD groups, respectively; *p* value was not significant by ANOVA).

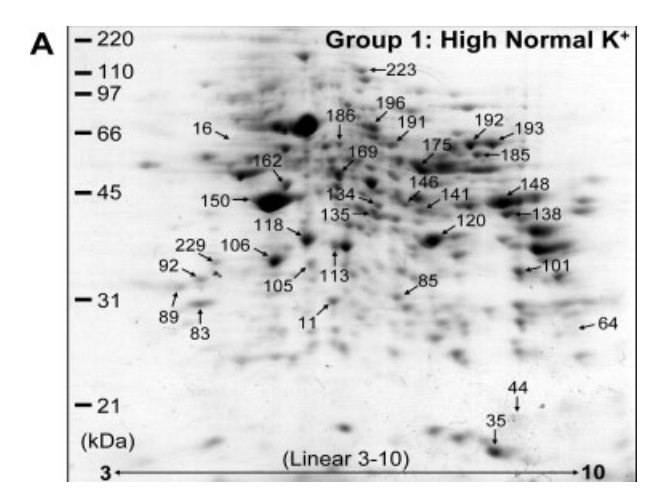
#### 4 Discussion

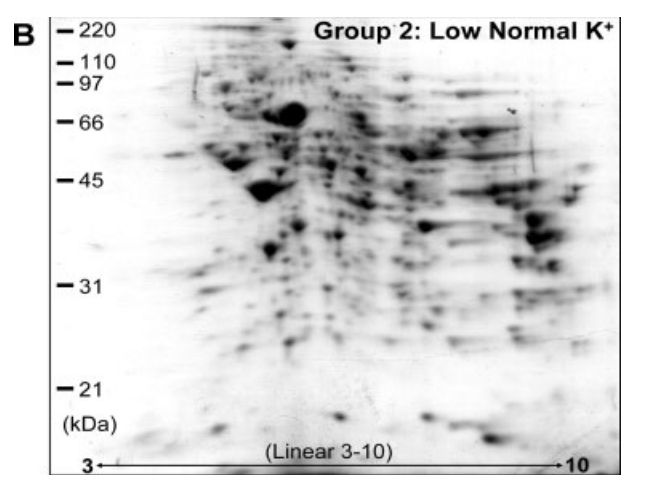
Proteomics has been successfully applied to address pathogenic mechanisms and pathophysiology of several diseases, including renal disorders [20-22]. Renal proteomics has shown its strength for linking the proteomic data to the normal renal physiology and pathophysiology of diseases. However, the field of renal proteomics is still in its early phase and current applications are limited to a relatively small number of renal disorders; there should be more applications to several other renal diseases. In the present study, we applied proteomics to identify previously unknown changes in renal protein expression that occur in hypokalemic nephropathy, which has been a well-known disease for a long time but the disease mechanisms remain unclear. Although K<sup>+</sup> repletion to normalize serum K<sup>+</sup> level can reverse renal ultrastructural changes observed in acute K+ deficiency state [15], this kind of treatment cannot abolish all of symptoms and renal changes occur in chronic KD or hypokalemic nephropathy, particularly when progressive tubulointerstitial damage occurs [11, 23]. It is therefore important to know the pathophysiology of hypokalemic nephropathy that may lead to further functional study to look for new therapeutic targets aiming to completely recover the disease.

2280 V. Thongboonkerd *et al. Proteomics* 2006, *6*, 2273–2285



Histopathological Figure 4. changes in the KD kidneys. There was no abnormal finding observed in the kidneys from the HNK (A and D) and LNK (B and E) groups. In contrast, severe tubular dilatation (labeled as \*) and intratubular deposition of amorphous and laminated materials (labeled as arrows) were seen in the KD kidneys (C, F-H). Additional findings in the latter group (I) included cellular cast (labeled as #) and tubular atrophy (labeled as §). There was no change observed in the glomeruli or renal vasculatures. Hematoxylin-eosin stain; magnification power was  $40 \times$  in (A-C) and 400  $\times$  in (D–I).





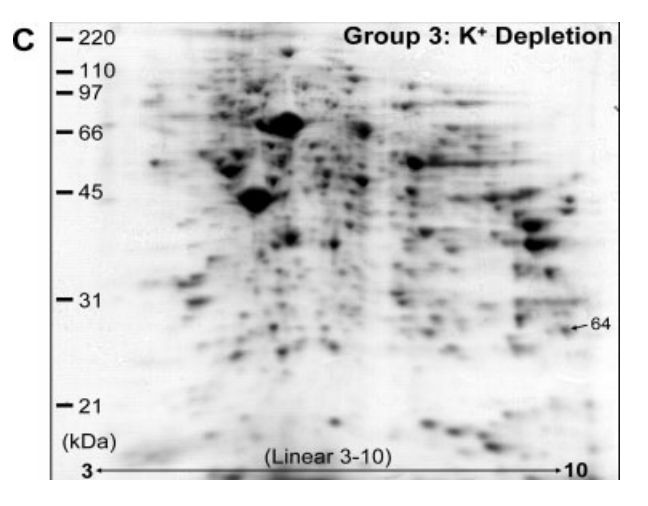
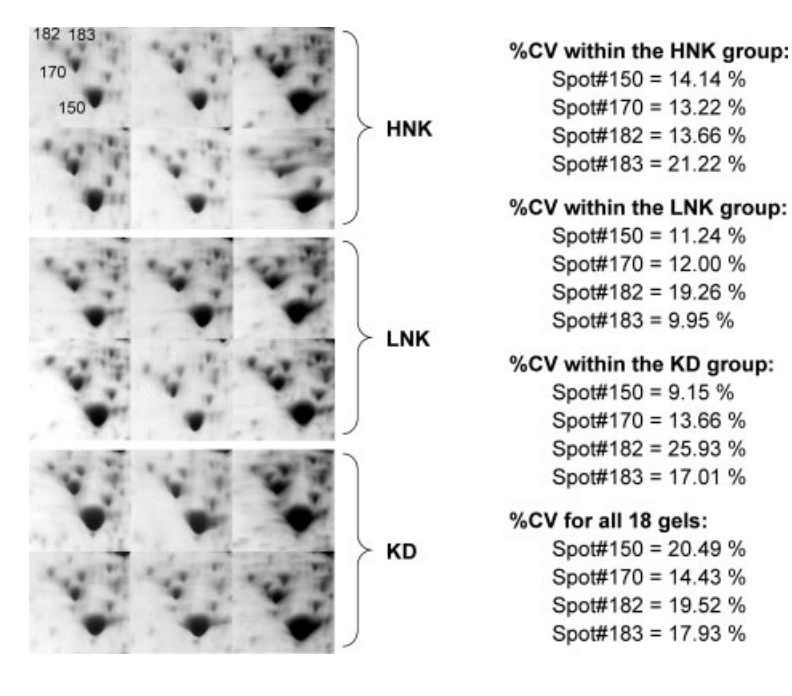


Figure 5. 2-D proteome map of differentially expressed proteins. Equal amount of 200  $\mu g$  total protein extracted from murine kidney (n=6 from different animals in each group) was loaded in each gel and resolved by 2-DE. Separated proteins were visualized by CBB stain. Quantitative intensity analysis was performed and only significant differences among groups by ANOVA with Tukey's post hoc test for multiple comparisons were subjected to mass spectrometric identification and are labeled. Numbers of protein spots correspond to those reported in Table 2.

Proteomics 2006, 6, 2273–2285 Clinical Proteomics 2281



**Figure 6.** Reproducibility of 2-D spot pattern. Zoom-in images of the selected portion of individual 2-D gels (n=18) show the corresponding area across different gels and demonstrate that the 2-D spot pattern was consistent but with some degrees of variations. To evaluate whether these variations were in acceptable range, CV was calculated (see Section 2). %CV for spots 150, 170, 182, and 183 varied from 9.15 to 25.93% for the analysis within the same group (n=6) and was 14.43–20.49% for the analysis across 18 gels.

We have generated a chronic hypokalemic mouse model by restricting K<sup>+</sup> in a given diet for 8 wk. Our model substantially differs from other hypokalemic animal models because almost all other models utilize rats and the duration of KD in such models is only 2–3 wk [9–11, 23–25]. In the present study, we used BALB/c mice and much longer duration of KD dietary exposure (8 wk). Our data clearly demonstrated that the KD mice developed chronic (>3 wk) severe hypokalemia and several clinical characteristics mimicking hypokalemic nephropathy in humans. Our model is, therefore, suitable for the study on chronic K<sup>+</sup> deficiency syndrome.

Because there was a variety of the  $K^+$  amounts in "normal  $K^+$ " rat chows [9–11, 23–25], we used two types of normal  $K^+$  diets, HNK (1%  $K^+$ ) and LNK (0.36%  $K^+$ ) to examine whether there is any difference in renal protein expression of mice given with two different  $K^+$  concentrations in diets. Plasma  $K^+$  levels were comparable between the HNK and LNK mice, although the average plasma  $K^+$  level was slightly lower in the LNK group. Differential proteomics analysis revealed differences in renal expression of eight proteins between the two groups. These results indicate that differential amounts of  $K^+$  intake have some effects on the renal physiology. Alterations in renal protein expression were more obvious when the KD diet was given to mice as demonstrated by a larger number of proteins that were differentially expressed between the KD and other mice.

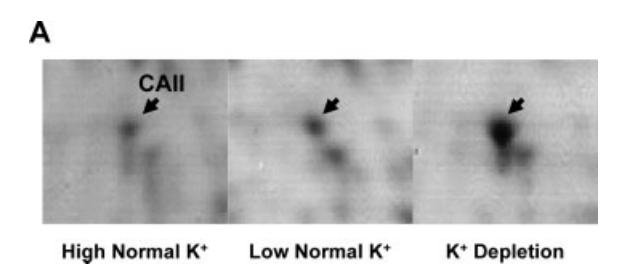
Recently, we have summarized alterations in renal protein expression in different renal diseases/disorders [20–22]. Interestingly, there are some specific patterns of changes that can potentially be useful to distinguish types of the diseases. For example, metabolic enzymes are the major components that are affected in lead nephrotoxicity, gentamicin

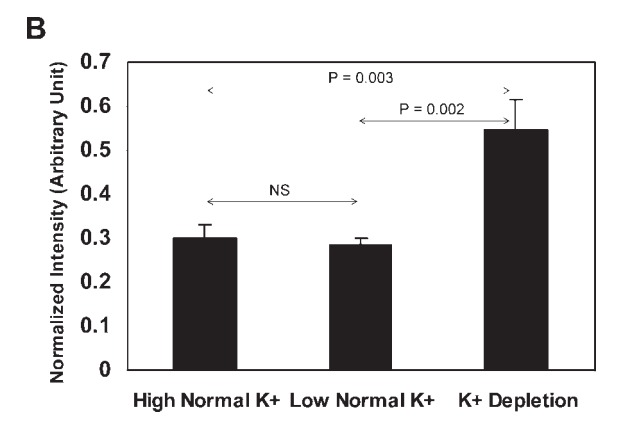
nephrotoxicity, renovascular hypertension, and renal cell carcinoma, whereas proteases, protease inhibitors, calciumbinding proteins, and transport regulators are the main compartments affected by diabetic nephropathy. These differences may imply the differential pathophysiological processes in a variety of renal diseases, as well as differential intrarenal microstructures that are involved. In the present study, we identified changes in three main groups of renal proteins in hypokalemic nephropathy: metabolic enzymes, signaling proteins, and cytoskeletal proteins. Of these altered proteins, some of them have been previously identified to be involved in other renal diseases (e.g., carbonic anhydrase in renal Fanconi syndrome and renal cancer; aldose reductase in lead nephrotoxicity, renovascular hypertension and renal cancer; argininosuccinate synthase, GST and sorbitol dehydrogenase in lead-induced tubular toxicity; GST, lactate dehydrogenase, cofilin 1 and ubiquinol-cytochrome C reductase in renal cancer; and actin and tropomyosin in several diseases) [22]. Interestingly, the major intrarenal microstructures that are affected in these diseases are renal tubules, which are also the main compartments affected by hypokalemic nephropathy. Similarity of the altered proteins across different diseases implicate that these diseases, on the other hand, have some similar pathophysiological processes. In the present study, we have focused our attention on changes in particular metabolic enzymes and signaling proteins as these changes may explain the pathophysiological processes that occur in hypokalemic nephropathy, especially acid-base imbalance, polyuria, and tubular injury.

Carbonic anhydrase is an ancient ubiquitous enzyme found in every tissue and cell type, in many subcellular organelles, and in all species ranging from unicellular bacteria through mammals [26]. Carbonic anhydrase isoform II

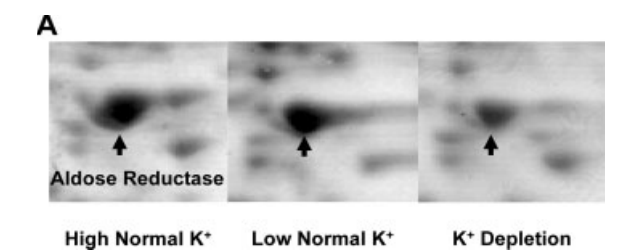
(CAII) is one among 11 isoforms in α-class of CA found in mammals [27]. We identified an up-regulation of renal CAII (approximately two-fold) in the KD mice (Fig. 7). CAII is responsible for reversible catalyzing reaction of CO2 and H<sub>2</sub>O to be H<sup>+</sup> and HCO<sub>3</sub><sup>-</sup>, acid-base balance, tubular anionic transport (coordinating with anionic exchanger protein 1, or AE1 in controlling Cl<sup>-</sup>/HCO<sub>3</sub><sup>-</sup> countertransport) and metabolic process at the cellular level [26–28]. Chronic KD is associated with increased proximal tubular bicarbonate reabsorption and thus hypokalemic alkalosis [29, 30]. Administration of carbonic anhydrase to animals with hypokalemia enhances bicarbonate reabsorption along S3 segment of proximal tubules, the loop of Henle, and/or early segment of the distal nephron [31]. These data indicate that the up-regulation of renal CAII is related, at least in part, to metabolic alkalosis that occurs in hypokalemic nephropathy.

Another metabolic enzyme that was significantly altered in hypokalemic nephropathy is aldose reductase (other synonyms are aldehyde reductase, aldo-keto reductase, and alcohol dehydrogenase). Its renal expression was down-regulated approximately 50% from the baseline level (Fig. 8). Aldose reductase is an enzyme crucial for the first step of the polyol pathway, of which glucose is converted to sorbitol. In addition to catalyzing function in the polyol pathway, aldose reductase is involved in the pathogenesis of diabetic complications and myocardial ischemic injury, and may have multiple other activities relating to signal transduction and oxidative defense mechanisms [32, 33]. Aldose reductase has been thought to serve osmoregulatory function in the kidney





**Figure 7.** Up-regulation of renal CAII in hypokalemic nephropathy. (A) Magnified image of the up-regulated CAII in the KD kidney. (B) Quantitative data obtained from intensity analysis.



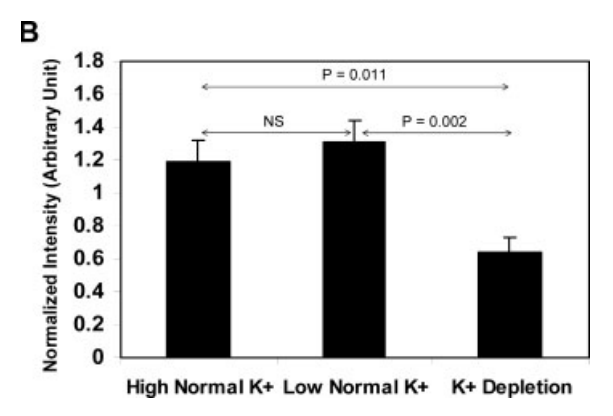
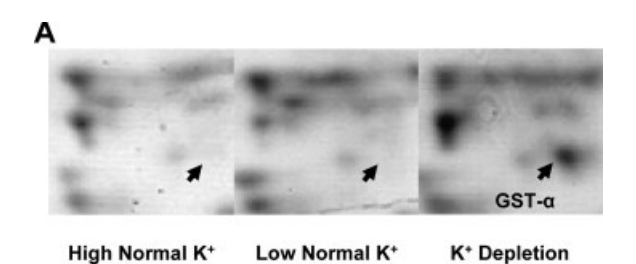


**Figure 8.** Down-regulation of renal aldose reductase in hypokalemic nephropathy. (A) Magnified image of the down-regulated aldose reductase in the KD kidney. (B) Quantitative data obtained from intensity analysis.

as renal inner medullary cells accumulate large amounts of organic osmolytes, including sorbitol, to compensate for the interstitial hypertonicity [34]. Interestingly, disruption of *Akr1b1*, an aldose reductase gene, causes defect in urinary concentrating ability [34]. Additionally, the decrease in aldose reductase mRNA expression level has been proven to be the cause of urinary concentrating defect or polyuria occurs in chronic KD [35]. Moreover, sorbitol dehydrogenase, another metabolic enzyme involved in the sorbitol/polyol pathway, was also identified as an altered protein in the present study. Our findings were consistent with the data reported in previous studies [34, 35] and indicate that the decrease in renal aldose reductase expression is associated with urinary concentrating defect or polyuria in hypokalemic nephropathy, perhaps *via* the sorbitol/polyol pathway.

GT41A is one of numerous members of GST-class  $\alpha$  that involves in conjugation of reduced glutathione to a wide number of exogenous and endogenous hydrophobic electrophiles. The up-regulation of renal GST-class  $\alpha$  has been observed in various models of renal tubular injury [36–38]. Whether its increased renal expression is the cause or the effect of renal tubular injury remains unclear. However, at least, its increased renal expression and urinary excretion may potentially be a marker for the injury at proximal renal tubules [36–38]. We identified the up-regulation of GT41A in the KD mice (Fig. 9). Its up-regulation in the KD animals might reflect renal tubular injury in hypokalemic nephropathy as renal tubules are the major intrarenal microstructures affected by prolonged hypokalemia.

Proteomics 2006, 6, 2273–2285 Clinical Proteomics 2283



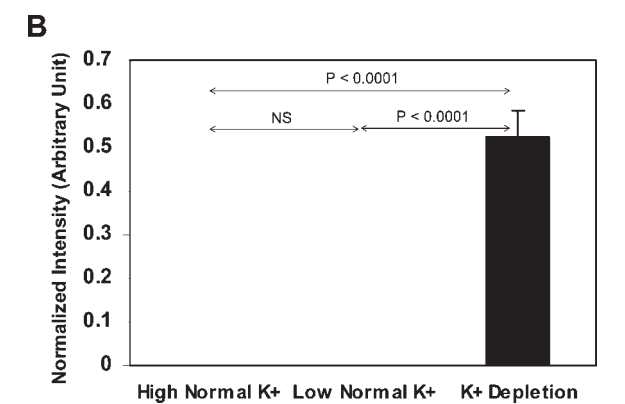
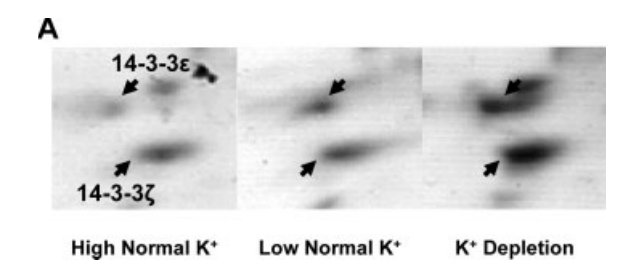
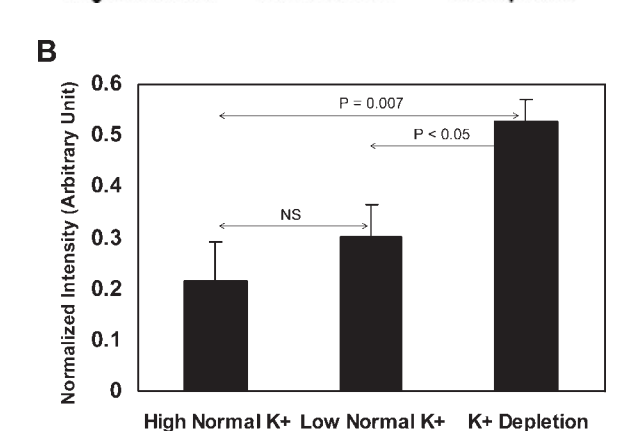


Figure 9. Up-regulation of renal glutathione S-transferase GT41A in hypokalemic nephropathy. (A) Magnified image of GT41A (GST-class  $\alpha$ ) spot that was detected only in the KD kidney and was below the detection limit in the other two groups. (B) Quantitative data obtained from intensity analysis.

14-3-3 proteins participate in protein kinase signaling pathways in all eukaryotic cells and play crucial role in regulating multiple cellular processes, including initiation and maintenance of cell cycle checkpoints and DNA repair, prevention of apoptosis, and coordination of cell adhesion and cytoskeletal dynamics [39]. 14-3-3 protein isoforms bind to specific phosphorylated sites on diverse target proteins in the context of a few additional neighboring amino acids [40-43]. Its role in K<sup>+</sup> transport (via interaction with K<sup>+</sup> channels) has been established in a few reports on plants [44], Xenopus oocytes [45, 46] and Chinese hamster embryo cells [47]. In the present study, we identified the up-regulation of two isoforms of 14–3-3 ( $\epsilon$  and  $\zeta$ ) in the KD kidney (Fig. 10). However, the role for 14–3-3 proteins in renal tubular K<sup>+</sup> transport and hypokalemic nephropathy is still unclear and needs to be further elucidated.

Some technical issues in the present study need to be discussed. First, protein spot pattern of mouse whole kidney on 2-D gel in the present study did not look like our 2-D proteome map of mouse whole kidney reported previously [48]. This difference was most likely due to different sample preparation protocols that were employed to solubilize kidney proteins. We utilized the simple lysis protocol using urea/thiourea buffer (see Section 2) to recover proteins in the present study, whereas the more complicated protocol involving three different sample buffers (with urea, but without thiourea) was employed in our previous study [48]. Ad-





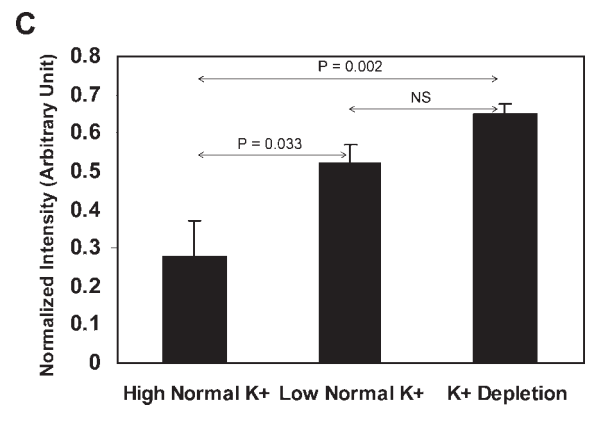


**Figure 10.** Up-regulation of renal 14–3-3 proteins in hypokalemic nephropathy. (A) Magnified image of the up-regulated 14–3-3  $\epsilon$  and  $\zeta$  isoforms in the KD kidney. Their quantitative data obtained from intensity analysis are shown in (B) and (C), respectively.

ditional minor factors are: (i) BALB/c mice were used in the present study, whereas FVB mice were employed in the previous study; and (ii) IPG strips were used in the present study, whereas mobilized tube gels were used for the IEF in our previous study. Therefore, it was not unexpected that 2-D spot pattern of mouse whole kidney in the present study was different from that reported in our previous study.

Second, we performed proteomic analysis of kidney tissues from 18 different animals and one of the most concerned issues in gel-based, differential proteomics is the reproducibility/comparability of 2-D spot pattern across different gels, in which variations may occur and make the analysis more difficult. In previous gel-based, proteome studies analyzing human tissues, cell lines, and body fluids,

up to 25% of CV was observed and acceptable for the reproducibility of 2-DE [49–51]. In the present study, we observed some degrees of variations in kidney tissues obtained from 18 mice. However, the %CV obtained from our present study was in an acceptable range. In addition, the summation of normalized intensity volumes of all spots in each 2-D gel was comparable among three different groups. Therefore, quantitative intensity analysis in our present study was justified.

Third, the total number of protein spots visualized in the present study was relatively small for the entire kidney proteome. This limitation might be because: (i) we used a small-format 2-D gel (using 7-cm-long IPG strip) in the present study that has some limitations in protein separation; much more spots should have been resolved using a large format (using 18 to 24-cm-long IPG strip); (ii) Coomassie Blue stain was employed instead of silver or fluorescence stains that are more sensitive in protein detection; and (iii) we used the highly stringent criteria or parameters for detection of "true protein spots" (see Section 2) in the present study; much more spots are expected to be detected when the lower stringent criteria or parameters are used.

Finally, we screened for changes in renal protein expression in hypokalemic nephropathy using the whole kidney. This kind of approach has a limitation in identification of all changes because major abundant proteins can obscure the identification of low-abundance proteins. Therefore, the total number of the altered proteins associated with hypokalemic nephropathy in our present study was underestimated. Surely, we can identify much more altered proteins using highly focused study to examine individual micro- and ultrastructures of the kidney (e.g., cortex, medulla, proximal tubules, distal tubules, etc.).

In summary, we have demonstrated that prolonged KD in mice caused several clinical, histopathological, and biochemical changes mimicking human hypokalemic nephropathy. Using differential proteomics analysis, we successfully identified alterations in expression of several metabolic enzymes and signaling proteins that may have significant roles in the pathophysiology of hypokalemia-induced metabolic alkalosis, polyuria, and renal tubular injury. These data may lead to a new roadmap for research on hypokalemic nephropathy and better understanding of the pathophysiology of this renal disease when the functional and physiological significances of these altered proteins are defined.

We thank Ms. Wipawanee Kasemworaphoom, Lt.Col. Duangporn Phulsuksombati and Mrs. Kanittar Srisook for their technical assistance, and Dr. Sumalee Nimmannit, Dr. Yasushi Nakagawa, Dr. Somkiat Vasuvattakul, Dr. Pa-Thai Yenchitsomanus, and Dr. Suchai Sritippayawan for their advice. This study was supported by the Thailand Research Fund to P. Malasit (Senior Research Scholar Program; Grant No. RTA4680017). V. Thongboonkerd is supported by Siriraj Preclinic Grant and Siriraj Foundation (D 2362: Surapongchai Fund). S. Chutipongtanate is a Ph.D. candidate in the Doctor of Philosophy

Programme in Immunology at Faculty of Medicine Siriraj Hospital and in the Medical Scholars Program (Ph.D./M.D.) supported by Mahidol University.

#### 5 References

- [1] Cohn, J. N., Kowey, P. R., Whelton, P. K., Prisant, L. M., Arch. Intern. Med. 2000, 160, 2429–2436.
- [2] Mount, D. B., Zandi-Nejad, K., in: Brenner, B. M. (Ed.), Brenner & Rector's The Kidney, 7th ed., W. B. Saunders, Philadelphia 2004, pp. 997–1040.
- [3] Gennari, F. J., N. Engl. J. Med. 1998, 339, 451-458.
- [4] Gennari, F. J., Crit. Care Clin. 2002, 18, 273-288.
- [5] Antes, L. M., Kujubu, D. A., Fernandez, P. C., Semin. Nephrol. 1998, 18, 31–45.
- [6] Relman, A. S., Schwartz, W. B., N. Engl. J. Med. 1956, 255, 195–203.
- [7] Hollander, W., Jr., N. C. Med. J. 1957, 18, 505-509.
- [8] Weissmann, G., Ludwig, A. M., J. Mt. Sinai. Hosp. NY 1958, 25, 454–458.
- [9] Tolins, J. P., Hostetter, M. K., Hostetter, T. H., J. Clin. Invest. 1987, 79, 1447–1458.
- [10] Berl, T., Linas, S. L., Aisenbrey, G. A., Anderson, R. J., J. Clin. Invest. 1977, 60, 620–625.
- [11] Ray, P. E., Suga, S., Liu, X. H., Huang, X. et al., Kidney Int. 2001, 59, 1850–1858.
- [12] Kaufman, A. M., Kahn, T., Am. J. Physiol. 1988, 255, F763– F770.
- [13] Peterson, L. N., Carpenter, B., Guttierrez, G. A., Fajardo, C. et al., Miner. Electrolyte Metab. 1987, 13, 57–62.
- [14] Stetson, D. L., Wade, J. B., Giebisch, G., Kidney Int. 1980, 17, 45–56.
- [15] Ordonez, N. G., Toback, F. G., Aithal, H. N., Spargo, B. J., Lab. Invest. 1977, 36, 33–47.
- [16] Fourman, P., Mccance, R. A., Parker, R. A., Br. J. Exp. Pathol. 1956, 37, 40–43.
- [17] Thongboonkerd, V., Gozal, E., Sachleben, L. R., Arthur, J. M. et al., J. Biol. Chem. 2002, 277, 34708–34716.
- [18] Thongboonkerd, V., Klein, E., Klein, J. B., Contrib. Nephrol. 2004, 141, 11–24.
- [19] Arthur, J. M., Thongboonkerd, V., Scherzer, J. A., Cai, J. et al., Kidney Int. 2002, 62, 1314–1321.
- [20] Thongboonkerd, V., Am. J. Nephrol. 2004, 24, 360-378.
- [21] Thongboonkerd, V., Malasit, P., Proteomics 2005, 5, 1033– 1042.
- [22] Thongboonkerd, V., Expert Rev. Proteomics 2005, 2, 349– 366.
- [23] Kimura, T., Nishino, T., Maruyama, N., Hamano, K. et al., Pathobiology 2001, 69, 237–248.
- [24] Amlal, H., Wang, Z., Soleimani, M., J. Clin. Invest. 1998, 101, 1045–1054.
- [25] Fryer, J. N., Burns, K. D., Ghorbani, M., Levine, D. Z., Kidney Int. 2001, 60, 1792–1799.
- [26] Henry, R. P., Annu. Rev. Physiol. 1996, 58, 523-538.
- [27] Tripp, B. C., Smith, K., Ferry, J. G., J. Biol. Chem. 2001, 276, 48615–48618.

Proteomics 2006, 6, 2273–2285 Clinical Proteomics 2285

[28] Sterling, D., Reithmeier, R. A., Casey, J. R., J. Biol. Chem. 2001, 276, 47886–47894.

- [29] Chan, Y. L., Biagi, B., Giebisch, G., Am. J. Physiol. 1982, 242, F532–F543.
- [30] Maddox, D. A., Gennari, F. J., *J. Clin. Invest.* 1986, 77, 709–
- [31] Capasso, G., Kinne, R., Malnic, G., Giebisch, G., J. Clin. Invest. 1986, 78, 1558–1567.
- [32] Petrash, J. M., Cell Mol. Life Sci. 2004, 61, 737-749.
- [33] Hwang, Y. C., Kaneko, M., Bakr, S., Liao, H. et al., FASEB J. 2004, 18, 1192–1199.
- [34] Aida, K., Ikegishi, Y., Chen, J., Tawata, M. et al., Biochem. Biophys. Res. Commun. 2000, 277, 281–286.
- [35] Nakanishi, T., Yamauchi, A., Yamamoto, S., Sugita, M. et al., Kidney Int. 1996, 50, 828–834.
- [36] Cressey, G., Roberts, D. R., Snowden, C. P., J. Cardiothorac. Vasc. Anesth. 2002, 16, 290–293.
- [37] Desmots, F., Rissel, M., Pigeon, C., Loyer, P. et al., Free Radic. Biol. Med. 2002, 32, 93–101.
- [38] Branten, A. J., Mulder, T. P., Peters, W. H., Assmann, K. J. et al., Nephron 2000, 85, 120–126.
- [39] Wilker, E., Yaffe, M. B., J. Mol. Cell Cardiol. 2004, 37, 633–642.

- [40] Mackintosh, C., Biochem. J. 2004, 381, 329-342.
- [41] Benzing, T., Yaffe, M. B., Arnould, T., Sellin, L. et al., J. Biol. Chem. 2000, 275, 28167–28172.
- [42] Mhawech, P., Cell Res. 2005, 15, 228-236.
- [43] Bridges, D., Moorhead, G. B., Sci. STKE 2004, 2004, re10.
- [44] van den Wijngaard, P. W., Sinnige, M. P., Roobeek, I., Reumer, A. et al., Plant J. 2005, 41, 43–55.
- [45] Benzing, T., Kottgen, M., Johnson, M., Schermer, B. et al., J. Biol. Chem. 2002, 277, 32954–32962.
- [46] Rajan, S., Preisig-Muller, R., Wischmeyer, E., Nehring, R. et al., J. Physiol. 2002, 545, 13–26.
- [47] Kagan, A., Melman, Y. F., Krumerman, A., McDonald, T. V., EMBO J. 2002, 21, 1889–1898.
- [48] Thongboonkerd, V., Barati, M. T., McLeish, K. R., Benarafa, C. et al., J. Am. Soc. Nephrol. 2004, 15, 650–662.
- [49] Hunt, S. M., Thomas, M. R., Sebastian, L. T., Pedersen, S. K. et al., J. Proteome. Res. 2005, 4, 809–819.
- [50] Terry, D. E., Desiderio, D. M., Proteomics 2003, 3, 1962–1979.
- [51] Molloy, M. P., Brzezinski, E. E., Hang, J., McDowell, M. T. et al., Proteomics 2003, 3, 1912–1919.

### Vascular Leakage in Severe Dengue Virus Infections: A Potential Role for the Nonstructural Viral Protein NS1 and Complement

Panisadee Avirutnan,¹ Nuntaya Punyadee,¹³ Sansanee Noisakran,⁴ Chulaluk Komoltri,² Somchai Thiemmeca,¹ Kusuma Auethavornanan,¹³ Aroonroong Jairungsri,¹ Rattiyaporn Kanlaya,¹³ Nattaya Tangthawornchaikul,⁴ Chunya Puttikhunt,⁴ Sa-nga Pattanakitsakul,¹ Pa-thai Yenchitsomanus,¹⁴ Juthathip Mongkolsapaya,¹ Watchara Kasinrerk,⁴⁵ Nopporn Sittisombut,⁴⁶ Matthias Husmann,⁵ Maria Blettner,⁵ Sirijitt Vasanawathana,² Sucharit Bhakdi,⁵ and Prida Malasit¹.⁴

<sup>1</sup>Medical Molecular Biology Unit and <sup>2</sup>Division of Clinical Epidemiology, Office for Research and Development, and <sup>3</sup>Department of Immunology, Faculty of Medicine, Siriraj Hospital, Mahidol University, Bangkok, <sup>4</sup>Medical Biotechnology Unit, National Center for Genetic Engineering and Biotechnology, National Science and Technology Development Agency, Pathumthani, <sup>5</sup>Department of Clinical Immunology, Faculty of Associated Medical Sciences, and <sup>6</sup>Department of Microbiology, Faculty of Medicine, Chiang Mai University, Chiang Mai, and <sup>7</sup>Pediatric Department, Khon Kaen Hospital, Ministry of Public Health, Khonkaen, Thailand; <sup>8</sup>Institute of Medical Microbiology and Hygiene and <sup>9</sup>Institute of Medical Biometry, Epidemiology, and Informatics, University Hospital, Johannes Gutenberg University, Mainz, Germany

**Background.** Vascular leakage and shock are the major causes of death in patients with dengue hemorrhagic fever (DHF) and dengue shock syndrome (DSS). Thirty years ago, complement activation was proposed to be a key underlying event, but the cause of complement activation has remained unknown.

*Methods.* The major nonstructural dengue virus (DV) protein NS1 was tested for its capacity to activate human complement in its membrane-associated and soluble forms. Plasma samples from 163 patients with DV infection and from 19 patients with other febrile illnesses were prospectively analyzed for viral load and for levels of NS1 and complement-activation products. Blood and pleural fluids from 9 patients with DSS were also analyzed.

**Results.** Soluble NS1 activated complement to completion, and activation was enhanced by polyclonal and monoclonal antibodies against NS1. Complement was also activated by cell-associated NS1 in the presence of specific antibodies. Plasma levels of NS1 and terminal SC5b-9 complexes correlated with disease severity. Large amounts of NS1, complement anaphylatoxin C5a, and the terminal complement complex SC5b-9 were present in pleural fluids from patients with DSS.

**Conclusions.** Complement activation mediated by NS1 leads to local and systemic generation of anaphylatoxins and SC5b-9, which may contribute to the pathogenesis of the vascular leakage that occurs in patients with DHF/DSS.

Dengue hemorrhagic fever (DHF) and dengue shock syndrome (DSS) are severe forms of dengue virus (DV) infection and are still one of the leading causes of morbidity and mortality in children of school age in tropical and subtropical regions. Major pathophysiological processes that distinguish DHF/DSS from mild dengue fe-

ver are abrupt onset of vascular leakage, hypotension, and shock, which are accompanied by thrombocytopenia and hemorrhagic diathesis in the absence of any characteristic histopathological vascular lesions [1, 2].

Four DV serotypes exist, and DHF/DSS occurs almost exclusively in patients who are reinfected with a different virus serotype [3, 4]. An enigmatic dysfunction of the immune system then leads to enhanced viral replication. This has been proposed to be due to an

Received 30 June 2005; accepted 28 October 2005; electronically published 9 March 2006.

Reprints or correspondence: Dr. Sucharit Bhakdi, Institute of Medical Microbiology and Hygiene, Hochhaus am Augustusplatz, 55101 Mainz, Germany (sbhakdi@uni-mainz.de); or Dr. Prida Malasit, Medical Molecular Biology Unit, Office for Research and Development and Dept. of Immunology, Siriraj Hospital, Mahidol University, Bangkok-noi, Bangkok 10700, Thailand (sipml@mahidol.ac.th).

The Journal of Infectious Diseases 2006; 193:1078–88

© 2006 by the Infectious Diseases Society of America. All rights reserved 0022-1899/2006/19308-0005\$15.00

Potential conflicts of interest: none reported.

Financial support: Senior Research Scholar Program of the Thailand Research Fund (TRF) (support to P.M.); Thailand Tropical Disease Research Program T2 (for clinical database and specimens); National Center for Genetic Engineering and Biotechnology, Thailand (support to P.A., P.M., P.Y., and N.T.). P.A. has been supported by a postdoctoral grant from the TRF and a preclinical grant from the Faculty of Medicine and the Vichit Suraphongchai Fund of Siriraj Foundation, Siriraj Hospital.

antibody-mediated increase in viral uptake in target cells [5, 6] or to cross-depletion of protective CD8 lymphocytes [7]. High viral loads and levels of circulating viral antigens are consequently found in these patients [8–10].

Thirty years ago, accelerated complement consumption and a marked reduction in plasma complement components were observed during shock in patients with DSS [11, 12], which led to the proposal that complement activation plays an important role in disease pathogenesis [13, 14]. In the following decades, the thrust of international research shifted toward the possible role of lymphocytes and cytokines [6, 15, 16], and the cause of complement activation has remained unknown. Previously, we observed that surfaces of DV-infected cells bind DV antibodies, which leads to complement activation and cytokine secretion [17]. The search for the responsible viral antigen led to NS1, a 45-kDa nonstructural protein that resides in the plasma membrane of infected cells [18] and is also released in oligomeric form to the extracellular milieu [19]. NS1 is strongly immunogenic, and type-specific anti-NS1 antibodies play a role in protection against disease [20-23]. High levels of NS1 are found in the circulation of DV-infected patients during the acute phase of the disease [10, 24, 25].

We report that soluble NS1 (NS1s) and membrane-associated NS1 (NS1m) activate human complement, that plasma levels of NS1s and the terminal SC5b-9 complement complex correlate with disease severity, and that massive complement activation probably occurs at the sites of vascular leakage. Complement anaphylatoxins and the terminal SC5b-9 complement complex increase vascular permeability [26, 27], and SC5b-9 increases lung hydraulic conductivity [28]. A link thus emerges between NS1 level, complement activation, and the clinical manifestation of DHF/DSS.

#### **PATIENTS AND METHODS**

Patient enrollment and study design. A total of 182 patients admitted to the ward of Khon Khan Provincial Hospital, Thailand, between November 2001 and December 2003 who met the following 2 sets of criteria were enrolled in this prospective study. The first set of criteria included (1) age 1-15 years; (2) pyrexia for not more than 4 days, with no obvious source of infection; and (3) tourniquet test positivity or history of signs/ symptoms of bleeding/hemorrhagic diathesis. These patients subsequently all tested positive for DV by reverse-transcription polymerase chain reaction (RT-PCR), virus isolation, and DV antibody ELISA profiling. The second set of criteria included (1) age 1-15 years and (2) <3 days of fever with no obvious source of infection. Patients who subsequently tested positive for DV were included in the dengue fever (DF) and DHF groups, whereas those with negative RT-PCR and DV antibody results were assigned to the control "other febrile illness" (OFI)

group. Blood specimens were collected daily in 5 mmol/L EDTA until 1 day after defervescence, and plasma samples were stored at  $-70^{\circ}$ C. DV infection was confirmed by measuring anti-DV IgM/IgG and by RT-PCR [32]. Pleural fluid was aspirated only in patients experiencing severe respiratory difficulty, as a part of therapeutic measures to alleviate the pulmonary insufficiency caused by rapidly accumulated fluid.

Grading of DHF followed World Health Organization criteria [33]: DHF3 is assigned to patients with signs of circulatory failure, DHF2 is assigned to patients with spontaneous bleeding, and DHF1 is assigned to patients with fever who are tourniquet-test positive. Study day 0 was defined as the calendar day during which the patient's temperature fell and stayed below 37.8°C. The study protocol was approved by the Ministry of Public Health (approval date, 7 May 2003), the Faculty of Medicine Siriraj Hospital (certificates of approval 156/2002 and 115/2004), and the Khon Khan Hospital (approval date, 31 October 2002). Informed consent was individually obtained from all subjects.

**Reagents.** IgG from pooled convalescent-phase serum (PCS) samples (hemagglutination titer, ≥1/25600) and control serum samples (DV antibody–negative serum [DNS]) were purified by protein G column chromatography (Pharmacia). NS1-specific monoclonal antibody (MAb) clones 2G6, 1A4, 1B2, 1F11, 2E11, and 2E3 have been described elsewhere [29].

Cells and viruses. The swine fibroblast cell line (PsCloneD) and the insect cell line C6/36 were cultured at 37°C and 28°C, respectively, in L-15 medium (Life Technologies) containing 10% tryptose phosphate broth (Sigma) and 10% fetal bovine serum (FBS) (Hyclone). The human kidney epithelial cell line HEK-293T was grown in RPMI 1640 (GIBCO) containing 10% FBS, 100 U/mL penicillin, and 100  $\mu$ g/mL streptomycin. DV serotype 1 (DEN-1), DEN-2, DEN-3, and DEN-4 (strain Hawaii, 16681, H-87, and H-241, respectively) were propagated in C6/36 cells [17].

Two HEK-293T cell lines expressing NS1 were conventionally generated [30]. Cells were transfected with pcDNA3.1/Hygro (Invitrogen) containing the coding sequence of NS1s (the complete sequence of NS1) or NS1m (the complete NS1 sequence connected to the 26-aa region at the N-terminus of NS2A).

*NS1 purification.* Fibroblast monolayers were infected with DEN-1, -2, -3, and -4 at an MOI of 1 and were cultured in protein-free medium (Ultradoma). Culture supernatants were harvested 3 days later, centrifuged at 200,000 *g*, and subjected to immunoaffinity chromatography with a column prepared with anti-NS1 MAb 2G6.

For isolation of NS1s from transfected cells, culture supernatants were harvested every 3 days and replaced with fresh medium. Supernatants were passed through a 0.2- $\mu$ m filter before immunoaffinity chromatography. Purified NS1 was passed over a protein G column twice to remove any traces of contaminating antibodies.

*NS1 ELISA.* Microtiter plates (Nunc) were coated with MAb 2E11 (5  $\mu$ g/mL) overnight at 4°C. After blocking with PBS containing 15% FBS, wells were washed 5 times with PBS/0.05% Tween-20. Samples (100  $\mu$ L) were added to each well and incubated for 1 h at room temperature. After 5 washes, 100  $\mu$ L of MAb 2E3 (50  $\mu$ g/mL) was added to each well and incubated for 1 h. The ELISA was developed conventionally, using horseradish peroxidase–conjugated goat anti-mouse IgG (Sigma).

Assay for fluid-phase complement activation. Cell supernatants or purified NS1s from DV-2 were incubated with 12.5% normal human serum (NHS) (final concentration) in a 0.2-mL total assay volume in the presence or absence of anti-DV antibodies for 60 min at 37°C. Heat-inactivated serum or serum containing 10 mmol/L EDTA served as a negative control. Hemolytic complement titers (CH<sub>50</sub>) were determined in the conventional manner. SC5b-9 measurements were performed using a commercial ELISA from Quidel.

Assay for complement activation on cells. HEK-293T cells were infected with DV-2 at an MOI of 10 and were harvested 24 h after infection. DV-infected cells or cells expressing NS1m (1 × 106) were incubated with purified PCS, DNS, a mix of anti-NS1 MAbs, or isotype controls, in the presence of 12.5% NHS. Washed cells were incubated with a MAb against C3dg, provided by P. J. Lachmann, or against SC5b-9 complexes (Quidel); this was followed by staining with fluorescein isothiocyanate (FITC)-labeled rabbit F(ab'), anti-mouse immunoglobulin. Double staining for C3 and NS1 was performed by first reacting cells with a mix of anti-NS1 MAbs at 37°C for 1 h. After 1 wash, cells were fixed with 2% paraformaldehyde for 10 min and incubated with rabbit anti-human C3c and C3d (Dakopatts). Stainings were developed with FITC-conjugated swine anti-rabbit immunoglobulins (Dako) and Cy3-conjugated goat anti-mouse immunoglobulin (Jackson Immuno Research Laboratories). Washed cells were resuspended in 50% fluorescent mounting medium (Dako) and observed under a Zeiss LSM 510 META confocal microscope (Carl Zeiss).

**Quantitative RT-PCR.** RNA was extracted from DV-infected cell supernatants or patients' plasma by use of QIAamp Viral RNA Mini Kit (Qiagen), aliquoted, and stored at  $-70^{\circ}$  C. Viral RNA was quantified by a single-tube 1-step real-time RT-PCR using a LightCycler instrument and software version 3.5 (Roche Molecular Biochemicals), as described by Shu et al. [31].

**Measurement of anaphylatoxins.** C3a and C5a were quantified using a commercial cytometric bead array kit (Becton Dickinson).

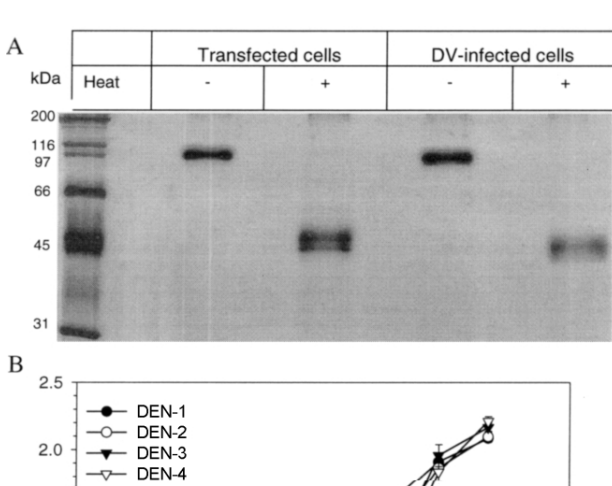
Statistical analysis. Data analysis was performed using SAS (version 8.1; SAS Institute). Viral load, NS1 level, and SC5b-9 level are presented as mean and SD and, in cases of skewness, as median and range. The  $\chi^2$  test and 1-way analysis of variance

were used to compare differences in sex and age, respectively, between groups of patients.

Since viral load, NS1 level, and SC5b-9 level were repeatedly observed over time and there were some missing data, a mixed model (MixMod) was employed as a multivariate statistical method. The purpose was to test the differences in patterns of viral load, NS1 level, and SC5b-9 level over time between different groups of patients. Under a random intercept model, mixed models with day (-3, -2, -1, 0, 1, and 2) as a quantitative variable were fitted. Only patients with data on at least 3 consecutive days were included in the analysis. Since viral load, NS1, and SC5b-9 were positively skewed, a common log transformation was applied. Residual analysis was performed to assure that model assumptions were satisfied. All analyzed P values were 2-sided.

#### **RESULTS**

*Study participants.* The overall male-to-female ratio among the 182 patients was 1:1, and the mean  $\pm$  SD age was 9.6  $\pm$ 



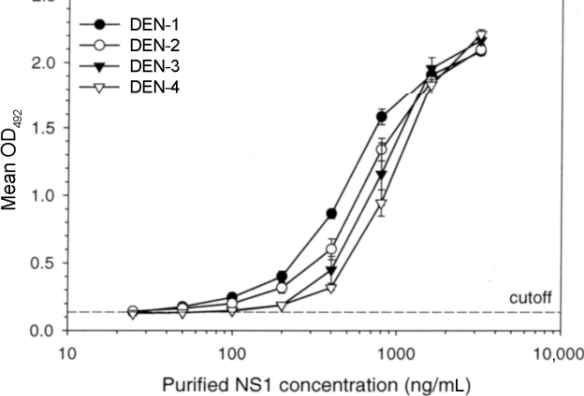


**Figure 1.** *A*, SDS-PAGE of purified soluble NS1 from dengue virus (DV)—infected cells and from cells stably expressing NS1. Purified NS1 was unheated or heated (at 95°C for 3 min) before SDS-PAGE. Markers are shown. *B*, Standard curves for NS1 capture ELISA with purified NS1 from DEN-1, -2, -3, and -4. Data points represent the mean and SD for 3 replicates. The cutoff value was set at twice the mean optical density value for negative control samples (mean  $\pm$  SD, 0.103  $\pm$  0.025).

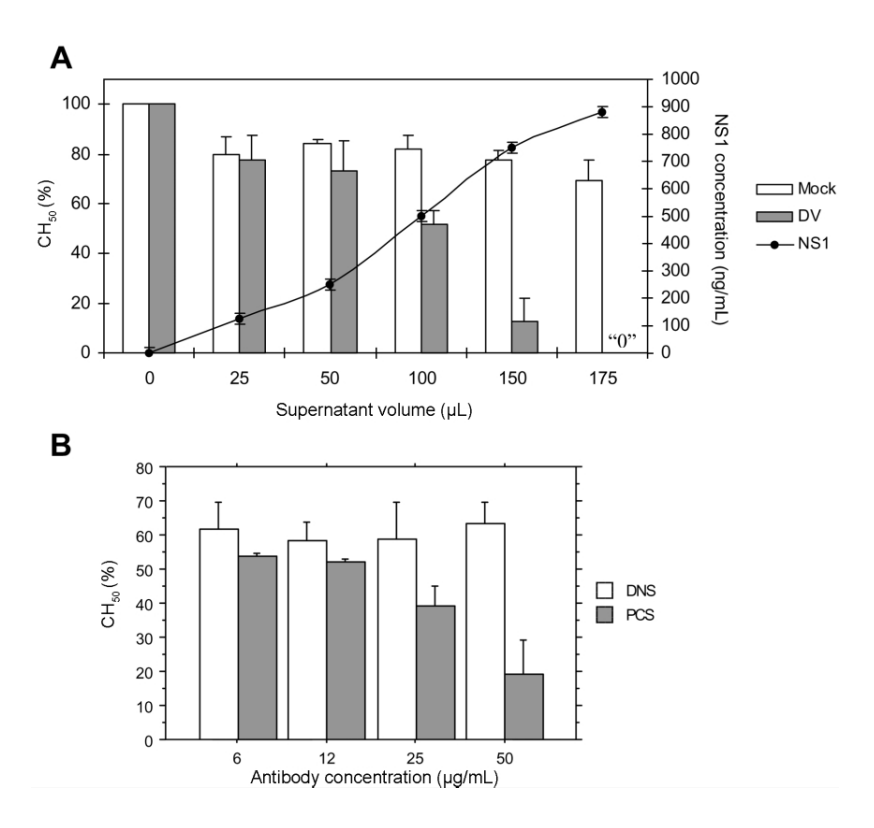


**Figure 2.** Complement activation by supernatants of dengue virus (DV)—infected cells. *A,* Dose dependency of spontaneous complement activation. The given amounts of culture supernatants were mixed with 25  $\mu$ L of normal human serum (NHS), and buffer was added to give a total of 200  $\mu$ L/sample. CH<sub>50</sub> was determined after incubation at 37°C for 1 h. Data are displayed as the mean  $\pm$  SD of the percentage CH<sub>50</sub> over serum controls from 3 independent experiments. Final concentrations of NS1 in the samples are given on the second *Y*-axis. *B,* Enhancement of complement activation by DV-specific antibodies. Culture supernatants (100  $\mu$ L) from DV-infected cells were mixed with purified antibodies from pooled convalescent-phase serum (PCS) and DV antibody—negative serum (DNS) at the given final concentrations and 25  $\mu$ L of NHS. CH<sub>50</sub> was determined after 60 min at 37°C. Data are displayed as the mean  $\pm$  SD of percentage CH<sub>50</sub> over serum controls from 3 independent experiments. "0" indicates that the value of CH<sub>50</sub> in the DV experiment was not detectable.

3 years (range, 2–15 years; median, 9 years). There were no major differences in sex ratios and mean ages of patients in each group. There were 49 patients with DF, 44 with DHF1, 44 with DHF2, 26 with DHF3/DSS, and 19 with OFIs. DV RT-PCR results were positive for 151 (92.6%) of 163 patients infected with DV. The virus types identified were DEN-1 (n = 87), DEN-2 (n = 52), DEN-3 (n = 6), and DEN-4 (n = 6). Secondary infection was diagnosed in 148 patients (90.8%), and primary infection was diagnosed in 15 patients (9.2%). Of the primary infection cases, 67% were classified as DF (n = 10), and the rest were classified as DHF1 (n = 2), DHF2 (n = 2), or DHF3 (n = 1).

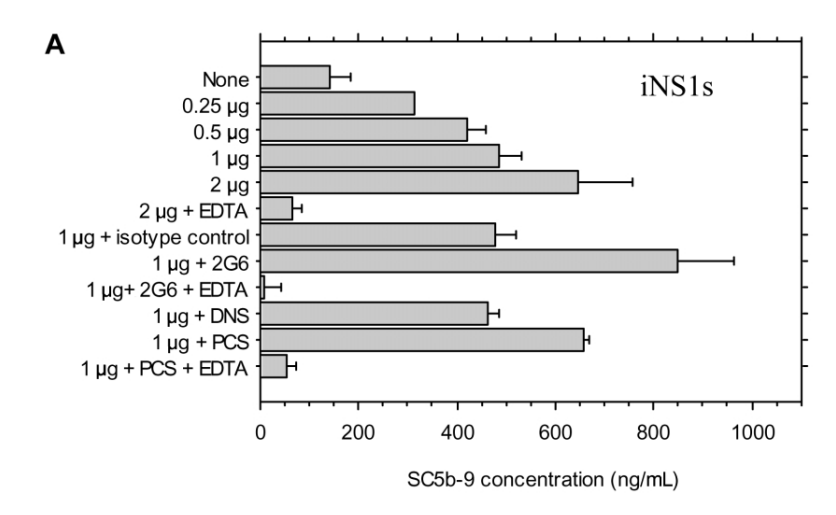
**Purification of NS1s.** Figure 1A depicts SDS-PAGE of purified NS1. As described by Winkler et al. [18], the 80-kDa dimeric form was converted to the 40-kDa monomer by heating. The same bands appeared in Western blots with NS1-specific MAbs (data not shown). The mean  $\pm$  SD NS1 level in 3-day supernatants of infected cells ranged from 900.3  $\pm$  46.7 to 1029.4  $\pm$  62.4 ng/mL, and the yield of NS1 was 334  $\pm$  87.5

and 237.4  $\pm$  38.5  $\mu$ g/L of culture from DV-infected cells and from NS1-transfected cells, respectively.

*NS1 capture ELISA*. Antibodies employed in the capture ELISA cross-reacted with NS1 from all 4 DV serotypes. The detection limit for NS1 was found to be ∼50 ng/mL from DV-1 and DV-2, 120 ng/mL for DV-3, and 160 ng/mL for DV-4 (figure 1*B*).

Activation of complement by NS1s. Supernatants from DV-infected cells, but not from mock-infected cells, dose dependently consumed complement in pooled human serum (figure 2A). Addition of purified immunoglobulin fractions from PCS but not control DNS enhanced complement consumption (figure 2B). An increase in complement activation was also observed when a mix of MAbs against NS1 was employed (data not shown).

NS1s purified from supernatants of infected cells also activated complement and caused a decrease in  $CH_{50}$  similar to that caused by the unfractionated culture supernatants. Complement activation occurred to completion with formation of



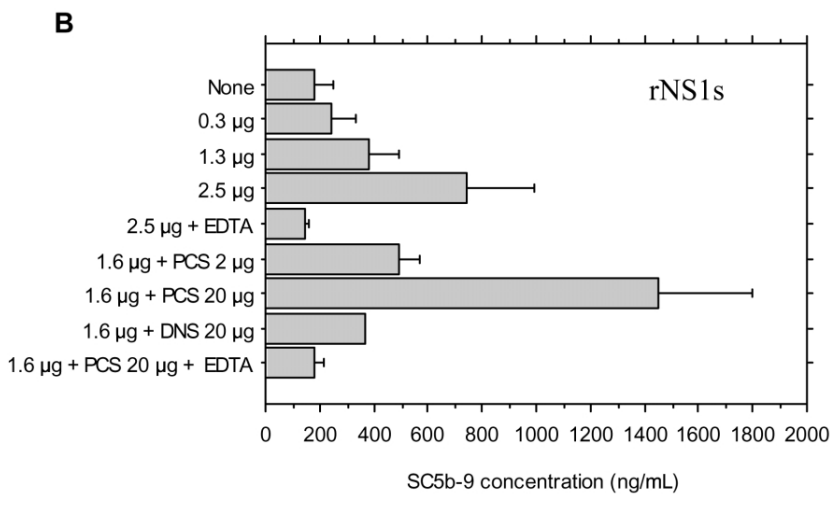


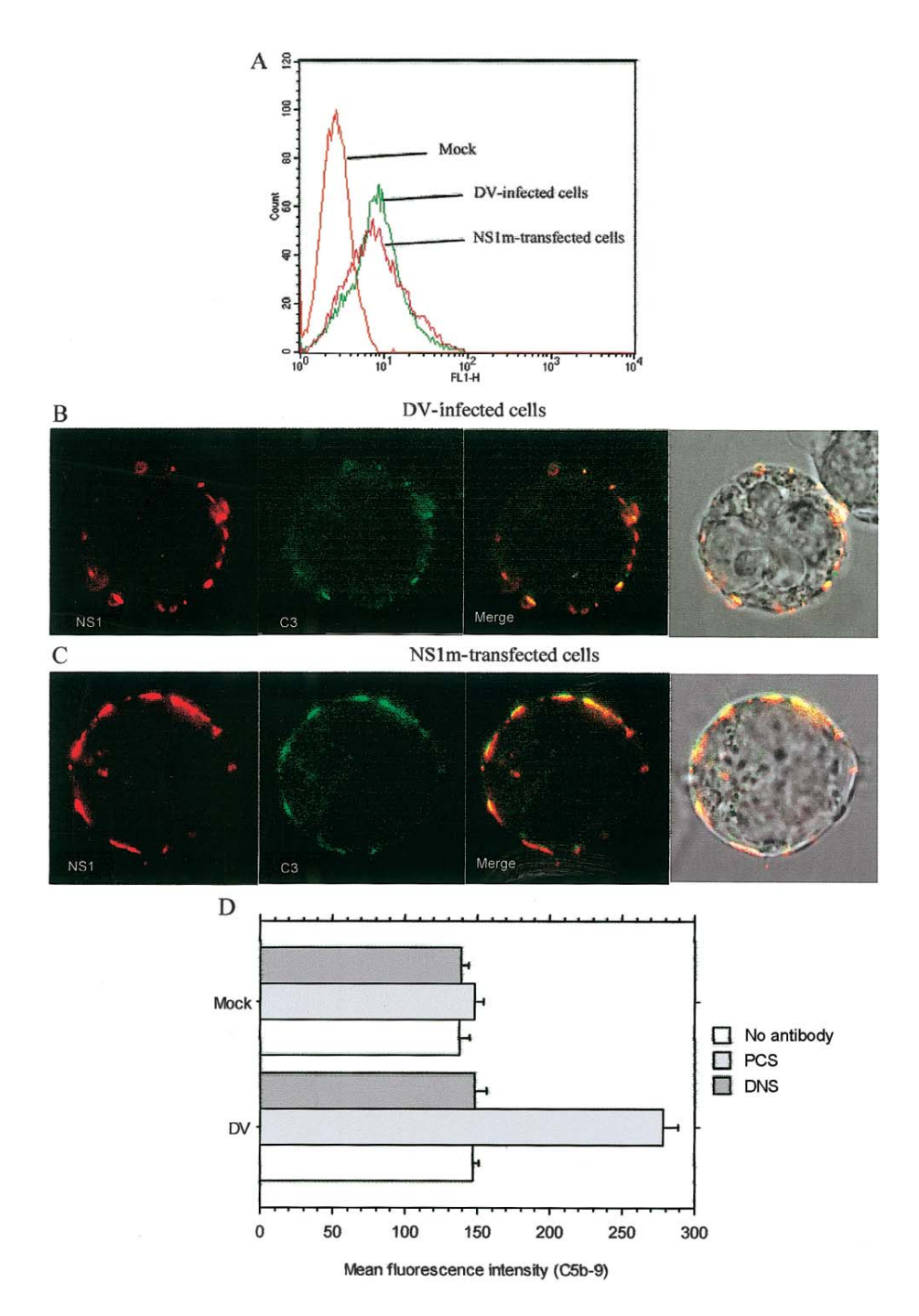
Figure 3. Activation of complement to completion by purified dengue virus (DV) NS1 protein. A, Purified soluble NS1 from DV-infected cells (iNS1s) at the given final concentrations was incubated in 12.5% normal human serum in the presence or absence of NS1-specific monoclonal antibody 2G6 (10  $\mu$ g/mL) or pooled convalescent-phase serum (PCS) (20  $\mu$ g/mL) at 37°C for 1h, and the SC5b-9 level was measured. B, Purified soluble NS1 from NS1 stably expressing cells (rNS1s) at the given final concentrations, tested for complement activation, as described in panel A. Equivalent concentrations of isotype control antibody and DV antibody—negative serum (DNS) were used as controls. EDTA (10 mmol/L) was added to inhibit complement activation for negative controls. Data are displayed as the mean  $\pm$  SD from 3 independent experiments.

SC5b-9 (figure 3*A*) and was enhanced by NS1-specific MAbs and by purified immunoglobulin fractions from PCS but not by isotype-control antibodies or by purified immunoglobulin from DNS (figure 3*A*). Similar results were obtained with purified recombinant NS1s from transfected cells (figure 3*B*). Fractions from the protein G columns containing little or no NS1 had no complement-consuming activity.

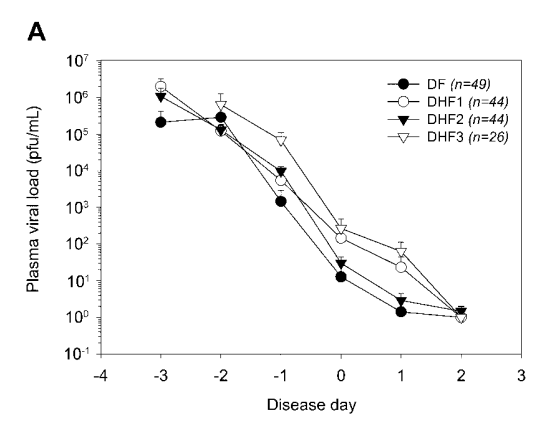
Antibody dependency of complement activation by cell-associated NS1. NS1 was expressed on the surface of DV-infected cells and on NS1m-transfected cells (figure 4A). When DV-infected cells were incubated with 12.5% NHS, no complement activation was observed, as was evident from negative staining for C3dg (data not shown) and C5b-9 (figure 4D) on cell surfaces. However, the presence of purified antibodies

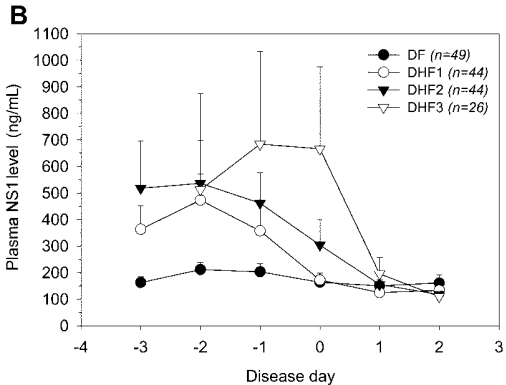
against NS1 triggered complement activation, as evidenced by colocalization of complement C3 and NS1 on the cells (figure 4*B*). Similar results were obtained with purified immunoglobulin from PCS (data not shown). Antibody-dependent complement activation was induced by all 4 clones of NS1-specific MAbs tested but not by isotype control antibodies. Colocalization of NS1 and C3dg was also observed after antibody-dependent complement activation on NS1m-transfected cells (figure 4*C*). Parallel immunofluorescent staining for C5b-9 revealed its deposition on the plasma membrane of DV-infected (figure 4*D*) and transfected (data not shown) cells.

*DV RNA, NS1s, and complement activation products in clinical specimens.* Measurements of DV RNA, NS1s, and SC5b-9 were performed in a blinded manner. Figure 5 displays



**Figure 4.** Activation of complement to completion by membrane-associated NS1 (NS1m) in the presence of NS1-specific antibodies. *A*, Surface expression of dengue virus (DV) NS1 on DV-infected cells and on cells stably expressing NS1. Cells were stained with NS1-specific monoclonal antibody (MAb) 1A4, followed by fluorescein isothiocyanate (FITC)—conjugated anti-mouse immunoglobulin. Histogram plots were determined from data acquired from 5000 events in viable cells. The representative set of histograms is derived from 1 of 3 independent experiments. *B* and *C*, Colocalization of NS1 and complement C3 fragments on the surfaces of complement-attacked cells. DV-infected cells or cells expressing NS1m were incubated with 12.5% normal human serum (NHS) in the presence of a mix of purified NS1-specific MAbs. After 1 h at 37°C, cells were stained with fluorescent-conjugated secondary antibodies and observed by confocal microscopy. NS1 (Cy3; *red*) and complement (FITC; *green*) colocalized on the membranes. *D*, Formation of C5b-9 on cells. Mockor DV-infected cells were incubated with purified antibodies from pooled convalescent-phase serum (PCS) and DV antibody—negative serum (DNS) in the presence of 12.5% NHS. The deposition of membrane attack complexes was detected by flow cytometry after staining with a MAb against C5b-9 and FITC-conjugated secondary antibodies. Analysis was performed on 5000 viable cells. Data are displayed as the mean  $\pm$  SD from 3 independent experiments.





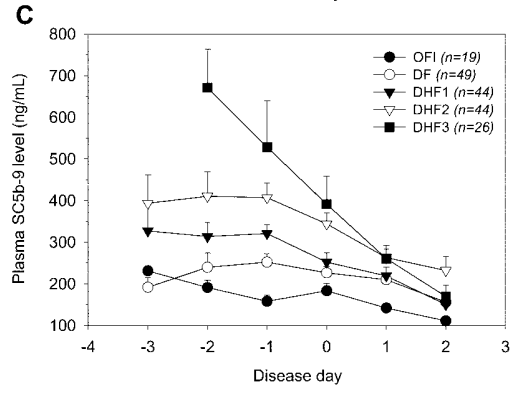


**Figure 5.** Viral loads, NS1 levels, and terminal SC5b-9 complexes in the circulation of patients with dengue fever (DF) and dengue hemorrhagic fever (DHF) and dengue shock syndrome. Plasma samples were assayed for dengue virus (DV) RNA levels by use of quantitative real-time reverse-transcription polymerase chain reaction, and soluble NS1 and SC5b-9 complexes were quantified by ELISA. Disease day 0 was defined as the calendar day during which the temperature fell and stayed below 37.8°C. Plasma samples from patients with acute febrile diseases other than dengue (other febrile illnesses [OFIs]) were also used as controls. Plots show the mean and SE. NS1 levels were not detectable in patients with OFIs.

cross-sectional analysis of the mean and SD of each variable (viral load, NS1 level, and SC5b-9 level) over time, based on all available data. The highest viral loads were detected early during clinical illness in all patients and gradually declined to undetectable levels on day +1 in patients with DF or on day

+2 in patients with DHF (figure 5*A*), in accordance with previous reports [9, 34]. The mean  $\pm$  SD level of NS1s in patients with DHF (383.9  $\pm$  620 ng/mL) was higher than that in patients with DF (181.6  $\pm$  120 ng/mL) during acute illness (figure 5*B*). NS1 was undetectable in patients with OFIs. Similarly, mean  $\pm$  SD plasma SC5b-9 levels were higher in patients with DHF (306.9  $\pm$  174 ng/mL) than in patients with DF (225.3  $\pm$  97 ng/ml) or OFIs (170.3  $\pm$  57 ng/mL) during acute illness (figure 5*C*).

Because of missing viral load, NS1 level, and SC5b-9 level data at some time points, a mixed model of multivariate statistical analysis was applied. Only patients with at least 3 consecutive measurements were included in the analysis. This resulted in 83 patients and 301 observations for viral load, 89 patients and 319 observations for NS1 level, and 85 patients and 312 observations for SC5b-9 level. Figure 6 displays plots of predicted viral load, NS1 level, and SC5b-9 level obtained from the quadratic mixed model against time.

Viral load for patients with DF, DHF1, DHF2, or DHF3 decreased over time (figure 6*A*). There was a statistically significant difference in plasma viral load between patients with DF and some groups of patients with DHF (DF vs. DHF1, P=.0856; DF vs. DHF2, P=.0087; DF vs. DHF3, P=.0599) and between patients with DF and all patients with DHF (P=.0035). However, no difference in viral load was found among the different groups of patients with DHF (DHF1 vs. DHF2, P=.1790; DHF1 vs. DHF3, P=.3577; DHF2 vs. DHF3, P=.4999).

NS1 levels significantly decreased over time in all groups of patients with DHF, whereas, in patients with DF, NS1 levels increased slightly during early acute illness, with a peak at day -1 or 0, and then gradually decreased (figure 6B). However, no statistically significant difference was observed among patients with the 3 types of DHF (DHF1 vs. DHF2, P = .2811; DHF1 vs. DHF3, P = .3158; DHF2 vs. DHF3, P = .9123). The pattern of change in NS1 levels over time in patients with DF was significantly different from that in patients with DHF1 or DHF2 (DF vs. DHF1, P = .0002; DF vs. DHF2, P = .0042) but not patients with DHF3 (P = .0761), which might have been due to the small sample size of this group. When all types of DHF were combined, a highly significant difference was found between patients with DF and patients with DHF (P< .0001). Importantly, levels of NS1 during the febrile phase (days -3 to -1) could be used to differentiate between patients with DF and all groups of patients with DHF (day -3 and -2, P < .0001; day -1, P = .021).

SC5b-9 levels exhibited a similar pattern in patients with DF and patients with DHF, reaching a peak at day -1 and day -2 for those with DF and those with DHF, respectively (figure 5*C*). No complement activation was found in patients with OFIs. Comparisons of SC5b-9 levels between patients with DF and all patients with DHF and between patients with DF and patients with OFIs revealed a statistical difference (P<.0001).

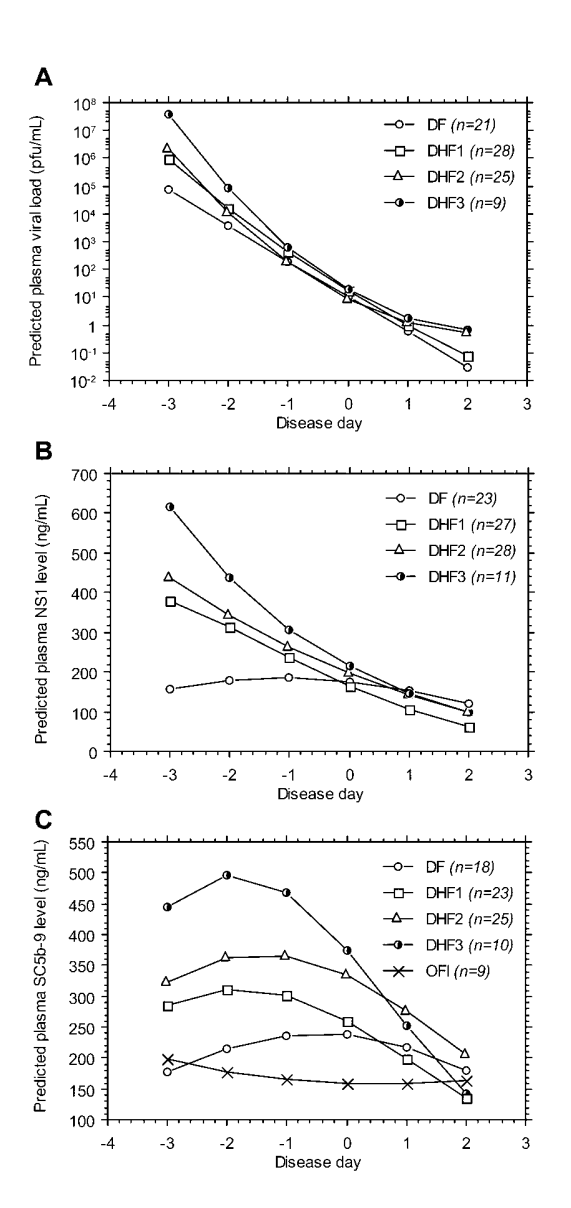


**Figure 6.** Predicted viral loads (A), NS1 levels (B), and SC5b-9 levels (C) from a mixed-model analysis. DF, dengue fever; DHF, dengue hemorrhagic fever; OFI, other febrile illness.

Levels of SC5b-9 observed during acute illness were highly correlated with disease severity—that is, the levels in patients with DHF3 were greater than those in patients with DHF2, and the levels in patients with DHF1 were greater than those in patients with DHF1 (DHF3 vs. DHF2, P=.0052; DHF2 vs. DHF1, P=.0507). Similar to NS1 levels, SC5b-9 levels in the febrile phase of DHF were significantly higher than those in patients with DF (day -3, P=.0001; day -2, P<.0001; day -1, P=.0004). Unlike NS1 levels, SC5b-9 levels could still be used to differentiate between DF and DHF at the day of defervescence (day 0, P=.0183).

*NS1s and complement activation products in pleural fluids from patients with DSS.* NS1, C3a and C5a, and SC5b-9 were

measured in pleural fluids and in plasma from 9 patients with DSS. Samples were collected at the day of shock or 1-2 days later. The results are shown in table 1. Pleural fluid levels of NS1 were similar to (patients 1-3) or higher than (patients 4-6) those in plasma. Pleural fluid levels of SC5b-9 were markedly higher than the plasma levels in all but 1 case. The mean  $\pm$ SD SC5b-9 level in pleural fluids was 2575.9  $\pm$  1121 ng/mL (range, 627-4865 ng/mL; median, 2312.5 ng/mL) and was significantly higher than the mean  $\pm$  SD level in plasma (1546.3 ± 943 ng/mL; range, 394–2935 ng/mL; median, 1722 ng/mL) (P = .04). A similar trend was found for C5a: the mean  $\pm$  SD level of this anaphylatoxin in pleural fluids was  $47.4 \pm 61.1$  ng/ mL (range, 7-227 ng/mL; median, 23 ng/mL) and was also greater than that in plasma (25.6  $\pm$  33.9 ng/mL; range, 5–114 ng/mL; median, 15 ng/mL) (P = .34). Results obtained for C3a were erratic, with no recognizable pattern (data not shown).

When the pleural fluid-to-plasma ratios of NS1, SC5b-9, and C5a levels were plotted against the respective quotients for albumin, almost all plotted values came to lie above the diagonal. This indicated relative accumulation of the analytes, probably as a result of their local generation at the leakage site (figure 7).

#### **DISCUSSION**

Two mutually nonexclusive mechanisms for immunological enhancement of infection have been proposed. The first involves nonneutralizing, cross-reactive antibodies against DV enhancing the uptake of the virus into susceptible cells [5, 6]. The second involves DV-specific CD8 lymphocytes undergoing apoptotic depletion when confronted with cells infected with the heterotypic virus [7]. In both cases, a loss of immunological

Table 1. Measurements of NS1, C5a, SC5b-9, and albumin in EDTA-treated plasma (P) and pleural fluid (PF) from 9 children with dengue shock syndrome.

		S1 /el, /mL	lev	5a /el, /mL	lev	ōb-9 ⁄el, ′mL		umin I, g/L
Patient	Р	PF	Р	PF	Р	PF	Р	PF
1	117	139	10	16	876	1369	13.6	12.9
2	120	122	20	17	2935	3516	26.7	19.5
3	2333	2058	10	21	1801	3353	3.3	2.5
4	116	337	5	7	691	627	9.8	9.6
5	141	3234	15	49	1722	2307	10.3	17.3
6	117	220	28	50	394	2764	29.5	20.6
7	ND	ND	19	14	1838	2270	13.4	3.7
8	ND	ND	9	20	750	1869	1	1.5
9	ND	ND	114	227	2910	4865	1.2	1.2

NOTE. ND, not detectable.

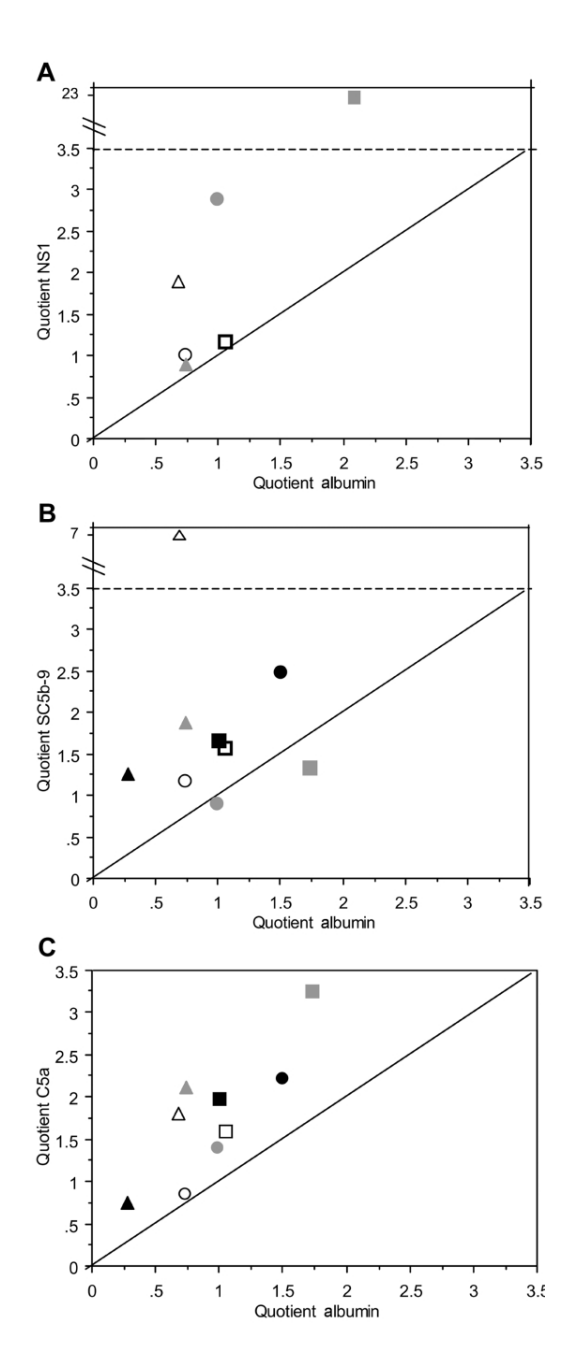


**Figure 7.** Relative accumulation of NS1, SC5b-9, and C5a in pleural fluids. The quotients between pleural fluid and plasma levels of these analytes are plotted against the respective albumin quotients. Each symbol represents 1 patient.

control over viral replication ensues. Indeed, the severity of disease does correlate with viral load [8–10].

However, viral load alone does not explain why vascular leakage should occur. In general, overproduction of cytokines by DV-infected cells or by activated lymphocytes is widely believed to be critical [15, 16], and the possible relevance of complement has received virtually no attention since 1973 [11]. We now propose that NS1, the major nonstructural DV protein,

is an important trigger for complement activation. Expression of NS1 on infected cells may result in binding of heterotypic, nonneutralizing antibodies and complement attack. Furthermore, NS1 released from infected cells can directly activate complement in the fluid phase. NS1-mediated complement activation occurs to completion. Membrane-associated C5b-9 might trigger cellular reactions and the production of inflammatory cytokines [35], and SC5b-9 can independently provoke other local and systemic effects [27, 28, 36–38].

In accordance with results of a recent study in which similar concentrations of NS1 were measured during early illness [10], high levels of NS1 were detected in plasma from patients with DHF/DSS during the febrile phase. A novel finding here was that plasma SC5b-9 levels followed a similar course and appeared to correlate with disease severity. A major challenge for the future will be to identify the major sites of DV infection and to assess the local presence of complement activation products. According to one report, DV antigen is present in alveolar macrophages and endothelial cells of the lung [39], which would fit nicely with our finding that pleural fluids from patients with DSS contain high levels of NS1 and SC5b-9 and that quotients formed between SC5b-9 in pleural fluids versus plasma are higher than the corresponding albumin ratios. It follows that local complement activation likely occurs at these sites, and C5a was indeed detected at high levels in pleural fluids. Although anaphylatoxins bind to cells and are also rapidly inactivated in vivo, the terminal SC5b-9 complex is stable. The half-life in plasma is ~1 h [40, 41], but it is probably considerably longer in closed compartments. SC5b-9 enhances endothelial permeability in vitro and in vivo at a concentration of just a few micrograms per milliliter [27]. These concentrations were reached in the pleural fluids from 8 of the 9 patients in this study.

A unifying concept can thus be formulated to explain the pathogenesis of vascular leakage in DHF/DSS. The antibody response to a primary infection generates nonneutralizing antibodies against heterotypic DVs. Viral replication is augmented because of immunological enhancement during secondary infections. Although it is not excluded that other viral proteins may contribute to complement activation, all of the results of the present study implicate a major role for NS1. The protein is released in copious amounts from infected cells and is probably identical to the soluble viral antigen that was reported in 1970 to bind anti-DV antibodies and activate guinea pig complement [42, 43]. At the same time, antibodies against NS1 direct complement attack to the infected cells, causing generation of membrane-damaging C5b-9 and bystander SC5b-9 complexes. DV infection may also induce the production of inflammatory cytokines, and interleukin-8 and RANTES have been found in high concentrations in pleural fluids from patients with DSS [17]. Complement-activation products and cytokines may synergize locally to incur vascular leakage. Pending availability of bedside assays, it should become possible to establish whether plasma levels of NS1 and/or SC5b-9 can serve as predictive markers, allowing patients at high risk for developing vascular leakage to be identified before the manifestation of the catastrophic events that claim the lives of so many children around the globe.

#### **Acknowledgments**

We thank Ladda Damrikarnlerd and Siraporn Sawasdivorn for managing the dengue clinical database, Kerstin Paprotka for excellent technical assistance, Steffen Schmitt for advice and help in performing anaphylatoxin cytometric bead analysis, and Suchitra Nimmannittya for valuable discussions on the history of dengue research. We also thank Peter J. Lachmann for providing C3dg-specific monoclonal antibodies (clone 9), Ananda Nisalak for pooled convalescent-phase serum and dengue virus antibody–negative serum, and Ronnachai Viriyataveekul for reagents used for CH<sub>50</sub> tests.

#### References

- Nimmannitya S. Clinical spectrum and management of dengue haemorrhagic fever. Southeast Asian J Trop Med Public Health 1987; 18: 392–7.
- Bhamarapravati N, Tuchinda P, Boonyapaknavik V. Pathology of Thailand haemorrhagic fever: a study of 100 autopsy cases. Ann Trop Med Parasitol 1967; 61:500–10.
- Sangkawibha N, Rojanasuphot S, Ahandrik S, et al. Risk factors in dengue shock syndrome: a prospective epidemiologic study in Rayong, Thailand. I. The 1980 outbreak. Am J Epidemiol 1984; 120:653–69.
- Guzman MG, Kouri G, Valdes L, et al. Epidemiologic studies on dengue in Santiago de Cuba, 1997. Am J Epidemiol 2000; 152:793–9.
- Halstead SB, O'Rourke EJ. Dengue viruses and mononuclear phagocytes. I. Infection enhancement by non-neutralizing antibody. J Exp Med 1977; 146:201–17.
- Halstead SB. Pathogenesis of dengue: challenges to molecular biology. Science 1988; 239:476–81.
- Mongkolsapaya J, Dejnirattisai W, Xu XN, et al. Original antigenic sin and apoptosis in the pathogenesis of dengue hemorrhagic fever. Nat Med 2003: 9:921–7.
- Vaughn DW, Green S, Kalayanarooj S, et al. Dengue viremia titer, antibody response pattern, and virus serotype correlate with disease severity. J Infect Dis 2000; 181:2–9.
- Murgue B, Roche C, Chungue E, Deparis X. Prospective study of the duration and magnitude of viraemia in children hospitalised during the 1996–1997 dengue-2 outbreak in French Polynesia. J Med Virol 2000: 60:432–8.
- Libraty DH, Young PR, Pickering D, et al. High circulating levels of the dengue virus nonstructural protein NS1 early in dengue illness correlate with the development of dengue hemorrhagic fever. J Infect Dis 2002; 186:1165–8.
- Bokisch VA, Top FH Jr, Russell PK, Dixon FJ, Muller-Eberhard HJ. The potential pathogenic role of complement in dengue hemorrhagic shock syndrome. N Engl J Med 1973; 289:996–1000.
- Pathogenetic mechanisms in dengue haemorrhagic fever: report of an international collaborative study. Bull World Health Organ 1973; 48: 117–33.
- Malasit P. Complement and dengue haemorrhagic fever/shock syndrome. Southeast Asian J Trop Med Public Health 1987; 18:316–20.
- Bhakdi S, Kazatchkine MD. Pathogenesis of dengue: an alternative hypothesis. Southeast Asian J Trop Med Public Health 1990; 21:652–7.

- Kurane I, Rothman AL, Livingston PG, et al. Immunopathologic mechanisms of dengue hemorrhagic fever and dengue shock syndrome. Arch Virol Suppl 1994; 9:59–64.
- Halstead SB. Antibody, macrophages, dengue virus infection, shock, and hemorrhage: a pathogenetic cascade. Rev Infect Dis 1989; 11(Suppl 4):S830–9.
- Avirutnan P, Malasit P, Seliger B, Bhakdi S, Husmann M. Dengue virus infection of human endothelial cells leads to chemokine production, complement activation, and apoptosis. J Immunol 1998; 161:6338

  –46.
- Winkler G, Maxwell SE, Ruemmler C, Stollar V. Newly synthesized dengue-2 virus nonstructural protein NS1 is a soluble protein but becomes partially hydrophobic and membrane-associated after dimerization. Virology 1989; 171:302–5.
- Flamand M, Megret F, Mathieu M, Lepault J, Rey FA, Deubel V. Dengue virus type 1 nonstructural glycoprotein NS1 is secreted from mammalian cells as a soluble hexamer in a glycosylation-dependent fashion. J Virol 1999; 73:6104–10.
- Schlesinger JJ, Brandriss MW, Walsh EE. Protection of mice against dengue 2 virus encephalitis by immunization with the dengue 2 virus non-structural glycoprotein NS1. J Gen Virol 1987; 68:853–7.
- Henchal EA, Henchal LS, Schlesinger JJ. Synergistic interactions of anti-NS1 monoclonal antibodies protect passively immunized mice from lethal challenge with dengue 2 virus. J Gen Virol 1988; 69:2101–7.
- Falgout B, Bray M, Schlesinger JJ, Lai CJ. Immunization of mice with recombinant vaccinia virus expressing authentic dengue virus nonstructural protein NS1 protects against lethal dengue virus encephalitis. J Virol 1990; 64:4356–63.
- Qu X, Chen W, Maguire T, Austin F. Immunoreactivity and protective effects in mice of a recombinant dengue 2 Tonga virus NS1 protein produced in a baculovirus expression system. J Gen Virol 1993; 74:89–97.
- Young PR, Hilditch PA, Bletchly C, Halloran W. An antigen capture enzyme-linked immunosorbent assay reveals high levels of the dengue virus protein NS1 in the sera of infected patients. J Clin Microbiol 2000; 38:1053–7.
- 25. Alcon S, Talarmin A, Debruyne M, Falconar A, Deubel V, Flamand M. Enzyme-linked immunosorbent assay specific to dengue virus type 1 nonstructural protein NS1 reveals circulation of the antigen in the blood during the acute phase of disease in patients experiencing primary or secondary infections. J Clin Microbiol 2002; 40:376–81.
- Hugli T, Muller-Eberhard HJ. Anaphylatoxins: C3a and C5a. Adv Immunol 1978; 26:1–55.
- Bossi F, Fischetti F, Pellis V, et al. Platelet-activating factor and kinindependent vascular leakage as a novel functional activity of the soluble terminal complement complex. J Immunol 2004; 173:6921–7.
- Ishikawa S, Tsukada H, Bhattacharya J. Soluble complex of complement increases hydraulic conductivity in single microvessels of rat lungs. J Clin Invest 1993; 91:103–9.
- Puttikhunt C, Kasinrerk W, Srisa-ad S, et al. Production of anti-dengue NS1 monoclonal antibodies by DNA immunization. J Virol Methods 2003; 109:55–61.
- Sambrook J, Russell DW. Introducing cloned genes into cultured mammalian cells: calcium-phosphate-mediated transfection of eukaryotic cells with plasmid DNAs. 3th ed. New York: Cold Spring Harbor Laboratory Press, Cold Spring Harbor, 2001.
- Shu PY, Chang SF, Kuo YC, et al. Development of group- and serotypespecific one-step SYBR green I-based real-time reverse transcription-PCR assay for dengue virus. J Clin Microbiol 2003;41:2408–16.
- Yenchitsomanus PT, Sricharoen P, Jaruthasana I, et al. Rapid detection and identification of dengue viruses by polymerase chain reaction (PCR). Southeast Asian J Trop Med Public Health 1996; 27:228–36.
- Dengue haemorrhagic fever: diagnosis, treatment, prevention and control. Geneva: World Health Organization, 1997.
- Sudiro TM, Zivny J, Ishiko H, et al. Analysis of plasma viral RNA levels during acute dengue virus infection using quantitative competitor reverse transcription-polymerase chain reaction. J Med Virol 2001; 63: 29–34.

- Morgan BP. Regulation of the complement membrane attack pathway.
   Crit Rev Immunol 1999; 19:173–98.
- 36. Tedesco F, Pausa M, Nardon E, Introna M, Mantovani A, Dobrina A. The cytolytically inactive terminal complement complex activates endothelial cells to express adhesion molecules and tissue factor procoagulant activity. J Exp Med 1997; 185:1619–27.
- Dobrina A, Pausa M, Fischetti F, et al. Cytolytically inactive terminal complement complex causes transendothelial migration of polymorphonuclear leukocytes in vitro and in vivo. Blood 2002; 99:185–92.
- Casarsa C, De Luigi A, Pausa M, De Simoni MG, Tedesco F. Intracerebroventricular injection of the terminal complement complex causes inflammatory reaction in the rat brain. Eur J Immunol 2003; 33:1260–70.
- 39. Jessie K, Fong MY, Devi S, Lam SK, Wong KT. Localization of dengue

- virus in naturally infected human tissues, by immunohistochemistry and in situ hybridization. J Infect Dis 2004;189:1411–8.
- 40. Hugo F, Berstecher C, Kramer S, Fassbender W, Bhakdi S. In vivo clearance studies of the terminal fluid-phase complement complex in rabbits. Clin Exp Immunol 1989;77:112–6.
- Greenstein JD, Peake PW, Charlesworth JA. The kinetics and distribution of C9 and SC5b-9 in vivo: effects of complement activation. Clin Exp Immunol 1995; 100:40–6.
- 42. Brandt WE, Chiewslip D, Harris DL, Russell PK. Partial purification and characterization of a dengue virus soluble complement-fixing antigen. J Immunol 1970; 105:1565–8.
- McCloud TG, Brandt WE, Russell PK. Molecular size and charge relationships of the soluble complement-fixing antigens of dengue viruses. Virology 1970; 41:569–72.

#### LABORATORY INVESTIGATION

### A Novel H572R Mutation in the Transforming Growth Factor-β-Induced Gene in a Thai Family with Lattice Corneal Dystrophy Type I

La-ongsri Atchaneeyasakul<sup>1\*</sup>, Binoy Appukuttan<sup>2\*</sup>, Sarinee Pingsuthiwong<sup>3</sup>, Pa-thai Yenchitsomanus<sup>4</sup>, Adisak Trinavarat<sup>1</sup>, Chatchawan Srisawat<sup>3</sup>, and The Study Group

<sup>1</sup>Department of Ophthalmology, Siriraj Hospital Mahidol University, Bangkok, Thailand; <sup>2</sup>Casey Eye Institute, Oregon Health & Science University, Portland, Oregon, USA;

#### Abstract

**Purpose:** To describe a large Thai family with lattice corneal dystrophy (LCD) type I and to determine whether this LCD is associated with mutations within the transforming growth factor- $\beta$ -induced (*TGFBI*) gene.

**Methods:** A six-generation family with LCD type I was identified and diagnosed on the basis of clinical and/or histopathologic evaluation. Visual acuity testing and slit-lamp biomicroscopic evaluation were carried out and corneal photography was documented. All 17 exons and flanking intron sequences of the *TGFBI* gene were sequenced.

**Results:** Thirty-three participants demonstrated LCD in both eyes, most of which was symmetrical. Age at onset of decreased vision was the mid- to late twenties. Visual acuity varied from 6/6 to no light perception. Two patients, 74 and 42 years of age, demonstrated a thick yellowish plaque covering the corneal surfaces. DNA sequencing revealed a heterozygous mutation in exon 13 (A1762G), changing histidine to arginine at codon 572 (H572R). Ten of 42 clinically unaffected family members, all under 25 years of age, exhibited the same mutation.

**Conclusions:** This is the first report of a molecular analysis of LCD type I in Thai patients. The novel mutation identified is associated with distinct phenotypes and later onset of the disease compared with the more common R124C mutation. **Jpn J Ophthalmol** 2006;50:403–408 © Japanese Ophthalmological Society 2006

**Key Words:** genotype–phenotype correlation, lattice corneal dystrophy, mutation, transforming growth factor-β-induced gene

#### Introduction

Received: September 26, 2005 / Accepted: May 17, 2006
Correspondence and reprint requests to: La-ongsri Atchaneeyasakul, Department of Ophthalmology, Siriraj Hospital Mahidol University, 2 Prannok Road, Bangkoknoi, Bangkok 10700, Thailand e-mail: atchanee@hotmail.com

\*These authors contributed equally to this work. See Appendix for members of the Study Group

Understanding of the molecular events associated with corneal dystrophies has expanded during the past decade. At least nine genes are associated with corneal dystrophies.<sup>1</sup> Mutations in the transforming growth factor-β-induced (*TGFBI*) gene are responsible for various types of hereditary corneal dystrophies.<sup>2</sup> Lattice corneal dystrophy (LCD) has been reported in different ethnic groups to be associated with mutations in the *TGFBI* gene.<sup>3-10</sup> LCD type I is inherited in an autosomal dominant fashion. Progressive

<sup>&</sup>lt;sup>3</sup>Department of Biochemistry, Siriraj Hospital Mahidol University, Bangkok, Thailand;

<sup>&</sup>lt;sup>4</sup>Department of Research and Development, Siriraj Hospital Mahidol University, Bangkok, Thailand

corneal opacities lead to severe visual loss in the fourth or fifth decade. The most common mutation in the *TGFBI* gene reported in LCD type I is the Arg124Cys mutation. Other uncommon mutations found in families with LCD type I include the Leu518Pro and Leu569Arg mutations.<sup>8,11</sup>

Although the TGFBI protein is implicated as a cell adhesion molecule and may play a role in tissue morphogenesis, the exact function of this protein within the cornea is far from understood. It dentification of new mutations that lead to new or modified phenotypes may enlighten us as to the cellular function of this protein in relation to corneal dystrophies. We report a large Thai family with LCD type I through six generations, four of which are affected with the disease. We identify a novel mutation in the *TGFBI* gene in this family and discuss the phenotypes and distinct age of onset of visual impairment associated with this mutation.

#### **Subjects and Methods**

A Thai family with LCD type I, consisting of more than 150 family members from six generations, was studied. Seventy-five members participated in visual acuity testing, slit-lamp biomicroscopy, and blood collection for DNA analysis. Ocular examination and blood collection were carried out at the village where the family members live. Corneal photography and DNA analysis were conducted at Siriraj Hospital Mahidol University, Bangkok, Thailand. Preliminary DNA analysis was performed at the Casey Eye Institute, Portland, Oregon, USA. Informed consent was signed by all participants prior to the ocular examination and blood collection. The consent for mutation analysis of the *TGFBI* gene was indicated in the informed consent for blood collection.

#### Amplification and Sequencing of Genomic DNA

Genomic DNA was isolated from peripheral blood leukocytes. Individual exons of *TGFBI* were amplified from genomic DNA by polymerase chain reaction (PCR) using primer pairs specific to the flanking intron sequences of the corresponding exons. Most of the primers used in this study were the same as (or slightly modified from) those described previously. The PCR product was purified using QIAquick PCR or Gel Purification Kits (QIAGEN, Hilden, Germany) and subsequently sequenced using a DYEnamic ET Terminator Cycle Sequencing Kit (Amersham, Buckinghamshire, UK) and run on an ABI Prism 3100 automated sequencer (Applied Biosystems, Foster, CA, USA). The sequences were compared to the published sequence of the human *TGFBI* gene (GenBank accession number AY149344).

## Mutation Detection Using Allele-Specific Amplification

The presence of wild-type or novel mutant alleles of *TGFBI* in each individual was detected using allele-specific ampli-

fication (ASA). Two separate PCR reactions were performed using either the wild-type (5'-GGAACTTGC CAACATCCTTAAATACAA-3') or mutant-specific ASA primer (5'-GGAACTTGCCAACATCCTTAAATACAG-3') as forward primers and the same exon 13-specific primer (5'-CTGGGGAAATTTAGCCAGCC-3') as the reverse primer. Each PCR amplification was carried out in a 50-µl reaction using standard conditions. PCR amplification of exon 5 of *TGFBI* was simultaneously performed in each ASA reaction to serve as an internal control; forward primer (5'-TAAACACAGAGTCTGCAGCC-3') and reverse primer (5'-TTCATTATGCACCAAGGGCC-3') were used for amplification.

#### Results

The pedigree, which is typical for autosomal dominant inheritance, is shown in Fig. 1. Of the 75 participants, 50 were women and 25 were men. Thirty-three were clinically

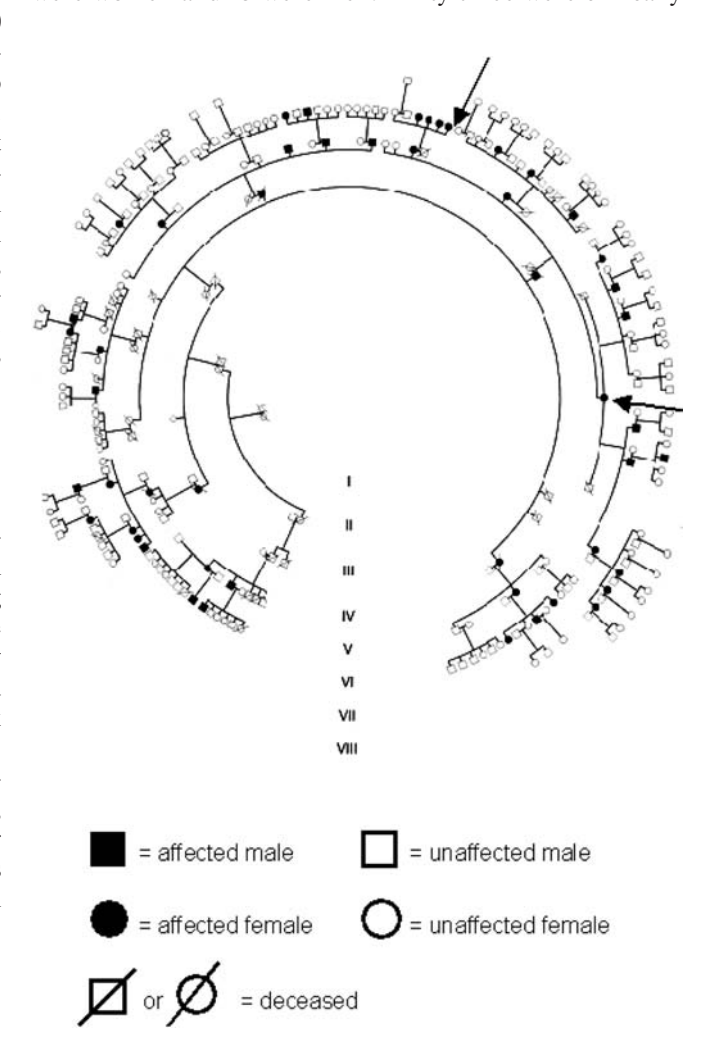
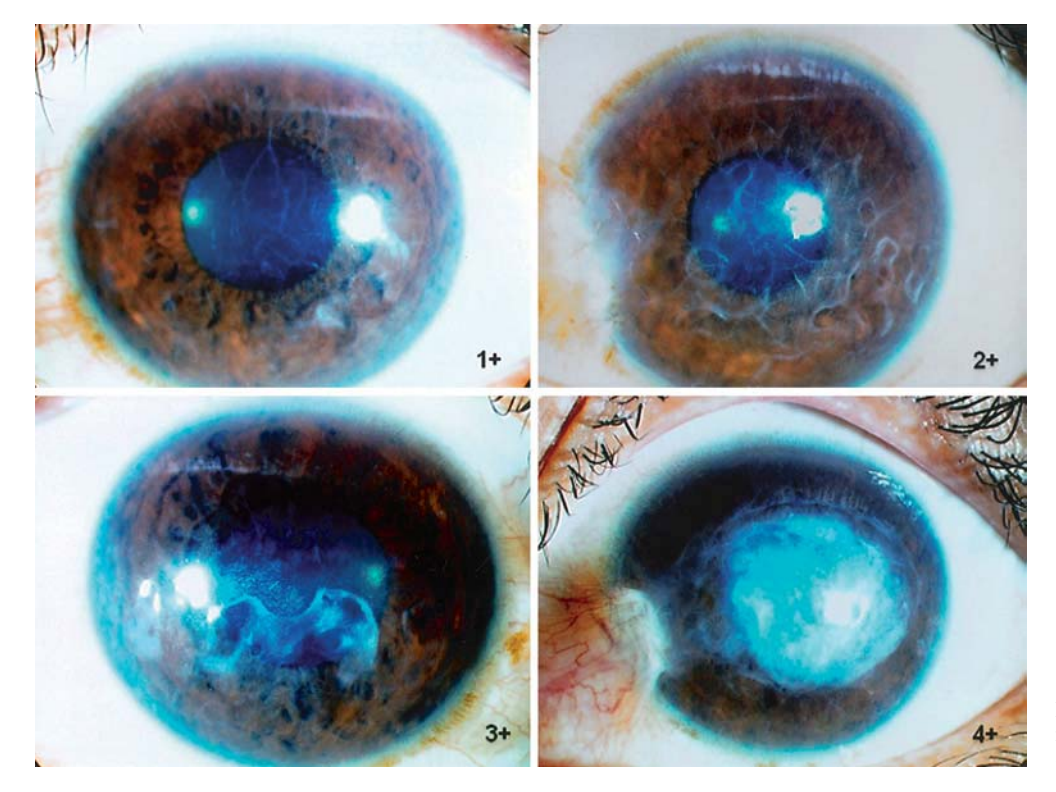


Figure 1. The pedigree of a Thai family with lattice corneal dystrophy type I. *Arrows* indicate the two patients with yellowish corneal plaques. ■ Affected male; □ unaffected male; ○ unaffected female; □ or Ø deceased.



**Figure 2.** Grading of corneal involvement with lattice corneal dystrophy.

affected with LCD, 21 women and 12 men. The average age at examination of the affected participants was  $45.2 \pm 13.8$ years (range, 24–74) with the average age of onset of symptoms  $28.6 \pm 8.1$  years (range, 20–50). The average age of visual impairment was  $37.6 \pm 13.3$  years (range, 24–70), and 84% had a history of recurrent corneal erosion. The severity of corneal involvement was graded from 1+ to 4+ depending on the magnitude of obscuration of the iris detail (Fig. 2). More than half of the clinically affected members had visual acuity in the better eye of less than 20/200. All cases of LCD were bilateral, and systemic involvement was ruled out. The histopathologic results from the corneal buttons obtained from two affected family members revealed amyloid deposits with positive Congo red staining and characteristic apple green birefringence throughout the stroma under polarized light (data not shown). A more detailed pathological and clinical description regarding corneal haziness, surface irregularity, history of recurrent corneal erosion, and quality of life of the clinically affected members is reported elsewhere.13

One affected female patient aged 74 and her niece aged 42 developed thick yellowish corneal plaques covering the central part of the corneas (Fig. 3). These plaques were located in the anterior corneal stroma. The corneal epithelium was intact in both cases. Visual acuity in the 74-year-old patient was no light perception in the right eye and finger counting at 1 foot (about 30 cm) in the left. The corneal plaques were documented in the right eye. In the left eye, the corneal graft from a penetrating keratoplasty performed several years previously appeared cloudy at the

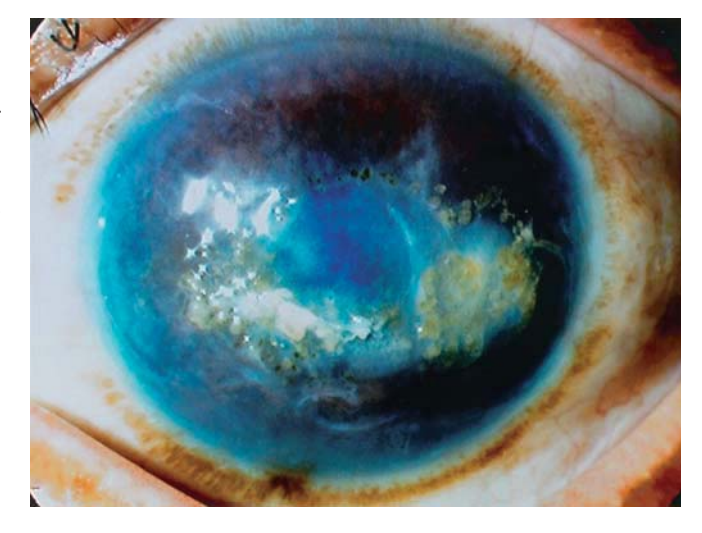


**Figure 3.** Yellowish plaques covering the corneal surface, found in two closely related female patients.

time of examination. For the 42-year-old patient, visual acuity was 20/100 and 20/800 in the right and left eye, respectively. Corneal plaques were seen in the left eye only, whereas the right eye, which had received a corneal transplant, showed cloudiness of the corneal graft. To our knowledge, these yellowish corneal plaques have not been observed in LCD or in any other corneal dystrophy.

#### DNA Analyses

Preliminary DNA analysis of the previously reported mutations of TGFBI gene responsible for LCD revealed none of the following mutations: R124C, P501T, L518P, L527R, N622H, or H626R.<sup>3,7,14,15</sup> Therefore, all 17 exons and the flanking introns were studied using DNA samples from five clinically affected participants, and two unaffected participants aged 41 and 38. The results showed seven nucleotide positions that were different from the wild type (GenBank accession number AY149344). These comprised 698 C/G in exon 6, 1028 A/G in exon 8, 1463 C/T in exon 11, 1667 T/C in exon 12, IVS12 +23 G/A, 1762 A/G in exon 13, and IVS14 +44 T/C. The first four are single base substitutions that do not alter the encoded amino acids of the TGFBI protein, previously reported as polymorphisms. Nucleotide substitutions in IVS12 and IVS14 have also been reported as sequence variations in the TGFBI gene.

A single base transition from A to G at nucleotide position 1762 in exon 13 (A1762G) was found only in clinically affected participants as a heterozygous mutation in the *TGFBI* gene (Fig. 4). This mutation results in a change of

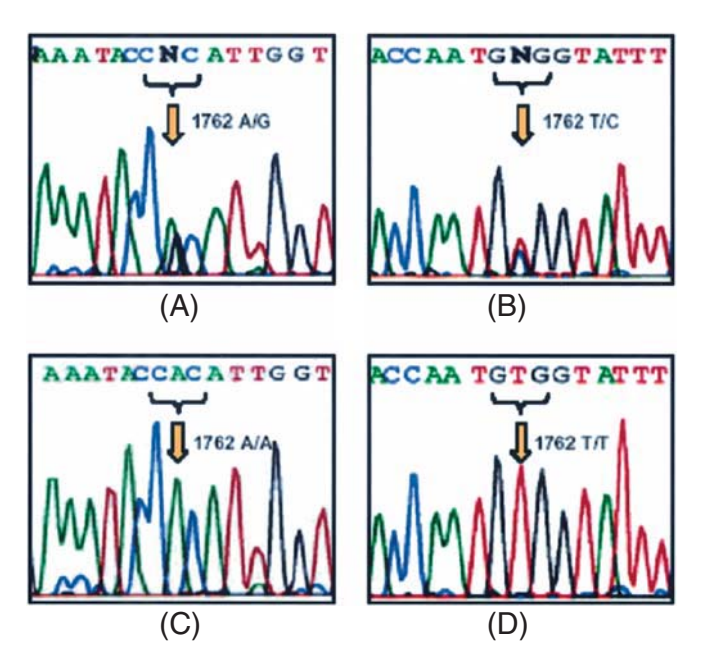


**Figure 4A–D.** Direct sequencing of exon 13 of the *TGFBI* gene. **A** Sense and **B** antisense sequence from a clinically affected participant. **C** Sense and **D** antisense sequence from an unaffected participant.

codon from CAC (histidine) to CGC (arginine) at position 572 (H572R) of the TGFBI protein.

To confirm the mutation, ASA analysis was performed in all participants as well as in 100 unrelated normal volunteers. The H572R mutation was absent in all normal volunteers, whereas all clinically affected participants harbored this heterozygous alteration. Interestingly, 10 of 42 unaffected participants also carried the H572R mutation. All except one of these ten participants were less than 20 years old at the time of the ocular examination. Table 1 summarizes the clinical characteristics and mutations in the *TGFBI* gene reported in LCD type I.

#### Discussion

We present a large Thai family with LCD type I with typical autosomal dominant inheritance. We have identified a novel mutation in exon 13 of the TGFBI gene that results in a substitution of an arginine for a histidine residue at codon 572 and that segregates with the disease phenotype. The majority of the clinically affected participants demonstrated distinct lattice lines in the corneal stroma. Two female patients aged 74 and 42 developed yellowish plaques in the anterior corneal stroma. The manifestation of yellowish plaques has not been reported previously in any type of LCD, or in any other corneal dystrophy. Whether this clinical feature represents a unique finding associated with LCD type I or an accompanying corneal degeneration is unclear at present. Histopathology of the corneal button containing the yellowish plaques may reveal the nature of these deposits. At the time of examination both patients had already had penetrating keratoplasty in one eye; thus, it is uncertain whether the corneal plaques developed bilaterally prior to the surgery. We did not detect the development of corneal plaques on the corneal grafts in either patient. It is interesting that the two patients are closely related (Fig. 1), and it is possible that there may be other genetic or environmental influences that contributed to the development of this particular manifestation.

All clinically affected participants reported significant visual impairment in their 20s or 30s. This study also revealed ten unaffected participants who also carried the disease-causing mutation. These individuals are likely to be presymptomatic cases. Regular follow-up examinations should identify the onset of corneal changes and also help document the disease penetrance. Genetic counseling should be given to the patients and their offspring, which

**Table 1.** TGFBI gene mutations in lattice corneal dystrophy type I and their clinical characteristics

Mutation/exon	Nationality	Age at onset	Corneal erosion	PKP	Reference nos.
Arg124Cys/exon 4	Worldwide	1st Decade	1st decade	Frequently required	2, 5, 6, 10
Leu518Pro/exon 12 Leu569Arg/exon 13	Japan USA	2nd Decade 1st Decade	4th decade 1st decade	Frequently required Frequently required	11 8
His572Arg/exon 13	Thailand	3rd Decade	NA	Frequently required	This report

PKP, penetrating keratoplasty; NA, not available.

will also make possible more precise predictions of the development of the disease in unaffected individuals. The time of onset of visual impairment in this family is different from that reported previously (Table 1). This novel mutation bestows a later onset of LCD type I than previously described mutations. How this H572R mutation results in a later onset of disease is unknown and open to speculation.

TGFBI is a secreted 68-kDa extracellular matrix protein that contains putative integrin-binding motifs and mediates cell adhesion. 16-18 Mutations within the TGFBI gene may disrupt protein folding, protein secretion, or proteinprotein interactions to cause corneal opacity. The histidine at codon 572 is situated within the fourth of four fasciclin-I (FAS1) domains within TGFBI and is invariably conserved in FAS1 domains from various organisms ranging from bacteria to plants to mammals. 16,17 One study suggests that histidine-572, together with tyrosine-571, is essential for αVβ5-integrin binding and mediation of human lung fibroblast cell adhesion in vitro. 17 This evidence suggests that the H572R change may disrupt cell-cell adhesion mediated by αVβ5 integrin within the cornea. However, another study, based on a homology model and X-ray crystallographic mapping, suggests that histidine-572 is totally hidden within hydrophobic residues in the FAS1 motif, and is unlikely to be involved in binding to  $\alpha V\beta 5$  integrin or in any other protein-protein interaction. 16,18 The secondary structure of each FAS1 domain consists of seven β-sheets and five αhelices. Histidine-572 is situated at the start of  $\beta$ 2 and forms hydrogen bonds with the central spine of  $\beta$ 1, which involves a conserved proline (P542) at the end of β1. Owing to the lack of supporting disulfide bonds within the FAS1 domains, it is thought that conserved hydrogen bonds are necessary for proper folding and stability.<sup>18</sup> It is possible that the substitution of the highly conserved histidine for arginine may have a deleterious effect on protein folding, since the more basic and longer side chain of arginine might not be accommodated well within the hydrophobic core of the FAS1 domains. As a result, protein secretion or stability may be disrupted. It would be of interest to analyze the mutant H572R cDNA isolated from affected patients to test within a cell culture system whether this H572R product is secreted or if it is able to bind to integrin.

In conclusion, we have identified a novel mutation in the *TGFBI* gene in a large Thai family with LCD type I. This mutation results in later onset of the disease compared with other mutations. The mutated residue is highly conserved throughout all FAS1 domains. More information on the structure and function of LCD-related mutations in the *TGFBI* gene will provide a basis for future interventions, either prevention or treatment, for LCD patients.

#### **Appendix: Members of the Study Group**

La-ongsri Atchaneeyasakul and Adisak Trinavarat, Department of Ophthalmology, Siriraj Hospital Mahidol University, Bangkok, Thailand; Binoy Appukuttan, Trevor J McFarland, and J. Timothy Stout, Casey Eye Institute, Oregon Health & Science University, Portland, Oregon, USA; Sarinee Pingsuthiwong, Patcharee Wichyanuwat, and Chatchawan Srisawat, Department of Biochemistry, Siriraj Hospital Mahidol University, Bangkok, Thailand; and Pa-thai Yenchitsomanus and Wanna Thongnoppakhun, Department of Research and Development, Siriraj Hospital Mahidol University, Bangkok, Thailand.

Acknowledgments. The study design, data collection, and analysis were supported by a Siriraj Grant for Research Development and Medical Education, the Clayton Foundation for Research, Houston, TX, USA, and Research to Prevent Blindness, New York, NY, USA. The authors thank all the participants for their valuable contributions, Dr. Pinnita Prabhasawat for referring this LCD family to us, and Dr. Mongkol Uiprasertkul for providing the histopathologic findings.

#### References

- Klintworth GK. The molecular genetics of the corneal dystrophies—current status. Front Biosci 2003;8:d687–713.
- Munier FL, Frueh BE, Othenin-Girard P, et al. BIGH3 mutation spectrum in corneal dystrophies. Invest Ophthalmol Vis Sci 2002;43:949–954.
- Stewart H, Black GC, Donnai D, et al. A mutation within exon 14 of the *TGFBI (BIGH3)* gene on chromosome 5q31 causes an asymmetric, late-onset form of lattice corneal dystrophy. Ophthalmology 1999:106:964–970.
- Schmitt-Bernard CF, Guittard C, Arnaud B, et al. BIGH3 exon 14 mutations lead to intermediate type I/IIIA of lattice corneal dystrophies. Invest Ophthalmol Vis Sci 2000;41:1302–1308.
- Mashima Y, Yamamoto S, Inoue Y, et al. Association of autosomal dominantly inherited corneal dystrophies with BIGH3 gene mutations in Japan. Am J Ophthalmol 2000;130:516–517.
- Afshari NA, Mullally JE, Afshari MA, et al. Survey of patients with granular, lattice, avellino, and Reis-Bucklers corneal dystrophies for mutations in the *BIGH3* and *gelsolin* genes. Arch Ophthalmol 2001:119:16–22.
- 7. Chau HM, Ha NT, Cung LX, et al. H626R and R124C mutations of the *TGFBI* (*BIGH3*) gene caused lattice corneal dystrophy in Vietnamese people. Br J Ophthalmol 2003;87:686–689.
- 8. Warren JF, Abbott RL, Yoon MK, Crawford JB, Spencer WH, Margolis TP. A new mutation (Leu569Arg) within exon 13 of the *TGFBI* (*BIGH3*) gene causes lattice corneal dystrophy type I. Am J Ophthalmol 2003;136:872–878.
- Klintworth GK, Bao W, Afshari NA. Two mutations in the TGFBI (BIGH3) gene associated with lattice corneal dystrophy in an extensively studied family. Invest Ophthalmol Vis Sci 2004;45: 1382–1388.
- Chakravarthi SV, Kannabiran C, Sridhar MS, Vemuganti GK. TGFBI gene mutations causing lattice and granular corneal dystrophies in Indian patients. Invest Ophthalmol Vis Sci 2005;46: 121–125
- Endo S, Nguyen TH, Fujiki K, et al. Leu518Pro mutation of the beta ig-h3 gene causes lattice corneal dystrophy type I. Am J Ophthalmol 1999;128:104–106.
- Ferguson JW, Mikesh MF, Wheeler EF, LeBaron RG. Developmental expression patterns of Beta-ig (betaIG-H3) and its function as a cell adhesion protein. Mech Dev 2003;120:851–864.
- Prabhasawat P, Thoongsuwan S, Tesavibul N, Uiprasertkul M, Atchaneeyasakul LO. Corneal lattice dystrophy, a concealed ophthalmic problem in Thailand. J Med Assoc Thai 2003;86:727–736.
- Yamamoto S, Okada M, Tsujikawa M, et al. The spectrum of beta ig-h3 gene mutations in Japanese patients with corneal dystrophy. Cornea 2000;19(3 Suppl):S21–23.
- Fujiki K, Hotta Y, Nakayasu K, et al. Six different mutations of TGFBI (betaig-h3, keratoepithelin) gene found in Japanese corneal dystrophies. Cornea 2000;19:842–845.

- Clout NJ, Hohenester E. A model of FAS1 domain 4 of the corneal protein βig-h3 gives a clearer view on corneal dystrophies. Mol Vis 2003;9:440–448.
- 17. Kim JE, Jeong HW, Nam JO, et al. Identification of motifs in the fasciclin domains of the transforming growth factor-beta-induced
- matrix protein betaig-h3 that interact with the alphavbeta5 integrin. J Biol Chem 2002;277:46159–46165.
- Clout NJ, Tisi D, Hohenester E. Novel fold revealed by the structure of a FAS1 domain pair from the insect cell adhesion molecule fasciclin I. Structure (Camb) 2003;11:197–203.



### Serial Changes in Urinary Proteome Profile of Membranous Nephropathy: Implications for Pathophysiology and Biomarker Discovery

Heidi Hoi-Yee Ngai,<sup>†</sup> Wai-Hung Sit,<sup>†</sup> Ping-Ping Jiang,<sup>†</sup> Ruo-Jun Xu,<sup>†</sup> Jennifer Man-Fan Wan,\*,<sup>\*</sup>,<sup>†</sup> and Visith Thongboonkerd\*,<sup>#</sup>,<sup>‡</sup>

Department of Zoology, The University of Hong Kong, HKSAR, P.R. China, and Medical Molecular Biology Unit, Office for Research and Development, Faculty of Medicine at Siriraj Hospital, Mahidol University, Bangkok, Thailand

#### Received March 28, 2006

Membranous nephropathy is one of the most common causes of primary glomerular diseases worldwide. The present study adopted a gel-based proteomics approach to better understand the pathophysiology and define biomarker candidates of human membranous nephropathy using an animal model of passive Heymann nephritis (PHN). Clinical characteristics of Sprague-Dawley rats injected with rabbit anti-Fx1A antiserum mimicked those of human membranous nephropathy. Serial urine samples were collected at Days 0, 10, 20, 30, 40, and 50 after the injection with anti-Fx1A (number of rats = 6; total number of gels = 36). Urinary proteome profiles were examined using 2D-PAGE and SYPRO Ruby staining. Quantitative intensity analysis and ANOVA with Tukey post-hoc multiple comparisons revealed 37 differentially expressed proteins among 6 different time-points. These altered proteins were successfully identified by MALDI-TOF MS and classified into 6 categories: (i) proteins with decreased urinary excretion during PHN; (ii) proteins with increased urinary excretion during PHN; (iii) proteins with increased urinary excretion during PHN, but which finally returned to basal levels; (iv) proteins with increased urinary excretion during PHN, but which finally declined below basal levels; (v) proteins with undetectable levels in the urine during PHN; and (vi) proteins that were detectable in the urine only during PHN. Most of these altered proteins have functional significance in signaling pathways, glomerular trafficking, and controlling the glomerular permeability. The ones in categories (v) and (vi) may serve as biomarkers for detecting or monitoring membranous nephropathy. After normalization of the data with 24-h urine creatinine excretion, changes in 34 of initially 37 differentially expressed proteins remained statistically significant. These data underscore the significant impact of urinary proteomics in unraveling disease pathophysiology and biomarker discovery.

Keywords: Heymann nephritis • urine • kidney • glomerulus • proteomics • proteome • biomarker • pathophysiology

#### Introduction

Membranous nephropathy, an idiopathic antibody-mediated autoimmune disease, is one of the most common causes of nephrotic syndrome in Caucasian adults. Approximately one-third of affected patients will develop end-stage renal disease (or chronic renal failure) and eventually require renal replacement therapy. Subepithelial immune complexes and complement activation lead to glomerular dysfunction and impairment

of the filtration barrier.<sup>4,5</sup> A primary clinical manifestation is proteinuria, which is nonspecific to membranous nephropathy. At present, there is no reliable noninvasive method for predicting and/or monitoring this glomerular disease. Urine is an ideal source of materials to search for potential disease-related biomarkers as it is produced by the affected tissues and can be obtained easily by noninvasive methods. Therefore, the availability of urinary biomarkers that would provide diagnosis and/or prognosis of membranous nephropathy would be a significant advance. The characterization of urinary proteins may also lead to identification of new therapeutic targets and to better understanding of the disease pathophysiology.

In the present study, we adopted a gel-based proteomics approach to examine the urinary proteome profile in an animal model of human membranous nephropathy. Male Sprague—Dawley (SD) rats were injected with anti-Fx1A to induce passive Heymann nephritis (PHN), of which the characteristics truly

<sup>\*</sup> Equal contributions as co-principal investigators

<sup>\*\*</sup>Correspondence to: Visith Thongboonkerd, MD, FRCPT, Medical Molecular Biology Unit, 12th Fl. Adulyadej Vikrom Bldg., Siriraj Hospital, 2 Prannok Rd., Bangkoknoi, Bangkok 10700, Thailand. Phone: 66-2-4184793; Fax: 66-2-4184793; E-mail: thongboonkerd@dr.com (or) Jennifer M. F. Wan, PhD. Department of Zoology, Kadoorie Biological Sciences Building, The University of Hong Kong, HKSAR, P. R. China. Phone: 852—22990838; Fax: 852—25599114; E-mail: jmfwan@hkusua.hku.hk.

<sup>†</sup> The University of Hong Kong.

<sup>&</sup>lt;sup>‡</sup> Mahidol University.

resemble those of human membranous glomerulopathy. These include subepithelial immune deposits and severe proteinuria without cellular infiltration or inflammatory change in the glomeruli.<sup>1,3</sup> Serial urine samples were collected at baseline (Day 0), 10, 20, 30, 40, and 50 days following the induction of PHN to the animals. Urinary proteins were isolated using a precipitation method and separated with two-dimensional polyacrylamide gel electrophoresis (2D-PAGE). Resolved protein spots were visualized using SYPRO Ruby stain. Quantitative intensity analysis and ANOVA with Tukey post-hoc multiple comparisons were performed to define differentially expressed proteins, which were subsequently identified by matrix-assisted laser desorption/ionization time-of-flight mass spectrometry (MALDI-TOF MS), followed by peptide mass fingerprinting using the NCBI protein database. A total of 37 proteins were identified as differentially expressed proteins. Their functional significance and potential roles in the pathophysiology of membranous nephropathy are discussed. Some proteins, which were undetectable or present only during the disease course, may be of further use as diagnostic or prognostic biomarkers.

#### **Materials and Methods**

**Animals.** Young male Sprague—Dawley (SD) rats (initial body weights = 180-200 g; n=6 for each group; total n=12) were used in this study. Animal care and treatment were conducted according to guidelines of the Department of Health, the Government of Hong Kong, SAR. All animals were housed in a room, in which the temperature was kept constant in a 12-h dark/12-h light cycle with ad libitum standard laboratory rat chow and tap water.

Induction of Passive Heymann Nephritis (PHN) Model. PHN was induced in 6 young male SD rats by intravenous injection of 1 mL rabbit anti-Fx1A antiserum. Fx1A was prepared from freshly isolated kidneys from normal SD rats (weight = 300-350 g) using standard protocol<sup>6</sup> and was utilized to immunize rabbits. Further 6 young male SD rats, with comparable body weights, were used as normal controls and were injected with an equal amount of normal rabbit serum. The efficacy of anti-Fx1A antiserum to induce PHN was tested by measuring urinary protein excretion and by renal histopathological and immunofluorescence examinations.

Renal Histopathological and Immunological Examinations. For light microscopic examination, snap-frozen kidneys of control and PHN rats at 14 days after injection (D14) with normal serum and anti-Fx1A antiserum, respectively, were cut into 5-µm-thick sections and stained with hematoxylin and eosin using a standard technique. For immunofluorescence examination, fresh tissues were embedded in OCT compound (Lab-Tek Products, Miles Laboratories, Naperville, IL) and snapfrozen in liquid nitrogen. Cryostat sections (5  $\mu$ m thick) of D14 control and PHN kidneys were transferred to Superfrost/Plus slides (Fisher Scientific, Pittsburgh, PA). Tissue sections were fixed in acetone at 4 °C for 20 min and blocked with 20% horse serum in PBS for 60 min. Sections were then washed with cold PBS and stained with goat anti-rat IgG (1:200) conjugated with FITC for 1 h. Immunofluorescence was viewed with a confocal laser scanning microscope (Leica DMRBE, Solms, Germany). All images were captured using the Leica DC Viewer Digital Imaging Systems software package, using identical settings for exposure time and gain.

**Urine Collection and Sample Preparation.** The animals were transferred to metabolic cages individually and received free access of water but without food (to prevent contamination

of proteins from food particles into the urine).<sup>7,8</sup> For total protein measurement, 24-h urine samples were collected on Day 0 and on Days 7, 14, 21, 28, 35, and 42 after anti-Fx1A antiserum injection. For proteomic analysis, 4-h urine samples were collected on Days 0, 10, 20, 30, 40, and 50. To minimize protein degradation, the urine samples for proteomic analysis were collected in 1 mL of protease-inhibitors cocktail (0.1 mg/ mL leupeptin, 0.1 mg/mL phenylmethylsulfonyl fluoride, and 1 mM sodium azide in 1 M Tris, pH 6.8) in iceboxes.<sup>7,8</sup> Immediately after collection, the urine samples were centrifuged at  $1000 \times g$  for 5 min. After removal of cell debris and nuclei, proteins in supernatant were precipitated with 20% trichloroacetic acid in acetone containing 20 mM dithiothreitol (DTT) at -20 °C overnight followed by three washes with acetone/20 mM DTT. The pellets were centrifuged at 12 000  $\times$ g for 5 min and resuspended in a buffer containing 7.92 M urea, 0.06% SDS, 120 mM DTT, 3.2% Triton X-100, 22.4 mM Tris-HCl, and 17.6 mM Tris base (pH 8). Protein concentration of each sample was measured by spectrophotometry using Bio-Rad protein microassay based on the method of Bradford.9

**2D-PAGE.** A fixed amount of 200  $\mu$ g of protein was taken from each sample for 2D-PAGE. The protein solution was then mixed with rehydration buffer containing 7 M urea, 2 M thiourea, 2% (w/v) 3-[(3-cholamidopropyl)dimethylamino]-1propanesulfonate (CHAPS), 2% (v/v) ampholytes (pH 3-10), 120 mM DTT, 40 mM Tris-base, and bromophenol blue before loading onto an immobilized pH gradient (IPG) strip (linear pH gradient 3 to 10, 7-cm long; Amersham Biosciences, Uppsala, Sweden).<sup>7,8</sup> The samples were electrofocused to reach 9084 V·hours. After the completion of isoelectric focusing, the IPG strips were incubated in a buffer containing 6 M urea, 50 mM Tris (pH 8.8), 30% v/v glycerol, and 2% SDS with 65 mM DTT for 15 min and subsequently with 260 mM iodoacetamide for another 15 min. The second dimensional separation was performed with 50 mA in 15% acrylamide gel. The resolved 2D spots were visualized with SYPRO Ruby fluorescent dye (Bio-Rad, Hercules, CA) according to the manufacturer's instruction.

Quantitative Intensity Analysis. Image Master 2D Platinum (Amersham Biosciences) software was used for matching and analyzing protein spots on 2-D gels. Parameters used for spot detection were (i) minimal area = 10 pixels; (ii) smooth factor = 2.0; and (iii) saliency = 2.0. A reference gel was created from an artificial gel combining all of the spots presenting in different gels into one image. The reference gel was then used for matching of corresponding protein spots between gels. Background subtraction was performed and the intensity volume of individual spot was normalized with total intensity volume (summation of the intensity volumes obtained from all spots in the same 2-D gel).

Normalization of Intensity Data with 24-h Urine Creatinine. Urine creatinine concentrations of individual samples (from individual animals at each time-point) were measured using a standard spectrophotometric protocol. Briefly, urine samples were added into picric acid and sodium hydroxide containing SDS. Then the samples were allowed to stand at room temperature for 10 min and the absorbance was measured by a UV—visible spectrophotometer at  $\lambda 505$  nm. The 24-h urine creatinine excretion was calculated using the measured creatinine concentrations and 24-h urine volume, and was then used for normalization of the intensity data from individual protein spots.

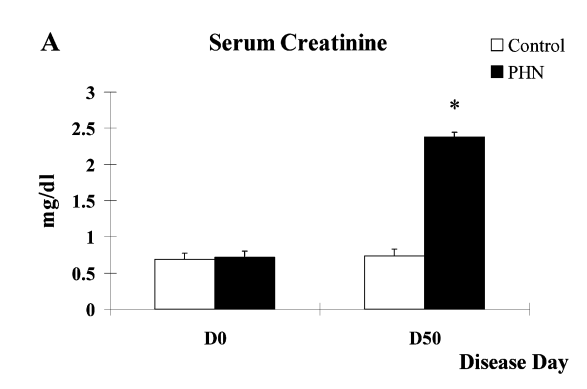
**Statistical Analysis.** ANOVA with Tukey post-hoc multiple comparisons using the SPSS software (version 10.0) were

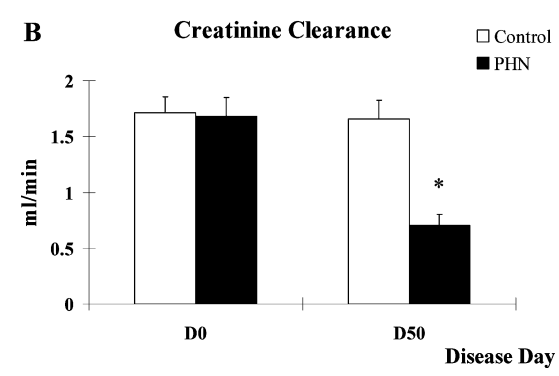
research articles Ngai et al.

Table 1. Total Urine Protein Excretion in Control and PHN Animals

	urine prot	urine protein (mg/24h) <sup>a</sup>					
days	control	PHN					
0	$6.47 \pm 1.11$	$6.29 \pm 0.44$					
7	$7.39 \pm 0.33$	$62.43 \pm 5.55^{b,c}$					
14	$9.72 \pm 0.65$	$142.76 \pm 11.71^{b,c}$					
21	$8.12 \pm 0.88$	$231.62 \pm 25.17^{b,c}$					
28	$9.70 \pm 2.23$	$261.69 \pm 59.19^{b,c}$					
35	$9.23 \pm 1.58$	$293.47 \pm 42.10^{b,c}$					
42	$10.69 \pm 2.10$	$317.09 \pm 32.60^{b,c}$					

 $^a$  Data are expressed as Mean  $\pm$  SEM; n=6 for each groups.  $^b$  p < 0.001 versus controls on the same day.  $^c$  p < 0.001 versus day 0 of the PHN animals.





**Figure 1.** Serum creatinine level and creatinine clearance. (A) Rats had comparable serum creatinine levels at the baseline (D0). At D50, serum creatinine was increased significantly in the PHN rats compared to the controls. (B) Creatinine clearance, which represents renal function, significantly declined in the PHN rats. (n = 6 for each bar). \* = p < 0.001; PHN vs controls.

performed to define significant differences among the different groups (time-points) of samples. P values less than 0.05 were considered statistically significant. A statistical power analysis was further conducted according to the method described by Hunt et al.  $^{10}$  to ensure significant differences of the differentially expressed proteins among different time-points. The computational tool used to calculate such statistical power of significance was adapted from www.emphron.com. Setting of the statistical power was significance level of 5%, effect size of 100% and intensity changes of 2-fold, and the analysis was based on the experimental design of 6 individual rats at 6 different time-points.

MALDI-TOF MS and Peptide Mass Fingerprinting. Differentially expressed protein spots were subjected to identification using a reflectron MALDI-TOF mass spectrometer (Autoflex; Bruker Daltonics, Leipzig, Germany). These spots were excised

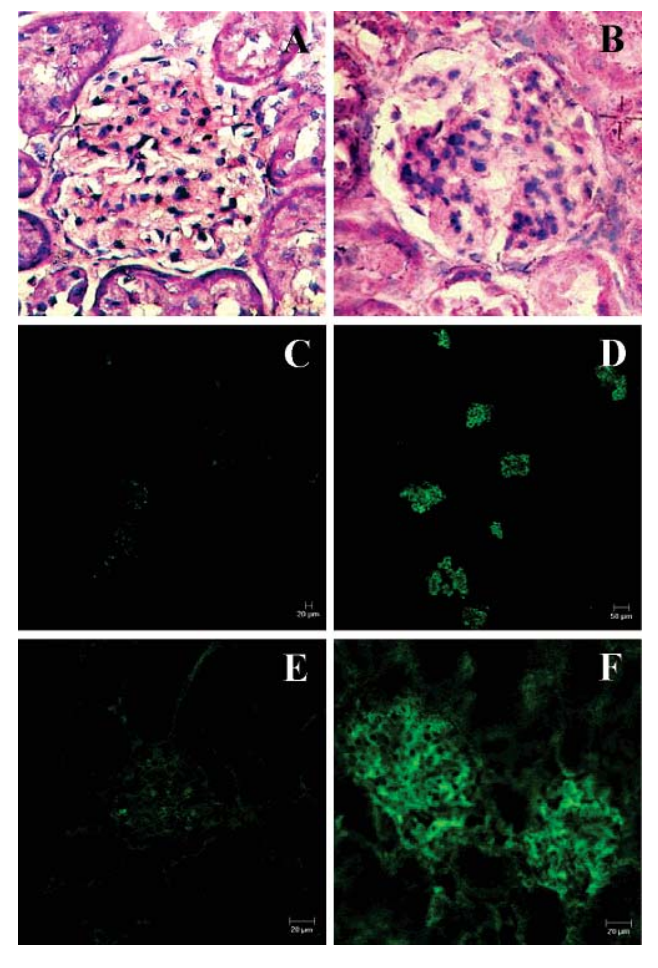
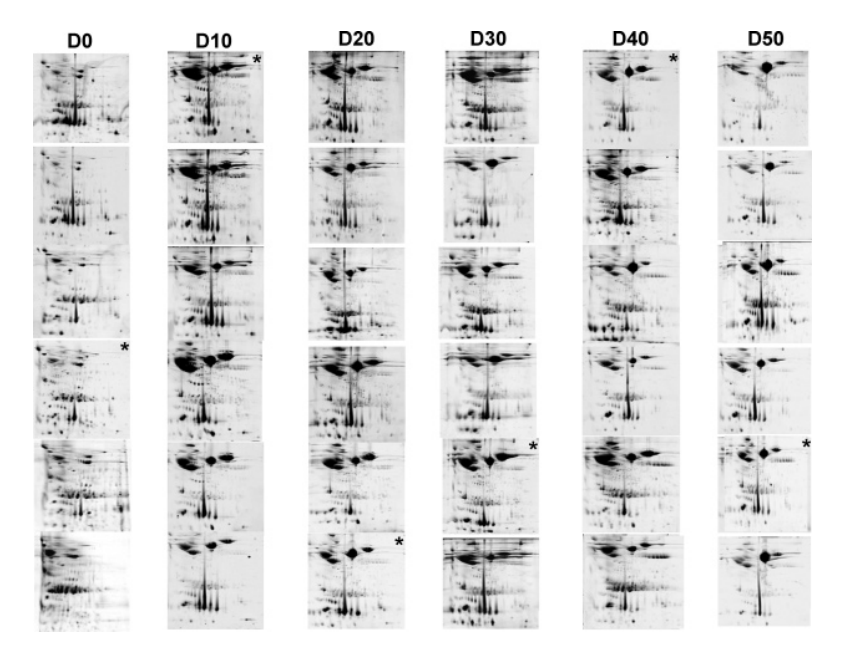


Figure 2. Histopathology and immunofluorescence study. Hematoxylin and eosin staining showed (A) normal glomerular structure of control rats and (B) the glomerulus with mesangial expansion and thickened glomerular basement membranes in PHN rats. Immunofluorescence study revealed tensed granular deposition of  $\lg G$  in the glomeruli of PHN rats (D,F) that is typical for membranous nephropathy, whereas those in control rats had only weak background stain (C,E). Magnification powers were  $400 \times$  for (A), (B), (E), and (F) and  $100 \times$  for (C) and (D).

and digested with trypsin according to the method described by Shevchenko et al.  $^{11}$  The digests were desalted with ZipTip (Millipore, Boston, MA) and further analyzed by MALDI-TOF MS. Peptide mass fingerprinting was performed using Pro-Found search tool, which is available at http://129.85.19.192/ProFound\_bin/WebProFound.exe, as well as MASCOT search engine, which is available at http://www/matrixscience.com, based on the entire NCBI protein database. The search was limited with a mass tolerance of 150 ppm. Only one missed cleavage per peptide was allowed and cysteine residues were assumed to be carbamidomethylated with acrylamide adducts and methionine residues were in oxidized form. Significant matching required Z score of >1.65 or probability-based MOWSE score of >78 (p < 0.05).

#### Results

**24-h Urinary Protein Excretion.** There were no significant differences of 24-h urine volumes between the controls and the PHN rats and among the different days of the disease (data not shown). But the total urine protein excreted over the 24-h



**Figure 3**. Urinary proteome profiles of PHN rats at different time-points of the disease. Urinary proteins were isolated using a precipitation method and resolved with 2D-PAGE using 7-cm-long, linear 3–10 pH gradient, IPG strips and 15% acrylamide gel. Resolved proteins were visualized with SYPRO Ruby stain. N = 6 gels from individual animals in each disease day. D0 = baseline, whereas D10-D50 = Day 10-Day 50. \* = Represented gel series shown in Figure 4.

period in the PHN animals was significantly elevated (p < 0.001) throughout the disease course when compared to the controls at the same time-points and when compared to Day 0 (D0) of the PHN rats (Table 1). At the baseline (D0), rats in both groups (controls and PHN rats) had comparable urinary protein excretion levels (6.47  $\pm$  1.11 and 6.29  $\pm$  0.44 mg/24 h in controls and PHN rats, respectively). After 7 days (D7) of injection with rabbit anti-Fx1A antiserum to the PHN rats and normal rabbit serum to the controls, urinary protein levels of the control rats remained normal, whereas rats that received the anti-Fx1A antiserum developed significant proteinuria (7.39  $\pm$  0.33 vs  $62.43 \pm 5.55 \text{ mg/}24 \text{ h}$ ; controls vs PHN; p < 0.001; averaged PHN/controls ratio = 8.45). The PHN rats had progressive proteinuria throughout the study and urine protein levels at the end of experiment (D50) were 10.69  $\pm$  2.10 mg/24 h in controls and 317.09  $\pm$  32.60 mg/24 h in PHN rats (p < 0.001), and the averaged PHN/controls ratio was 29.65 (Table 1).

Serum Creatinine Level and Creatinine Clearance. Rats in both groups had comparable renal function at the baseline (D0). At D50, serum creatinine was increased significantly in the PHN rats compared to the controls (0.735  $\pm$  0.097 vs 2.378  $\pm$  0.071 mg/dl; controls vs PHN; p < 0.001) (Figure 1A). As a result, the creatinine clearance, which represents renal function, significantly declined in the PHN rats (1.657  $\pm$  0.171 vs 0.703  $\pm$  0.102 mL/min; controls vs PHN; p < 0.001) (Figure 1B).

Histopathological Findings. At D14, the glomeruli of control rats were normal (Figure 2A), whereas those of PHN rats had thickened glomerular basement membranes and increased mesangial matrix, while number of mesangial cells was not increased (Figures 2B). Immunofluorescence study showed extensive granular deposition of IgG in the glomeruli of PHN rats that is typical for membranous nephropathy<sup>4</sup> (Figure 2D,F).

Serial Changes of the Urinary Proteome Profile and Identification of Differentially Expressed Proteins. Serial collection of urine samples from 6 PHN rats was performed at D0, D10, D20, D30, D40, and D50 (days after the injection of

anti-Fx1A antiserum) (total number of samples was 36). The contamination of proteins from food particles that might occur and interfere with the analysis was avoided by housing the rats in metabolic cages with free access of water but without food for 4 h.7,8 The volume of urine collected from each animal over the 4-h period was comparable among different time-points  $(2.63 \pm 0.31,\, 4.28 \pm 0.82,\, 4.40 \pm 0.87,\, 4.60 \pm 0.89,\, 3.58 \pm 0.33$ and  $3.82 \pm 0.45$  mL for D0, D10, D20, D30, D40, and D50, respectively, p = 0.340 by ANOVA). Cell, debris, and other particulate matters were discarded from the urine immediately after the collection. Urinary proteins were then concentrated from all these samples using a precipitation method. For qualitative analysis of the proteome profile and for quantitative intensity analysis to compare relative amounts of individual proteins among different time-points of the disease, the equal amount of total protein (200 µg) isolated from each urine sample was used for such comparisons. The isolated proteins were resolved with 2D-PAGE and visualized with SYPRO Ruby fluorescence dye. Figure 3 shows all 2D gels of individual urine samples (n = 36). A clear difference among groups (timepoints) of samples can be observed.

Quantitative intensity analysis using a 2D analysis software (Image Master 2D Platinum; Amersham Bioscience) and ANO-VA with Tukey post-hoc multiple comparisons revealed differential expression of 37 proteins among groups (time-points) (labeled in Figure 4). Power calculation revealed that the statistical power of the study is greater than 80% with the significance level of 5% and intensity changes of 2-fold. The differentially expressed proteins were then identified by MALDI-TOF MS (Table 2). Their expected pI, molecular size, sequence coverage (%Cov), Z score, probability-based MOWSE score, and quantitative intensity data are shown in Table 3. These proteins can be divided into 6 main categories: (i) proteins with decreased urinary excretion during PHN; (iii) proteins with increased urinary excretion during PHN; (iii) proteins with increased urinary excretion during PHN, but which finally

research articles Ngai et al.

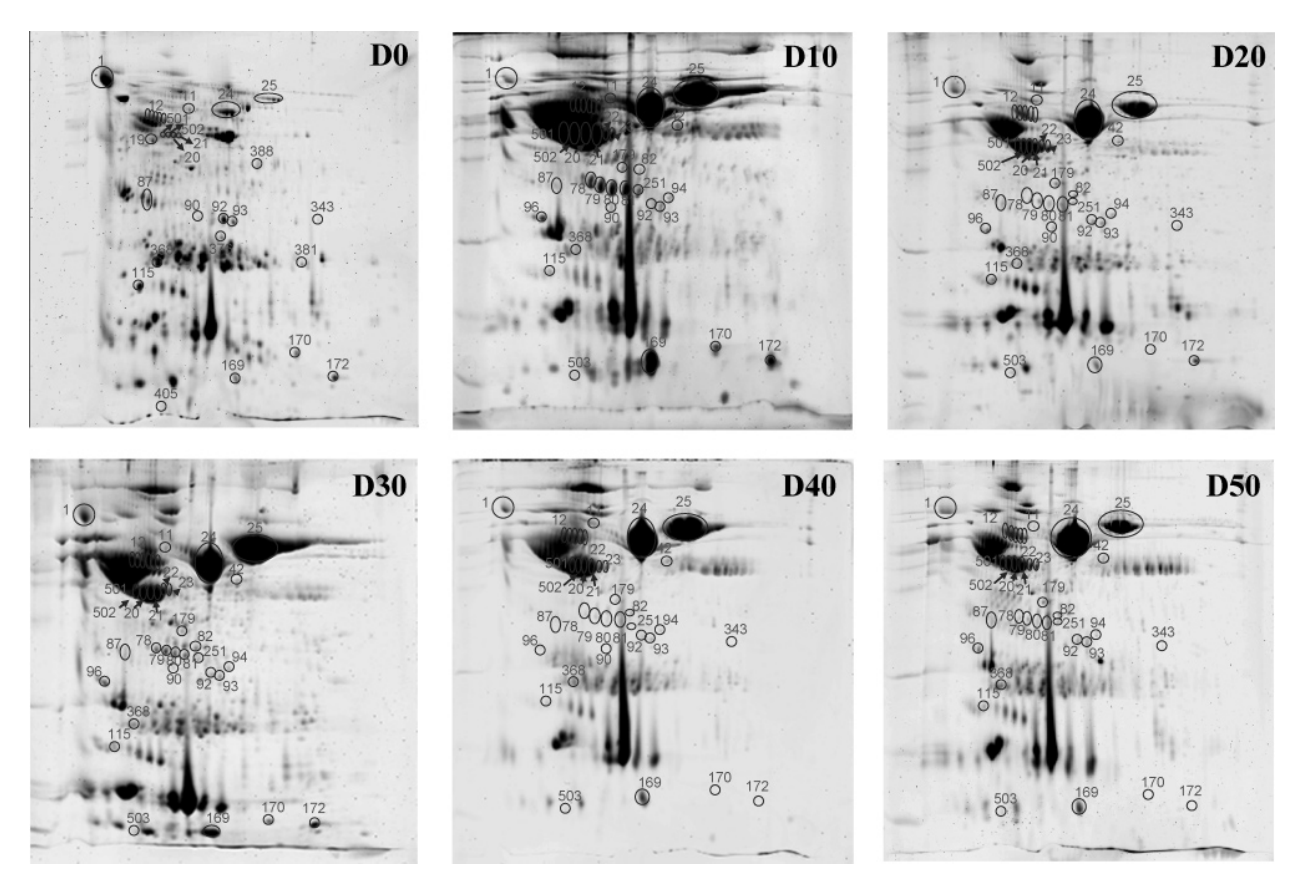


**Figure 4.** 2D map of differentially expressed proteins. Quantitative intensity analysis using Image Master 2D Platinum software (Amersham Bioscience) and ANOVA with Tukey post-hoc multiple comparisons revealed 37 differentially expressed proteins. All of these altered proteins were identified by MALDI-TOF MS and are labeled with numbers correspond to those in Tables 1 and 2. (p < 0.05, power > 80%)

returned to basal levels; (iv) proteins with increased urinary excretion during PHN, but which finally declined below basal levels; (v) proteins with undetectable levels in the urine during PHN; and (vi) proteins that were detectable in the urine only during PHN. Of all these differentially expressed proteins, the ones in categories (v) and (vi) may serve as biomarkers for detecting or monitoring membranous nephropathy.

Normalization of the Intensity Data with 24-h Urine Creatinine. To strengthen and standardize our data, we also normalized the intensity data with 24-h urine creatinine excretion. Table 4 shows the normalized quantitative data (x 10<sup>-3</sup> arbitrary units per mg creatinine per 24 h). After normalization, changes in 34 of initially 37 differentially expressed proteins remained statistically significant by ANOVA and Tukey post-hoc multiple comparisons with the same pattern of changes as mentioned in Tables 2 and 3. The normalized data of the other 3 spots (#11, #20, and #251), although did not reach the statistically significant threshold, tended to be altered during different time-points. These consistent results strengthened our quantitative data.

#### **Discussion**

The diagnosis and treatment of glomerular diseases are presently based primarily on clinical manifestations, urinary protein excretion levels, and renal histopathology. <sup>12</sup> Inevitably, urinary protein excretion levels are not able to differentiate types of glomerular diseases. Renal biopsy, though providing specific diagnosis, is an invasive procedure with considerably

significant complications, particularly in patients with bleeding tendency or skin infection on the flank. Thus, a renal biopsy may not be possible or contraindicated in certain high-risk patients. Serial renal biopsies, which can be used to monitor the outcome of treatment with immunosuppressant regimen, are frequently avoided because of the risk for serious complications. As the excretion levels of albumin and total protein can be affected by several factors (e.g., glomerular function, glomerular filtration rate, renal plasma flow, urine output, etc.), evaluation only for total protein or albumin excretion levels may be insufficient to monitor the therapeutic response or disease activity.<sup>13</sup> Defining a novel biomarker in the urine for each specific type of glomerular disease is therefore required and such biomarkers can serve as a noninvasive test for more effective prediction of the disease, earlier diagnosis, and better monitoring of the disease activity.

In the present study, we employed the passive Heymann nephritis (PHN) rat model to evaluate whether there is a set of urinary proteins that can be used as novel biomarkers for human membranous nephropathy. Clinical characteristics of the PHN rats mimicked those in human membranous nephropathy. These included progressive proteinuria, declined renal function, mesangial expansion, thickened glomerular basement membrane, and granular deposition of IgG. The urinary protein and creatinine clearance data presented herein are consistent with those reported in previous study that rats with PHN produce significant proteinuria and have impaired renal function. Hence, this animal model is suitable for such

Table 2. Differentially Expressed Proteins among Different Time-Points

	altered proteins	GenInfo ID	accession
I. Protei	ins with decreased excretion levels in the urine during PHN		
#1	epithelial-cadherin precursor (E-cadherin) (Uvomorulin) (Cadherin-1)	gi 13431333	O9R0T4
#87	phosphatase subunit gene g4–1 [Mus musculus]	gi 19354389	AAH24754
#90	tropomyosin beta chain (Tropomyosin 2) (Beta-tropomyosin)	gi 20178269	P58775
#92	kallikrein 7; kallikrein 1 [Rattus norvegicus]	gi 6981132	NP_036725
#93	kallikrein 7; kallikrein 1 [Rattus norvegicus]	gi 6981132	NP_036725
#115	alpha-2u globulin	gi 204264	AAA41199
#343	aldehyde dehydrogenase family 1, subfamily A1 [Mus musculus]	gi 32484332	AAH54386
#368	Mpp7 protein [Mus musculus]	gi 29437038	AAH49662
	eins with increased excretion levels in the urine during PHN	81/20101000	71111110002
#12	mKIAA1601 protein [Mus musculus]	gi 37360470	BAC98213.1
#20	alpha-1-antitrypsin; serine (or cysteine) proteinase inhibitor clade A	gi 51036655	NP_071964
1120	(alpha-1 antiproteinase antitrypsin) member 1 [Rattus norvegicus]	g1 31030033	141_071304
#21	alpha-1-antitrypsin; serine (or cysteine) proteinase inhibitor clade A	gi 51036655	NP_071964
#41		g1 31030033	NF_071304
//O.4	(alpha-1 antiproteinase antitrypsin) member 1 [Rattus norvegicus]	1110500	Doorgo
#24	serum albumin precursor	gi 113580	P02770
#25	serotransferrin precursor (Transferrin) (Siderophilin) (Beta-1-metal binding globulin)	gi 6175089	P12346
#501	1-phosphatidylinositol-4,5-bisphosphate phosphodiesterase delta 1	gi 130228	P10688
	(Phosphoinositide phospholipase C) (PLC-delta-1) (PLC-III)		
#502	glycerol-3-phosphate dehydrogenase, mitochondrial precursor (GPD-M) (GPDH-M)	gi 2494650	Q64521
	eins with increased excretion levels in the urine during PHN, but which finally returned to b		
#11	embryonic growth-associated protein EGAP [Mus musculus]	gi 21539896	AAM52342
#169	chain D, Rat Transthyretin	gi 3212535	1GKE
	eins with increased excretion levels in the urine during PHN, but which finally declined belo		
#170	pancreatitis associated protein III [Rattus norvegicus]	gi 463280	AAA41809
#172	pancreatitis associated protein III [Rattus norvegicus]	gi 463280	AAA41809
	eins with undetectable excretion in the urine during PHN		
#19	progesterone-induced blocking factor 1 isoform a [Mus musculus]	gi 46852193	NP_083596
#376	unnamed protein product [Mus musculus]	gi 26353410	BAC40335
#381	ribosomal protein L5 [Rattus norvegicus]	gi 38014831	AAH60561
#388	vimentin [Rattus norvegicus]	gi 38197662	AAH61847
#405	similar to tropomyosin isoform 6 [Mus musculus]	gi 38083544	XP_355057
VI. Prot	eins that were detectable in the urine only during PHN		
#22	alpha-1-antitrypsin precursor	gi 203063	AAA40788
#23	alpha-1-antiproteinase precursor (Alpha-1-antitrypsin) (Alpha-1-proteinase inhibitor)	gi 112889	P17475
#42	serotransferrin precursor (Transferrin) (Siderophilin) (Beta-1-metal binding globulin)	gi 6175089	P12346
#78	bal-647 [Rattus norvegicus]	gi 33086640	AAP92632
#79	haptoglobin precursor	gi 123513	P06866
#80	bal –647 [Rattus norvegicus]	gi 33086640	AAP92632
#81	bal – 647 [Rattus norvegicus]	gi 33086640	AAP92632
#82	serum albumin precursor	gi 113580	P02770
#94	CTP:phosphocholine cytidylyltransferase	gi 455294	AAA53526
#96	similar to anti-idiotype immunoglobulin M light chain [Rattus norvegicus]	gi 34869770	XP_213585
#179	serum albumin precursor	gi 113580	P02770
#251	preprohaptoglobin	gi 204657	AAA41349
	vascular endothelial growth factor A splice variant VEGF 102 [Mus musculus]	gi 32699992	AAP86647

purpose. Moreover, the extensive study of urinary proteins in this animal model may also lead to better understanding of the disease pathophysiology in human membranous nephropathy.<sup>14</sup>

Gel-based proteomic methodology was applied to examine serial changes in the urinary proteome profile of PHN rats. To our knowledge, this is the first study that evaluates the urinary proteome at several different time-points, which directly refer to the disease course. The information obtained is more dynamic than studying only at a single time-point. We thus believe that this approach is most suitable for identifying biomarkers for disease monitoring. Using quantitative intensity analysis and appropriate statistical tests for multiple comparisons, a total of 37 protein spots were defined as differentially expressed proteins among groups, either normal (at the baseline or D0) vs disease (D10 to D50), or among the disease at differential stages (D10 to D50). These differentially expressed proteins were then successfully identified by MALDI-TOF MS and peptide mass fingerprinting. They could be classified into several categories; a part of them may be helpful for better understanding of the pathogenic mechanisms or pathophysiology of membranous nephropathy, whereas some of them may potentially serve as biomarker candidates. Functional significance as well as potential roles of some of these altered proteins in human membranous nephropathy is highlighted as follows.

A. Potential Biomarkers for Membranous Nephropathy. Theoretically, suitable protein biomarkers should be the ones whose expression levels are detectable only in the disease of interest or, vice versa, the ones whose expression was absent or undetectable in the disease. The findings in our present study showed that several proteins could potentially be useful as novel biomarkers for the early diagnosis of human membranous nephropathy. These include the proteins whose excretion was absent or undetectable during PHN (i.e., progesteroneinduced blocking factor 1 isoform a, unnamed protein product, ribosomal protein L5, vimentin, and tropomyosin isoform 6), and those whose excretion levels were detectable only during PHN (i.e., alpha-1-antitrypsin, serotransferrin precursor, Ba1-647, haptoglobulin precursor, preprohaptoglobin, serum albumin precursor, CTP:phosphocholine cytidylyltransferase, similar to anti-idiotype immunoglobulin M light chain, and vascular research articles Ngai et al.

Table 3. Quantitative Data and Peptide Mass Fingerprint Scores<sup>a</sup>

spot	%			Z			intens	sity levels (mean	± SEM; arbitrary	units)	
no.	Cov	$\mathrm{p} I$	mw	score	MOWSE	D0	D10	D20	D30	D40	D50
							Group	I			
#1	14	4.7	99.21	2.33	44	$2.556 \pm 0.318$	$0.457 \pm 0.135$	$0.723 \pm 0.234$	$1.134 \pm 0.314$	$0.960 \pm 0.174$	$0.545 \pm 0.129$
#87	26	5.1	53.62	2.43	$N/A^b$	$0.349 \pm 0.051$	$0.044 \pm 0.017$	$0.098 \pm 0.021$	$0.127 \pm 0.050$	$0.094 \pm 0.019$	$0.067 \pm 0.014$
#90	61	4.7	32.93	2.43	45	$0.161 \pm 0.074$	$0.041 \pm 0.013$	$0.033 \pm 0.011$	$0.020 \pm 0.008$	$0.007 \pm 0.003$	$0.000 \pm 0.000$
#92	29	5.6	29.52	2.21	60	$0.416\pm0.061$	$0.046\pm0.006$	$0.068\pm0.010$	$0.053 \pm 0.009$	$0.055 \pm 0.011$	$0.078 \pm 0.016$
#93	29	5.6	29.52	1.28	42	$0.212 \pm 0.037$	$0.057 \pm 0.006$	$0.081 \pm 0.008$	$0.057 \pm 0.007$	$0.048 \pm 0.011$	$0.079 \pm 0.019$
#115	62	5.4	17.34	2.38	92	$0.802 \pm 0.199$	$0.136 \pm 0.046$	$0.075 \pm 0.019$	$0.134 \pm 0.026$	$0.083 \pm 0.013$	$0.083 \pm 0.023$
#343	39	8.3	55.08	2.43	46	$0.119 \pm 0.040$	$0.000 \pm 0.000$	$0.048 \pm 0.012$	$0.000 \pm 0.000$	$0.032 \pm 0.021$	$0.011 \pm 0.011$
#368	57	6.6	40.70	2.43	66	$1.856 \pm 0.441$	$0.087 \pm 0.015$	$0.162 \pm 0.045$	$0.091 \pm 0.020$	$0.258 \pm 0.058$	$0.079 \pm 0.017$
							Group 1	II			
#12	42	5.3	98.93	2.09	$N/A^b$	$0.283 \pm 0.047$	$2.343 \pm 0.341$	$2.844 \pm 0.436$	$1.311 \pm 0.237$	$2.955 \pm 0.465$	$1.919 \pm 0.229$
#20	25	5.7	46.28	1.85	68	$0.268 \pm 0.017$	$1.970 \pm 0.516$	$1.380 \pm 0.151$	$1.467 \pm 0.181$	$1.733 \pm 0.292$	$1.788 \pm 0.327$
#21	25	5.7	46.28	2.17	74	$0.180 \pm 0.023$	$1.432 \pm 0.302$	$1.135 \pm 0.151$	$0.781 \pm 0.102$	$1.013 \pm 0.159$	$1.002 \pm 0.220$
#24	34	6.1	70.70	2.42	164	$2.648 \pm 0.503$	$9.361 \pm 1.080$	$13.249 \pm 1.522$	$14.071 \pm 2.801$	$14.655 \pm 1.627$	$28.160 \pm 4.279$
#25	51	7.0	78.57	2.43	132	$1.373 \pm 0.174$	$10.176 \pm 0.879$	$9.830 \pm 1.397$	$11.225 \pm 1.604$	$10.955 \pm 1.602$	$6.828 \pm 0.580$
#501	19	5.9	86.80	2.43	37	$0.112 \pm 0.011$	$1.292 \pm 0.239$	$0.969 \pm 0.087$	$1.127 \pm 0.104$	$1.037 \pm 0.254$	$1.005 \pm 0.154$
#502	53	6.2	81.40	2.43	$N/A^b$	$0.201 \pm 0.037$	$1.179 \pm 0.441$	$1.567 \pm 0.192$	$1.571 \pm 0.080$	$1.500 \pm 0.317$	$1.447 \pm 0.220$
// 1	- 4	0.0	0400	0.40	40	0.015 ( 0.010	Group I		0.004   0.014	0.004   0.010	0.010   0.004
#11	54	6.9	84.36	2.43	40	0.017 ( 0.012	$0.064 \pm 0.011$	$0.076 \pm 0.010$	$0.034 \pm 0.014$	$0.024 \pm 0.013$	$0.012 \pm 0.004$
#169	73	6.0	13.11	2.43	97	$0.258 \pm 0.047$	$1.735 \pm 0.424$	$0.838 \pm 0.314$	$1.100 \pm 0.327$	$0.728 \pm 0.137$	$0.247 \pm 0.059$
<b>#150</b>	50	0.0	10.45	0.00	0.4	0.100   0.000	Group I		0.004   0.004	0.005   0.011	0.001   0.010
#170	50	8.0	19.47	2.30	64	$0.132 \pm 0.038$	$0.187 \pm 0.064$	$0.094 \pm 0.015$	$0.064 \pm 0.024$	$0.035 \pm 0.011$	$0.021 \pm 0.016$
#172	54	8.0	19.47	2.35	75	$0.796 \pm 0.366$	$0.803 \pm 0.222$	$0.303 \pm 0.053$	$0.212 \pm 0.051$	$0.114 \pm 0.051$	$0.027 \pm 0.016$
#10	4 =	<b>F</b> 0	00.00	2.17	56	0.004   0.072	Group		0.000   0.000	0.000   0.000	0.000   0.000
#19	45	5.9	90.00	2.17	$N/A^b$	$0.264 \pm 0.073$	$0.000 \pm 0.000$				
#376	21 17	5.6	40.02	2.43 2.43	$N/A^b$	$0.176 \pm 0.056$	$0.000 \pm 0.000$				
#381 #388	44	9.9 5.1	34.67 53.77	2.43	53	$0.083 \pm 0.025$ $0.224 \pm 0.062$	$0.000 \pm 0.000$ $0.000 \pm 0.000$				
#405	62	4.6	14.07	1.82	$N/A^b$	$0.224 \pm 0.062$ $0.207 \pm 0.075$	$0.000 \pm 0.000$ $0.000 \pm 0.000$				
π403	02	4.0	14.07	1.02	IV/A	0.207 ± 0.073	Group \		0.000 ± 0.000	0.000 ± 0.000	0.000 ± 0.000
#22	36	5.7	45.99	2.43	$N/A^b$	$0.000 \pm 0.000$	$0.429 \pm 0.031$	$0.311 \pm 0.038$	$0.303 \pm 0.031$	$0.308 \pm 0.062$	$0.229 \pm 0.029$
#23	35	5.7	46.29	2.43	$N/A^b$	$0.000 \pm 0.000$ $0.000 \pm 0.000$	$0.350 \pm 0.055$	$0.311 \pm 0.036$ $0.259 \pm 0.037$	$0.303 \pm 0.031$ $0.201 \pm 0.034$	$0.306 \pm 0.002$ $0.176 \pm 0.029$	$0.229 \pm 0.029$ $0.142 \pm 0.014$
#42	29	7.0	78.57	2.43	48	$0.000 \pm 0.000$ $0.000 \pm 0.000$	$0.051 \pm 0.007$	$0.259 \pm 0.007$ $0.059 \pm 0.007$	$0.201 \pm 0.004$ $0.040 \pm 0.005$	$0.170 \pm 0.029$ $0.047 \pm 0.010$	$0.142 \pm 0.014$ $0.016 \pm 0.004$
#78	26	6.1	43.08	2.40	76	$0.000 \pm 0.000$ $0.000 \pm 0.000$	$0.031 \pm 0.007$ $0.180 \pm 0.066$	$0.039 \pm 0.007$ $0.046 \pm 0.008$	$0.040 \pm 0.003$ $0.061 \pm 0.024$	$0.047 \pm 0.010$ $0.038 \pm 0.010$	$0.010 \pm 0.004$ $0.009 \pm 0.007$
#79	22	6.1	39.04	2.30	89	$0.000 \pm 0.000$ $0.000 \pm 0.000$	$0.100 \pm 0.000$ $0.281 \pm 0.084$	$0.040 \pm 0.000$ $0.080 \pm 0.011$	$0.001 \pm 0.024$ $0.094 \pm 0.037$	$0.050 \pm 0.010$ $0.057 \pm 0.012$	$0.003 \pm 0.007$ $0.017 \pm 0.011$
#80	22	6.1	43.08	2.35	54	$0.000 \pm 0.000$ $0.000 \pm 0.000$	$0.304 \pm 0.100$	$0.092 \pm 0.011$	$0.094 \pm 0.037$ $0.098 \pm 0.035$	$0.037 \pm 0.012$ $0.043 \pm 0.012$	$0.017 \pm 0.011$ $0.011 \pm 0.008$
#81	23	6.1	43.08	2.40	81	$0.000 \pm 0.000$ $0.000 \pm 0.000$	$0.504 \pm 0.100$ $0.527 \pm 0.132$	$0.309 \pm 0.051$	$0.149 \pm 0.070$	$0.043 \pm 0.012$ $0.067 \pm 0.015$	$0.041 \pm 0.000$ $0.043 \pm 0.029$
#82	27	6.1	70.70	2.17	72	$0.000 \pm 0.000$	$0.027 \pm 0.102$ $0.048 \pm 0.007$	$0.053 \pm 0.001$ $0.053 \pm 0.007$	$0.062 \pm 0.008$	$0.052 \pm 0.003$	$0.077 \pm 0.028$
#94	44	6.8	42.03	2.43	$N/A^b$	$0.000 \pm 0.000$ $0.000 \pm 0.000$	$0.036 \pm 0.007$	$0.049 \pm 0.007$	$0.002 \pm 0.000$ $0.029 \pm 0.002$	$0.032 \pm 0.003$ $0.034 \pm 0.009$	$0.077 \pm 0.020$ $0.051 \pm 0.019$
#96	28	5.0	26.24	2.43	40	$0.000 \pm 0.000$ $0.000 \pm 0.000$	$0.089 \pm 0.024$	$0.043 \pm 0.007$ $0.112 \pm 0.017$	$0.023 \pm 0.002$ $0.091 \pm 0.022$	$0.034 \pm 0.003$ $0.081 \pm 0.028$	$0.031 \pm 0.013$ $0.049 \pm 0.014$
#179	21	6.1	70.70	2.43	56	$0.000 \pm 0.000$ $0.000 \pm 0.000$	$0.058 \pm 0.024$	$0.066 \pm 0.011$	$0.051 \pm 0.022$ $0.053 \pm 0.018$	$0.031 \pm 0.020$ $0.032 \pm 0.017$	$0.043 \pm 0.014$ $0.088 \pm 0.028$
#251	36	7.2	30.43	2.40	90	$0.000 \pm 0.000$	$0.085 \pm 0.032$	$0.030 \pm 0.005$	$0.025 \pm 0.006$	$0.020 \pm 0.005$	$0.041 \pm 0.019$
#503	38	4.9	15.00	2.43	32	$0.000 \pm 0.000$	$0.006 \pm 0.002$	$0.040 \pm 0.010$	$0.031 \pm 0.015$	$0.013 \pm 0.008$	$0.019 \pm 0.007$
							= 2.001	= 0.010	= 2.010	= 2.000	

 $<sup>^</sup>a$  All spots had p < 0.05 by ANOVA with Tukey post-hoc multiple comparisons.  $^b$  N/A = Not applicable (not appeared in the first 20 hits by MASCOT search, but had a very high Z score (>1.65) using the ProFound search tool).

endothelial growth factor A splice variant VEGF 102). However, the interpretation for the latter group (those with detectable levels only during PHN) must be used with caution because a few proteins, particularly albumin and transferrin, have several isoforms in the urine and some are readily detectable in the normal urine. The presentation of some isoforms of these two proteins only in the diseased urine, as in the present study, is possible and deserves further investigations for specificity or type of such isoforms, which are most likely modified by the processes called "post-translational modifications".

B. Proteins with Potential Roles in the Pathogenic Mechanisms or Pathophysiology of Membranous Nephropathy: Proteins with Decreased Excretion Levels in the Urine During PHN. Cadherins are type I membrane, calcium-dependent, cell adhesion molecules. These proteins preferentially interact with themselves and other molecules [e.g., catenins, 16 nephrin 17 which is a key component of podocyte slit diaphragm determining glomerular permeability] in a homophilic manner in connecting cells. Cell adhesive mechanisms have an impact on cell migration and proliferation, which are involved in the

pathogenesis of various glomerular diseases. Down-regulation of cadherins, therefore, is associated with the glomerular permeability defects, thereby proteinuria. We identified a decrease in excretion of E-cadherin. Our data were consistent with the data reported previously of down-regulation of cadherins in several glomerular disorders. 18,19

Tissue kallikrein is a serine proteinase that is involved in the production of the potent vasodilator, kinin peptide, from kininogen substrate.<sup>20</sup> Tissue kallikrein level is reduced in humans and animal models with hypertension, cardiovascular and renal diseases.<sup>20,21</sup> Another protein with a decreased excretion level during PHN is aldehyde dehydrogenase which is capable of converting 9-cis and all-trans retinal to corresponding retinoic acid with high efficiency.<sup>22,23</sup> It is strongly expressed in kidney, lung, testis, intestine, stomach, and trachea, and weakly in liver. Its function has been suggested to involve in oxidative pathways.<sup>24</sup> However, its role in glomerular disease has not been previously studied and further investigation may lead to the discovery of novel disease mechanisms for membranous nephropathy.

Table 4. Quantitative Data after Normalization with 24-h Urine Creatinine Excretion<sup>a</sup>

	normalized intensity levels (x $10^{-3}$ )(mean $\pm$ SEM; arbitrary units/mg Cr/24 h)					
spot no.	D0	D10	D20	D30	D40	D50
			Group I			
#1	$3.4776 \pm 0.6191$	$0.2555 \pm 0.0769$	$0.5881 \pm 0.2006$	$0.6691 \pm 0.0963$	$0.7796 \pm 0.1573$	$0.3028 \pm 0.0618$
#87	$0.4823 \pm 0.1021$	$0.0258 \pm 0.0099$	$0.0772 \pm 0.0168$	$0.1068 \pm 0.0613$	$0.0774 \pm 0.0202$	$0.0382 \pm 0.0073$
#90	$0.2154 \pm 0.1016$	$0.0229 \pm 0.0074$	$0.0270 \pm 0.0087$	$0.0151 \pm 0.0077$	$0.0058 \pm 0.0030$	$0.0000 \pm 0.0000$
#92	$0.5323 \pm 0.0528$	$0.0267 \pm 0.0046$	$0.0582 \pm 0.0133$	$0.0351 \pm 0.0052$	$0.0466 \pm 0.0115$	$0.0477 \pm 0.0116$
#93	$0.2651 \pm 0.0308$	$0.0328 \pm 0.0053$	$0.0657 \pm 0.0095$	$0.0370 \pm 0.0038$	$0.0418 \pm 0.0114$	$0.0481 \pm 0.0126$
#115	$0.9783 \pm 0.1684$	$0.0781 \pm 0.0269$	$0.0630 \pm 0.0171$	$0.0870 \pm 0.0147$	$0.0645 \pm 0.0087$	$0.0460 \pm 0.0120$
#343	$0.1494 \pm 0.0453$	$0.0000 \pm 0.0000$	$0.0422 \pm 0.0117$	$0.0000 \pm 0.0000$	$0.0245 \pm 0.0161$	$0.0055 \pm 0.0055$
#368	$2.3027 \pm 0.4648$	$0.0532 \pm 0.0129$	$0.1172 \pm 0.0274$	$0.0533 \pm 0.0122$	$0.2101 \pm 0.0522$	$0.0451 \pm 0.0091$
			Group II			
#12	$0.3939 \pm 0.0926$	$1.3458 \pm 0.2366$	$2.1488 \pm 0.2228$	$0.9204 \pm 0.2172$	$2.3434 \pm 0.4214$	$1.1555 \pm 0.1877$
#20	$0.3618 \pm 0.0405$	$1.2269 \pm 0.4393$	$1.1117 \pm 0.1837$	$1.0700 \pm 0.2880$	$1.3142 \pm 0.1500$	$1.0754 \pm 0.2165$
#21	$0.2458 \pm 0.0459$	$0.8443 \pm 0.2416$	$0.9524 \pm 0.1925$	$0.5316 \pm 0.0884$	$0.7943 \pm 0.1169$	$0.5899 \pm 0.1309$
#24	$3.4104 \pm 0.4906$	$5.5143 \pm 0.9054$	$10.8350 \pm 1.8675$	$9.1490 \pm 1.8234$	$12.0471 \pm 2.0201$	$16.8190 \pm 3.1887$
#25	$1.7627 \pm 0.1073$	$5.9299 \pm 0.8054$	$7.5727 \pm 0.9350$	$7.8625 \pm 1.7960$	$8.9028 \pm 1.6294$	$4.0641 \pm 0.4872$
#501	$0.1456 \pm 0.0083$	$0.8030 \pm 0.1965$	$0.7620 \pm 0.0836$	$0.7901 \pm 0.1691$	$0.8298 \pm 0.2196$	$0.6060 \pm 0.1156$
#502	$0.2715 \pm 0.0634$	$0.7251 \pm 0.3049$	$1.2143 \pm 0.1455$	$1.0914 \pm 0.1955$	$1.1824 \pm 0.2578$	$0.8638 \pm 0.1553$
//3.3	0.0050   0.0100	0.0070   0.0000	Group III	0.0077   0.0150	0.0010   0.0110	0.00=0.1.0.0000
#11	$0.0259 \pm 0.0186$	$0.0379 \pm 0.0080$	$0.0575 \pm 0.0057$	$0.0277 \pm 0.0152$	$0.0219 \pm 0.0116$	$0.0073 \pm 0.0028$
#169	$0.3262 \pm 0.0389$	$1.0502 \pm 0.3092$	$0.5928 \pm 0.1587$	$0.8272 \pm 0.2979$	$0.6163 \pm 0.1236$	$0.1523 \pm 0.0405$
#170	0.1702   0.0507	0.1161   0.0400	Group IV $0.0762 \pm 0.0153$	0.0520   0.0272	0.0000   0.0000	0.0100   0.0005
#170 #172	$0.1783 \pm 0.0567$ $1.0803 \pm 0.4748$	$0.1161 \pm 0.0489$ $0.4429 \pm 0.1217$	$0.0762 \pm 0.0153$ $0.2452 \pm 0.0482$	$0.0539 \pm 0.0273$ $0.1532 \pm 0.0525$	$0.0298 \pm 0.0096$ $0.0958 \pm 0.0426$	$0.0108 \pm 0.0085$ $0.0143 \pm 0.0089$
#172	$1.0003 \pm 0.4740$	$0.4429 \pm 0.1217$	0.2452 ± 0.0462 Group V	$0.1332 \pm 0.0323$	$0.0936 \pm 0.0426$	$0.0145 \pm 0.0069$
#19	$0.3274 \pm 0.0732$	$0.0000 \pm 0.0000$				
#376	$0.2190 \pm 0.0582$	$0.0000 \pm 0.0000$				
#381	$0.1123 \pm 0.0354$	$0.0000 \pm 0.0000$				
#388	$0.2724 \pm 0.0557$	$0.0000 \pm 0.0000$				
#405	$0.2418 \pm 0.0712$	$0.0000 \pm 0.0000$				
			Group VI			
#22	$0.0000 \pm 0.0000$	$0.2424 \pm 0.0217$	$0.2482 \pm 0.0312$	$0.2178 \pm 0.0567$	$0.2582 \pm 0.0659$	$0.1328 \pm 0.0163$
#23	$0.0000 \pm 0.0000$	$0.1945 \pm 0.0258$	$0.2030 \pm 0.0250$	$0.1459 \pm 0.0403$	$0.1458 \pm 0.0286$	$0.0831 \pm 0.0092$
#42	$0.0000 \pm 0.0000$	$0.0299 \pm 0.0057$	$0.0449 \pm 0.0039$	$0.0295 \pm 0.0082$	$0.0377 \pm 0.0087$	$0.0098 \pm 0.0027$
#78	$0.0000 \pm 0.0000$	$0.1101 \pm 0.0485$	$0.0350 \pm 0.0062$	$0.0506 \pm 0.0270$	$0.0324 \pm 0.0084$	$0.0057 \pm 0.0044$
#79	$0.0000 \pm 0.0000$	$0.1674 \pm 0.0575$	$0.0614 \pm 0.0072$	$0.0792 \pm 0.0423$	$0.0479 \pm 0.0116$	$0.0107 \pm 0.0068$
#80	$0.0000 \pm 0.0000$	$0.1811 \pm 0.0685$	$0.0700 \pm 0.0089$	$0.0786 \pm 0.0367$	$0.0364 \pm 0.0103$	$0.0071 \pm 0.0050$
#81	$0.0000 \pm 0.0000$	$0.3016 \pm 0.0859$	$0.2542 \pm 0.0499$	$0.1137 \pm 0.0555$	$0.0564 \pm 0.0117$	$0.0270 \pm 0.0184$
#82	$0.0000 \pm 0.0000$	$0.0268 \pm 0.0035$	$0.0439 \pm 0.0090$	$0.0407 \pm 0.0057$	$0.0421 \pm 0.0048$	$0.0488 \pm 0.0199$
#94	$0.0000 \pm 0.0000$	$0.0213 \pm 0.0067$	$0.0413 \pm 0.0099$	$0.0205 \pm 0.0044$	$0.0300 \pm 0.0090$	$0.0322 \pm 0.0135$
#96	$0.0000 \pm 0.0000$	$0.0532 \pm 0.0180$	$0.0878 \pm 0.0154$	$0.0634 \pm 0.0179$	$0.0702 \pm 0.0267$	$0.0299 \pm 0.0098$
#179	$0.0000 \pm 0.0000$	$0.0339 \pm 0.0063$	$0.0561 \pm 0.0147$	$0.0375 \pm 0.0123$	$0.0294 \pm 0.0167$	$0.0545 \pm 0.0189$
#251	$0.0000 \pm 0.0000$	$0.0507 \pm 0.0219$	$0.0254 \pm 0.0059$	$0.0197 \pm 0.0083$	$0.0174 \pm 0.0056$	$0.0264 \pm 0.0132$
#503	$0.0000\pm0.0000$	$0.0027 \pm 0.0018$	$0.0341 \pm 0.0093$	$0.0212 \pm 0.0096$	$0.0098 \pm 0.0069$	$0.0110 \pm 0.0043$

<sup>&</sup>lt;sup>a</sup> Almost all spots (except only for #11, #20, and #251) had p < 0.05 by ANOVA with Tukey post-hoc multiple comparisons.

Proteins with Increased Excretion Levels in the Urine During PHN. Alpha-1-antitrypsin (AAT) is a member of the serine protease inhibitor (SERPIN) family. It is one of the most abundant proteins in urine of patients with proteinuria and has been suggested to be a marker for glomerulopathy. Recently, another potential role of AAT has been suggested to involve in regulation of inflammation and mesangial matrix accumulation. E5,26 We identified the increase in urinary AAT excretion in our present study. This is consistent with the findings reported in previous studies. 18,25,26

Vascular endothelial growth factor (VEGF; or vascular permeability factor) is a growth factor involved in angiogenesis, vasculogenesis, and endothelial cell growth. VEGF induces endothelial cell proliferation, promotes cell migration, inhibits apoptosis, enhances TGF-beta1 expression in mouse glomerular endothelial cells via mitogen-activated protein kinase and phosphatidylinositol 3-kinase, and induces permeabilization of blood vessels.<sup>27</sup> Our data are consistent with findings in several studies, which reported the up-regulation of VEGF in various glomerular diseases.<sup>28–33</sup> Another protein that plays a crucial role in protein kinase signaling pathways is 1-phosphatidyli-

nositol-4,5-bisphosphate phosphodiesterase delta 1 (other synonyms are phosphoinositide phospholipase C, PLC-delta-1, and PLC—III), which mediates the production of the second messenger molecules diacylglycerol (DAG) and inositol 1,4,5-trisphosphate (IP3).<sup>34</sup> We identified the increase in excretion of PLC-delta-1 in a rat PHN model. These data suggest that VEGF and PLC-delta-1 are likely to play critical roles in glomerular trafficking, leading to glomerular injury in membranous nephropathy.

Among these altered proteins, E-cadherin and alpha-1-antitrypsin have been also proven to have the decreased and increased excretion levels, respectively, in human membranous nephropathy in patients with lupus nephritis class V.<sup>18</sup> Although kallikrein has not been previously proven to have a role in the pathogenic mechanisms of human membranous nephropathy, kininogen, which is another protein involved in the renal kininogen-kinin-kallikrein system (indeed, it is the substrate for bradykinin generation), has been already demonstrated to have an altered (decreased) excretion level in human membranous nephropathy.<sup>18</sup> These data strengthen our results and

indicate that proteomic data obtained from PHN animal model are applicable to human membranous nephropathy.

C. Intermediate Modulators for the Disease Processes that may Potentially Be Useful as Novel Biomarkers for Monitoring or Predicting the Disease Course. This group of proteins may have potential roles in pathogenic mechanisms of membranous nephropathy as the intermediate modulators for the disease processes; hence, their increase in expression did not last long and returned to the basal levels or even lower than the baselines. Interestingly, as changes in urinary excretion of these proteins were dynamic, these proteins may potentially be useful as novel biomarkers for monitoring or predicting the disease course. This group of proteins included embryonic growth-associated protein, pancreatitis-associated protein III, and transthyretin. Whereas the role for the former two proteins in glomerular diseases remains unclear, defects in transthyretin has been previously shown to be associated with glomerulopathy, particularly amyloidosis-related kidney disease.35,36

**D.** Altered Proteins whose Sequences Have been Recently Submitted to the Database but their Functions Remain Unknown. These include MPP7 [submitted in 2002<sup>37</sup>], mKI-AA1601 protein [submitted in 2003<sup>38</sup>], unnamed protein product [submitted in 1999<sup>39</sup>], and Ba1–647 [direct submission in June 2003]. Functions or pathophysiological roles of these proteins remain unknown. Further investigations may lead to the discovery of novel pathogenic mechanisms of human membranous nephropathy.

#### **Conclusions**

Using a gel-based proteomic approach, we defined serial changes in urinary proteome profile of PHN rats. The altered proteins or those with differential urinary excretion levels during the disease course were successfully identified using mass spectrometry. Most of these 37 proteins have potential roles in the pathogenic mechanisms or pathophysiology of human membranous nephropathy, whereas some of them may potentially be novel biomarkers for early diagnosis, monitoring the disease course, and/or prediction of therapeutic outcome. With these preliminary data obtained from the animal model, our works on human membranous nephropathy will be highly focused as to further explore each individual protein in humans for future use in clinical practice.

**Abbreviations:** 2D-PAGE, two-dimensional polyacrylamide gel electrophoresis; CHAPS, 3-[(3-cholamidopropyl)dimethylamino]-1-propanesulfonate; DTT, dithiothreitol; IPG, immobilized pH gradient; MALDI-TOF MS, matrix-assisted laser desorption/ionization time-of-flight mass spectrometry; PHN, passive Heymann nephritis; SD, Sprague—Dawley

**Acknowledgment.** We thank Professor R. Grimble for his editorial help and thank S. Chutipongtanate, N. Songtawee, T. Semangoen, and R. Kanlaya for their technical assistance. This study was supported by the Hong Kong Healthcare Association, Ltd, HK, the Matching Grant Scheme under the University Grants Committee of the Hong Kong Special Administration Region, China (Project No. 20600305) (to J.M.W.), and by Siriraj Grant for Research and Development (to V.T.).

#### References

 Ronco, P.; Debiec, H. Molecular pathomechanisms of membranous nephropathy: from Heymann nephritis to alloimmunization. J. Am. Soc. Nephrol. 2005, 16, 1205–1213. (2) Wasserstein, A. G. Membranous glomerulonephritis. J. Am. Soc. Nephrol. 1997, 8, 664–674.

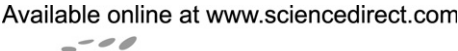
- (3) Glassock, R. J. Diagnosis and natural course of membranous nephropathy. Semin. Nephrol. 2003, 23, 324–332.
- (4) Couser, W. G. Membranous nephropathy: a long road but well traveled. J. Am. Soc. Nephrol. 2005, 16, 1184–1187.
- (5) Nangaku, M.; Shankland, S. J.; Couser, W. G. Cellular response to injury in membranous nephropathy. J. Am. Soc. Nephrol. 2005, 16, 1195–1204.
- (6) Salant, D. J.; Cybulsky, A. V. Experimental glomerulonephritis. Methods Enzymol. 1988, 162, 421–461.
- (7) Thongboonkerd, V.; Klein, J. B.; Pierce, W. M.; Jevans, A. W.; Arthur, J. M. Sodium loading changes urinary excretion: A proteomic analysis. Am. J. Physiol. Renal. Physiol. 2003, 284, F1155–F1163.
- (8) Thongboonkerd, V.; Klein, J. B.; Arthur, J. M. Proteomic identification of a large complement of rat urinary proteins. *Nephron. Exp. Nephrol.* 2003, 95, e69–e78.
- (9) Bradford, M. M. A rapid and sensitive method for the quantitation of microgram quantities of protein utilizing the principle of protein-dye binding. *Anal. Biochem.* 1976, 72, 248–254.
- (10) Hunt, S. M.; Thomas, M. R.; Sebastian, L. T.; Pedersen, S. K.; Harcourt, R. L.; Sloane, A. J.; Wilkins, M. R. Optimal replication and the importance of experimental design for gel-based quantitative proteomics. *J. Proteome Res.* 2005, 4, 809–819.
- (11) Shevchenko, A.; Wilm, M.; Vorm, O.; Mann, M. Mass spectrometric sequencing of proteins silver-stained polyacrylamide gels. *Anal. Chem.* 1996, 68, 850–858.
- (12) de Jong, P. E.; Gansevoort, R. T. Screening techniques for detecting chronic kidney disease. *Curr. Opin. Nephrol. Hypertens.* 2005, 14, 567–572.
- (13) Lamb, E. J.; Tomson, C. R.; Roderick, P. J. Estimating kidney function in adults using formulae. *Ann. Clin. Biochem.* 2005, 42, 321–345.
- (14) Cybulsky, A. V.; Quigg, R. J.; Salant, D. J. Experimental membranous nephropathy redux. Am. J. Physiol. Renal Physiol. 2005, 289, F660–F671.
- (15) Neale, T. J.; Ullrich, R.; Ojha, P.; Poczewski, H.; Verhoeven, A. J.; Kerjaschki, D. Reactive oxygen species and neutrophil respiratory burst cytochrome b558 are produced by kidney glomerular cells in passive Heymann nephritis. *Proc. Natl. Acad. Sci. U.S.A.* 1993, 90, 3645–3649.
- (16) Nakopoulou, L.; Lazaris, A. C.; Boletis, I. N.; Michail, S.; Giannopoulou, I.; Zeis, P. M.; Stathakis, C. P.; Davaris, P. S. Evaluation of E-cadherin/catenin complex in primary and secondary glomerulonephritis. *Am. J. Kidney Dis.* 2002, 39, 469–474.
- (17) Khoshnoodi, J.; Sigmundsson, K.; Ofverstedt, L. G.; Skoglund, U.; Obrink, B.; Wartiovaara, J.; Tryggvason, K. Nephrin promotes cell–cell adhesion through homophilic interactions. *Am. J. Pathol.* 2003. 163, 2337–2346.
- (18) Thongboonkerd, V.; Klein, J. B.; Jevans, A. W.; McLeish, K. R. Urinary proteomics and biomarker discovery for glomerular diseases. *Contrib. Nephrol.* 2004, 141, 292–307.
- (19) Xu, Z. G.; Ryu, D. R.; Yoo, T. H.; Jung, D. S.; Kim, J. J.; Kim, H. J.; Choi, H. Y.; Kim, J. S.; Adler, S. G.; Natarajan, R.; Han, D. S.; Kang, S. W. P-Cadherin is decreased in diabetic glomeruli and in glucose-stimulated podocytes in vivo and in vitro studies. *Neph*rol. Dial. Transplant. 2005, 20, 524-531.
- (20) Thongboonkerd, V.; Gozal, E.; Sachleben, L. R.; Arthur, J. M.; Pierce, W. M.; Cai, J.; Chao, J.; Bader, M.; Pesquero, J. B.; Gozal, D.; Klein, J. B. Proteomic analysis reveals alterations in the renal kallikrein pathway during hypoxia-induced hypertension. *J. Biol. Chem.* 2002, 277, 34708–34716.
- (21) Chao, J.; Chao, L. Kallikrein-kinin in stroke, cardiovascular and renal disease. Exp. Physiol. 2005, 90, 291–298.
- (22) Labrecque, J.; Dumas, F.; Lacroix, A.; Bhat, P. V. A novel isoenzyme of aldehyde dehydrogenase specifically involved in the biosynthesis of 9-cis and all-trans retinoic acid. *Biochem. J.* **1995**, 305 (Pt 2), 681–684.
- (23) Bhat, P. V.; Poissant, L.; Wang, X. L. Purification and partial characterization of bovine kidney aldehyde dehydrogenase able to oxidize retinal to retinoic acid. *Biochem. Cell Biol.* 1996, 74, 695–700.
- (24) Satriano, J.; Schwartz, D.; Ishizuka, S.; Lortie, M. J.; Thomson, S. C.; Gabbai, F.; Kelly, C. J.; Blantz, R. C. Suppression of inducible nitric oxide generation by agmatine aldehyde: beneficial effects in sepsis. *J. Cell Physiol.* 2001, *188*, 313–320.

- (25) Sharma, K.; Lee, S.; Han, S.; Lee, S.; Francos, B.; McCue, P.; Wassell, R.; Shaw, M. A.; RamachandraRao, S. P. Two-dimensional fluorescence difference gel electrophoresis analysis of the urine proteome in human diabetic nephropathy. Proteomics 2005, 5,
- (26) Machii, R.; Sakatume, M.; Kubota, R.; Kobayashi, S.; Gejyo, F.; Shiba, K. Examination of the molecular diversity of alpha1 antitrypsin in urine: deficit of an alpha1 globulin fraction on cellulose acetate membrane electrophoresis. J. Clin. Lab Anal. **2005**, 19, 16-21.
- (27) Li, Z. D.; Bork, J. P.; Krueger, B.; Patsenker, E.; Schulze-Krebs, A.; Hahn, E. G.; Schuppan, D. VEGF induces proliferation, migration, and TGF-beta1 expression in mouse glomerular endothelial cells via mitogen-activated protein kinase and phosphatidylinositol
- 3-kinase. *Biochem. Biophys. Res. Commun.* **2005**, 334, 1049–1060. (28) Feliers, D.; Chen, X.; Akis, N.; Choudhury, G. G.; Madaio, M.; Kasinath, B. S. VEGF regulation of endothelial nitric oxide synthase in glomerular endothelial cells. Kidney Int. 2005, 68, 1648-1659.
- (29) Cohen, M. P.; Chen, S.; Ziyadeh, F. N.; Shea, E.; Hud, E. A.; Lautenslager, G. T.; Shearman, C. W. Evidence linking glycated albumin to altered glomerular nephrin and VEGF expression, proteinuria, and diabetic nephropathy. Kidney Int. 2005, 68,
- (30) Namikoshi, T.; Satoh, M.; Horike, H.; Fujimoto, S.; Arakawa, S.; Sasaki, T.; Kashihara, N. Implication of peritubular capillary loss and altered expression of vascular endothelial growth factor in IgA nephropathy. *Nephron. Physiol.* **2006**, *102*, 9–16. Tang, Z.; Ren, H.; Yang, G.; Chen, H.; Zhou, H.; Zeng, C.; Liu, Z.;
- Li, L. Significance of vascular endothelial growth factor expression in renal tissue of patients with preeclamptic nephropathy. *Am. J. Nephrol.* **2005**, *25*, 579–585.
- (32) Schrijvers, B. F.; Flyvbjerg, A.; Tilton, R. G.; Rasch, R.; Lameire, N. H.; De Vriese, A. S. Pathophysiological role of vascular endothelial growth factor in the remnant kidney. Nephron Exp. Nephrol. 2005, 101, e9-15.
- (33) Cha, D. R.; Kang, Y. S.; Han, S. Y.; Jee, Y. H.; Han, K. H.; Han, J. Y.; Kim, Y. S.; Kim, N. H. Vascular endothelial growth factor is increased during early stage of diabetic nephropathy in type II diabetic rats. J. Endocrinol. 2004, 183, 183-194.
- (34) Cheng, H. F.; Jiang, M. J.; Chen, C. L.; Liu, S. M.; Wong, L. P.; Lomasney, J. W.; King, K. Cloning and identification of amino acid residues of human phospholipase C delta 1 essential for catalysis. *J. Biol. Chem.* **1995**, *270*, 5495–5505.

- (35) Lobato, L. Portuguese-type amyloidosis (transthyretin amyloidosis, ATTR V30M). J. Nephrol. 2003, 16, 438-442.
- (36) Lobato, L.; Beirao, I.; Silva, M.; Bravo, F.; Silvestre, F.; Guimaraes, S.; Sousa, A.; Noel, L. H.; Sequeiros, J. Familial ATTR amyloidosis: microalbuminuria as a predictor of symptomatic disease and clinical nephropathy. Nephrol. Dial. Transplant. 2003, 18, 532-
- (37) Strausberg, R. L.; Feingold, E. A.; Grouse, L. H.; Derge, J. G.; Klausner, R. D.; Collins, F. S.; Wagner, L.; Shenmen, C. M.; Schuler, G. D.; Altschul, S. F.; Zeeberg, B.; Buetow, K. H.; Schaefer, C. F.; Bhat, N. K.; Hopkins, R. F.; Jordan, H.; Moore, T.; Max, S. I.; Wang, J.; Hsieh, F.; Diatchenko, L.; Marusina, K.; Farmer, A. A.; Rubin, G. M.; Hong, L.; Stapleton, M.; Soares, M. B.; Bonaldo, M. F.; Casavant, T. L.; Scheetz, T. E.; Brownstein, M. J.; Usdin, T. B.; Toshiyuki, S.; Carninci, P.; Prange, C.; Raha, S. S.; Loquellano, N. A.; Peters, G. J.; Abramson, R. D.; Mullahy, S. J.; Bosak, S. A.; McEwan, P. J.; McKernan, K. J.; Malek, J. A.; Gunaratne, P. H.; Richards, S.; Worley, K. C.; Hale, S.; Garcia, A. M.; Gay, L. J.; Hulyk, S. W.; Villalon, D. K.; Muzny, D. M.; Sodergren, E. J.; Lu, X.; Gibbs, R. A.; Fahey, J.; Helton, E.; Ketteman, M.; Madan, A.; Rodrigues, S.; Sanchez, A.; Whiting, M.; Madan, A.; Young, A. C.; Shevchenko, Y.; Bouffard, G. G.; Blakesley, R. W.; Touchman, J. W.; Green, E. D.; Dickson, M. C.; Rodriguez, A. C.; Grimwood, J.; Schmutz, J.; Myers, R. M.; Butterfield, Y. S.; Krzywinski, M. I.; Skalska, U.; Smailus, D. E.; Schnerch, A.; Schein, J. E.; Jones, S. J.; Marra, M. A. Generation and initial analysis of more than 15,000 full-length human and mouse cDNA sequences. Proc. Natl. Acad. Sci. U.S.A. **2002**, 99, 16899-16903.
- (38) Okazaki, N.; Kikuno, R.; Ohara, R.; Inamoto, S.; Koseki, H.; Hiraoka, S.; Saga, Y.; Nagase, T.; Ohara, O.; Koga, H. Prediction of the coding sequences of mouse homologues of KIAA gene: III. the complete nucleotide sequences of 500 mouse KIAA-homologous cDNAs identified by screening of terminal sequences of cDNA clones randomly sampled from size-fractionated libraries. DNA Res. **2003**, 10, 167–180.
- (39) Carninci, P.; Hayashizaki, Y. High-efficiency full-length cDNA cloning. Methods Enzymol. 1999, 303, 19-44.

PR060122B









Biochemical and Biophysical Research Communications 350 (2006) 723-730

www.elsevier.com/locate/ybbrc

# Trafficking defect of mutant kidney anion exchanger 1 (kAE1) proteins associated with distal renal tubular acidosis and Southeast Asian ovalocytosis

Nunghathai Sawasdee <sup>a</sup>, Wandee Udomchaiprasertkul <sup>a</sup>, Sansanee Noisakran <sup>a</sup>, Nanyawan Rungroj <sup>b</sup>, Varaporn Akkarapatumwong <sup>c</sup>, Pa-thai Yenchitsomanus <sup>a,b,\*</sup>

<sup>a</sup> Division of Medical Molecular Biology and BIOTEC-Medical Biotechnology Unit, Department of Research and Development, and Department of Immunology and Immunology Graduate Program, Faculty of Medicine Siriraj Hospital, Mahidol University, Bangkok 10700, Thailand
 <sup>b</sup> Division of Molecular Genetics, Department of Research and Development, Faculty of Medicine Siriraj Hospital,
 Mahidol University, Bangkok 10700, Thailand

<sup>c</sup> Institute of Molecular Biology and Genetics, Mahidol University, Salaya Campus, Nakornpatom 73170, Thailand

Received 20 September 2006 Available online 2 October 2006

#### Abstract

Compound heterozygous *anion exchanger 1 (AE1)* SAO/G701D mutations result in distal renal tubular acidosis with Southeast Asian ovalocytosis. Interaction, trafficking and localization of wild-type and mutant (SAO and G701D) kAE1 proteins fused with hemagglutinin, six-histidine, Myc, or green fluorescence protein (GFP) were examined in human embryonic kidney (HEK) 293 cells. When individually expressed, wild-type kAE1 was localized at cell surface while mutant kAE1 SAO and G701D were intracellularly retained. When co-expressed, wild-type kAE1 could form heterodimer with kAE1 SAO or kAE1 G701D and could rescue mutant kAE1 proteins to express on the cell surface. Co-expression of kAE1 SAO and kAE1 G701D also resulted in heterodimer formation but intracellular retention without cell surface expression, suggesting their trafficking defect and failure to rescue each other to the plasma membrane, most likely the molecular mechanism of the disease in the compound heterozygous condition.

© 2006 Elsevier Inc. All rights reserved.

Keywords: Distal renal tubular acidosis (dRTA); Kidney anion exchanger 1 (kAE1); Southeast Asian ovalocytosis (SAO); Compound heterozygous mutation; Trafficking defect; Epitope tag; Green fluorescent protein (GFP); Thai

Erythroid and kidney anion exchanger 1 (eAE1 and kAE1) are encoded by *AE1* or *SLC4A1* gene located on chromosome 17q21-q22 [1]. kAE1 is a truncated isoform of eAE1 with lacking of 65 amino acids at the N-terminus owing to the use of differential transcription and translation start sites [2,3]. eAE1 regulates red blood cell (RBC) morphology and chloride/bicarbonate (Cl<sup>-</sup>/HCO<sup>-</sup><sub>3</sub>) exchange in RBC whereas kAE1 mediates chloride/bicarbonate exchange at basolateral membrane of acid-secreting

α-intercalated cells of distal nephron and collecting duct [3–7]. eAE1 defect results in morphological changes of RBC while kAE1 abnormality leads to distal renal tubular acidosis (dRTA)—a disease characterized by failure of kidney to appropriately acidify urine in the presence of systemic metabolic acidosis [8].

AEI mutations have been found to be associated with both autosomal dominant (AD) and autosomal recessive (AR) dRTA [8,9]. The mutations associated with AD dRTA such as R589H, R589C, R589S, and R901X still maintain substantial anion transport activities in RBC and Xenopus oocytes [10–14], suggesting that the defect dose not simply associate with a reduction of anion

<sup>\*</sup> Corresponding author. Fax: +662 4184793. E-mail address: grpye@mahidol.ac.th (P. Yenchitsomanus).

transport function. Trafficking of mutant proteins to the cell surface of human embryonic kidney 293 (HEK 293) cells was impaired, causing their intracellular retention [15–17]. Moreover, kAE1 R901X and G609R exhibited mis-targeting to apical surface in polarized Madin-Darby canine kidney (MDCK) cells [18,19]. Co-expression of kAE1 R589H or R901X with wild-type kAE1 also caused intracellular retention of wild-type protein attributable to their hetero-oligomer formation and dominant negative effect [15,16].

The AEI mutation associated with AR dRTA was first reported in two Thai patients who carried a homozygous AEI G701D ( $band 3 \ Bangkok I$ ) mutation and homozygous hemoglobin E (HBB E26K) and had severe hemolytic anemia and dRTA without abnormal RBC anion transport function [20]. eAE1 G701D and kAE1 G701D showed impaired chloride anion (Cl $^-$ ) transport and trafficking to the cell surface in Xenopus oocyte, which could be rescued by co-expression of glycophorin A (GPA)—an eAE1 chaperone [20]. The presence of dRTA phenotype without abnormal erythroid anion transport could be explained by the presence of GPA in RBC but absence in the kidney  $\alpha$ -intercalated cells; thus, kAE1 G701D might fail to move to basolateral membrane in the kidney  $\alpha$ -intercalated cells [21,22].

The combined dRTA and Southeast Asian ovalocytosis (SAO) condition was originally observed by our group in Thai patients who carried compound heterozygous SAO/ G701D mutations [23,24], and were also reported later by other groups [25,26]. AEI SAO is caused by a deletion of 27 base-pairs in codons 400–408, resulting in an in-frame 9-amino-acid deletion at the boundary between cytoplasmic and membrane domains of AE1. The heterozygous AE1 SAO mutation is insufficient to cause dRTA [23,25]. The transport function of eAE1 SAO is impaired in RBC and oocytes [25,27] although the protein could be inserted into plasma membrane [28]. The expression level and stability of eAE1 and kAE1 SAO proteins were significantly reduced and the mutant proteins were retained intracellularly in transfected HEK 293 and MDCK cells [29]. While homodimers of kAE1 and heterodimers of kAE1 and kAE1 SAO could traffic to the basolateral membrane of polarized cells, homodimers of kAE1 SAO were found to be retained in the endoplasmic reticulum and rapidly degraded.

To understand molecular mechanism of AR dRTA caused by compound heterozygous AEI SAO/G701D mutations, wild-type and mutant (SAO and G701D) kAE1 fused with different epitope tags or green fluorescent protein (GFP) were individually expressed and co-expressed in HEK 293 cells to examine protein expression, interaction, trafficking, and localization by several techniques. We found that trafficking defect of both kAE1 SAO and kAE1 G701D and their failure to rescue each other to the plasma membrane are most likely the molecular mechanism of the disease caused by this compound heterozygous condition.

#### Materials and methods

Plasmid construction. Wild-type (WT) kAE1 cDNA was amplified from pcDNA3-kAE1 (a gift from Professor Reinhart A. Reithmeier) by PCR and inserted into NotI/XhoI-digested pcDNA3.1/HisB (Invitrogen, USA) to construct pcDNA3-kAE1 WT-His. pcDNA3-kAE1-HA expressing kAE1 with HA epitope fusion at its C-terminus was a gift from Miss Thitima Keskanokwong and Professor Joseph R. Casey. To generate pcDNA3.1-GFP, GFP gene was amplified by PCR from pDs-Green and cloned into EcoRV/NotI-cleaved pcDNA3.1(+) vector (Invitrogen, USA). Then, kAE1 was inserted into this plasmid at the site downstream to GFP, yielding pcDNA3.1-GFP-kAE1. The expressed fusion protein contained GFP linked to the N-terminus of kAE1. The plasmid constructs transformed in Escherichia coli were prepared by using QIAprep Spin Miniprep Kit (Qiagen, Germany) and examined for correct reading frames by DNA sequencing.

Site-directed mutagenesis. pcDNA3-kAE1 WT-Myc, containing a sequence of Myc epitope inserted at the position 557 in the third extracellular loop of kAE1, was generated from pcDNA3-kAE1 by site-directed mutagenesis following the protocol of the QuickChange TM site-directed mutagenesis kit from Stratagene, USA. Eight plasmid constructs expressing kAE1 SAO or kAE1 G701D fused with either His, HA, Myc, or GFP (pcDNA3-kAE1 SAO-His, pcDNA3-kAE1 SAO-HA, pcDNA3-kAE1 SAO-Myc, pcDNA3.1 GFP-kAE1 SAO, pcDNA3-kAE1 G701D-His, pcDNA3-kAE1 G701D-HA, pcDNA3-kAE1 G701D-Myc or pcDNA3.1 GFP-kAE1 G701D) were created from the four plasmid constructs that were mentioned earlier by the site-directed mutagenesis method. Plasmid constructs propagated in E. coli were purified by QIA-prep Spin Miniprep Kit (Qiagen, Germany). Mutations in these plasmid constructs were confirmed by DNA sequencing.

Cell culture and transfection. HEK 293 cells were maintained in Dulbecco's modified Eagle's medium (DMEM) supplemented with 10% fetal bovine serum (PERBIO, UK), containing antibiotics, at 37 °C with 5% CO<sub>2</sub>. The cultured cells at 40–60% confluent growth in 6-well plates were transfected with 2–5 μg of recombinant plasmid DNA per well either by using Lipofectin (Invitrogen, USA) according to the manufacturer's protocol or DEAE-dextran method [30]. The HEK 293 cells were individually transfected with each of the twelve plasmid constructs (four containing wild-type kAE1 and eight consisting of mutant kAE1), and were also separately co-transfected with pcDNA-kAE1 WT-His and pcDNA-kAE1 SAO-HA (or pcDNA-kAE1 G701D-HA), pcDNA-kAE1 SAO-His and pcDNA-kAE1 G701D-HA, or pcDNA-kAE1 G701D-His and pcDNA-kAE1 SAO-HA, for expression or co-expression, affinity purification, co-timunoprecipitation, cellular localization, and cell-surface expression studies

SDS-PAGE and Western blot analysis. Two days after transfection, the transfected HEK 293 cells were washed once with phosphate buffer saline (PBS) and lysed with lysis buffer on ice for 30 min. Proteins were collected after centrifugation and subjected to electrophoresis on 8% SDS-PAGE before transferring to nitrocellulose membranes. The membranes were blocked for 1 h with 5% skim milk in TBST (TBS with 0.1% Tween 20) and then incubated with either anti-His, anti-HA, anti-Ct AE1, or anti-Myc antibody for 2 h. After washing three times with TBST for 5 min each, the membranes were incubated with secondary antibody conjugated to horseradish peroxidase (HRP) for 1 h. After washing another three times with TBST, the expressed proteins were detected by SuperSignal West Pico Chemiluminescent Substrate (Pierce, USA) plus Western Blotting Detection System for 5 min according to manufacturer's instruction. The chemiluminescence signal was detected by exposing the membrane to an X-ray film in a cassette for 1 min and the film was developed by a film-developing machine.

Affinity co-purification. In this study, HEK 293 cells were individually transfected with the plasmid constructs or were co-transfected with four different pairs of the constructs described above. Two days after transfection, the cells were detached with PBS and collected by centrifugation at 3000g for 5 min. The cells were lysed with  $500\,\mu$ l of lysis buffer containing protease inhibitor cocktail on ice for 15 min. The insoluble fraction was removed by centrifugation at 4 °C. An aliquot of  $400\,\mu$ l of cell lysate

was incubated with 40  $\mu$ l of washed Co<sup>2+</sup> chelate resins (BD Bioscience, USA) at 4 °C for 12–16 h with rotation. After incubation, the resins were collected by centrifugation and washed thoroughly with washing buffers. 6×Histidine-tagged-kAE1 proteins that bound to Co<sup>2+</sup> chelate resins were eluted with 2× SDS–PAGE sample loading buffer containing 2% (v/v) 2-mercaptoethanol and heated at 65 °C for 5 min. The samples were subjected to SDS–PAGE and the co-purified kAE1-HA proteins were detected by Western blot analysis using anti-HA antibody and HRP-conjugated secondary antibody as previously described.

Co-immunoprecipitation. The transfected and co-transfected HEK 293 cells were prepared as same as those in the previous section. The cells were similarly processed and lysed. The cell lysate was centrifuged to remove insoluble materials and the supernatant was transferred to new 1.5-mlmicrocentrifuge tubes containing 50 µl of Protein G-Sepharose resin mixture to eliminate (pre-clear) non-specific binding proteins in the lysate. The tubes were incubated at 4 °C for 2 h with constant rotation. The resins were then removed by centrifugation. One hundred microlitres of the supernatant was saved to serve as a total protein fraction and 400 µl of the supernatant were used for immunoprecipitation by adding 2 µl of rabbit anti-6×His antibody and 60 µl of protein G-Sepharose beads. The mixture was incubated at 4 °C with shaking for 12-16 h. Then, the resins were collected by centrifugation and washed thoroughly with washing buffers 1 and 2 as mentioned above. Protein complexes were eluted with 2× SDS-PAGE sample loading buffer containing 2% (v/v) 2-mercaptoethanol and heated at 65 °C for 5 min. The protein complexes were analyzed by SDS-PAGE and Western blot method using anti-HA antibody and HRPconjugated secondary antibody as previously described.

Immunofluorescence and confocal microscopy. To examine cellular localization of expressed proteins, HEK 293 cells were grown on round cover glasses in a 6-well plate for transfections and co-transfection with the recombinant plasmid constructs. To examine cellular localization of HA-tagged or Myc-tagged kAE1, after transfection for 48 h, the transfected HEK 293 cells were washed with PBS and fixed with 4% paraformaldehyde in PBS at room temperature for 1 h. After washing with 100 mM glycine in PBS for 5 min, the cells were permeabilized with 0.2% Triton X-100 for 15 min and were washed three times with PBS for 5 min each. The cells were incubated with 1% BSA in PBS for 30 min to block non-specific binding of antibody, followed by further washing with PBS. The cells were then incubated with an antibody (mouse anti-Myc antibody, rabbit anti-HA antibody, or mouse anti-CD147 antibody—a gift from Associate Professor Watchara Kasinrerk) in PBS containing 1% BSA for 1 h at room temperature. After washing three times with PBS, the cells were incubated with a secondary antibody conjugated with a fluoresceine dye (Cy3-conjugated donkey anti-rabbit IgG or goat anti-mouse Alexa 488-conjugated IgG) for 30 min at room temperature. The cells were washed three times with PBS and the cover glasses were mounted with antifade solution. Localization of the proteins was examined by a confocal microscope (Zeiss LSM510 META, Germany).

To examine cellular localization of GFP-tagged kAE1, the cells were washed once with PBS and fixed with 4% paraformaldehyde. After washing three times with PBS, the cover glasses were mounted with antifade solution. The cells were directly examined by a confocal microscope.

The image pixels of cell surface and total kAE1 protein expression were estimated by using Zeiss LSM510 META software. The percentage of relative cell surface expression of kAE1 protein was calculated, which is equal to  $100 \times$  (pixels of cell surface expression of kAE1/pixels of total expression of kAE1). The difference of means was analyzed by an unpaired Student's t test using Intercooled Stata 9.0 program for Windows (StataCorp LP, USA). The value of p < 0.05 was considered to be statistically significant.

Flow cytometry. Myc epitope inserted at the third extracellular loop of kAE1 would be expressed extracellularly. Thus, expression of kAE1-Myc on the cell surface could be determined by fluorescence staining and flow cytometry. HEK 293 cells were individually transfected or they were cotransfected with the plasmid constructs. Two days after transfections, the cells were collected by centrifugation at 4 °C. They were re-suspended in chilled DMEM containing with 2% fetal bovine serum, 1% BSA, and  $10 \text{ mM} \text{ NaN}_3$ , and permeabilized (for total protein analysis) with 0.2%

Triton X-100/PBS or non-permeabilized (for surface protein analysis) before incubated with mouse anti-Myc antibody for 1 h. After incubation, the cells were washed twice with chilled DMEM containing with 2% fetal bovine serum, 1% BSA, and 10 mM NaN₃. Then, goat anti-mouse antibody conjugated with Alexa 488 (Molecular Probes, Eugene, OR, USA) was used to probe mouse anti-Myc antibody for 30 min on ice. The cells were washed again and analyzed by using FACSort™ flow cytometer (Becton–Dickinson, USA.).

Number of cells with surface expression of kAE1 and number of cells with total expression of kAE1 were determined to quantify the percentage of relative cell surface expression of kAE1 which is equal to  $100 \times$  (number of cells with surface expression of kAE1 – number of cells with surface expression of vector control/number of cells with total expression of kAE1 – number of cells with total expression of kAE1 – number of cells with total expression of vector control). In addition, relative fluorescence intensity of cell surface expression was also calculated from mean fluorescence intensity (MFI) as follows: relative fluorescence intensity = (MFI of cell surface expression of kAE1 – MFI of cell surface expression of vector control)/MFI of cell surface expression of vector control. All experiments were repeated three times to calculate mean and standard deviation (SD). The difference of means was analyzed by an unpaired Student's t test. The value of t 0.05 was considered to be statistically significant.

#### Results and discussion

We have investigated into the molecular pathogenesis of compound heterozygous AEI SAO/G701D condition by in vitro studies. The recombinant plasmids expressing kAE1 WT, kAE1 SAO, and kAE1 G701D fused with either 6×His, HA, Myc, or GFP were constructed for the expression and co-expression studies in cultured HEK 293 cells in different experiments. The expression of wild-type and mutant kAE1 fusion proteins was initially analyzed by Western blot method, their interactions were studied by affinity co-purification and co-immunoprecipitation, and cellular localization and cell surface expression were investigated by confocal microscopy and flow cytometry.

Expressions and interaction of wild-type and mutant kAE1 fusion proteins in HEK 293 cells

The cells transfected with the recombinant plasmids expressed kAE1 WT, kAE1 SAO, or kAE1 G701D fused with an epitope tag (6×His, HA, or Myc) with the estimated molecular weight (MW) of  $\sim$ 96 kDa (Fig. 1A). The GFP-kAE1 and GFP-kAE1 G701D fusion proteins were expressed at  $M_{\rm W}$  of  $\sim$ 109 kDa while GFP-kAE1 SAO at  $M_{\rm W}$  of  $\sim$ 106 kDa (Fig. 1B).

The interactions between kAE1 WT and kAE1 SAO or kAE1 G701D, and between kAE1 SAO and kAE1 G701D co-expressed in HEK 293 cells were examined by affinity co-purification and co-immunoprecipitation methods based on the use of 6×His tag present on one interacting kAE1 partner. The results of affinity co-purification and co-immunoprecipitation are shown in Figs. 1C and D, respectively. Left panels of both Figs. 1C and D are the Western blot results of total cell lysates before the analyses whereas the right panels are the Western blot results of the affinity co-purification (Fig. 1C) and co-immunoprecipitation (Fig. 1D). The wild-type and mutant kAE1 fused with

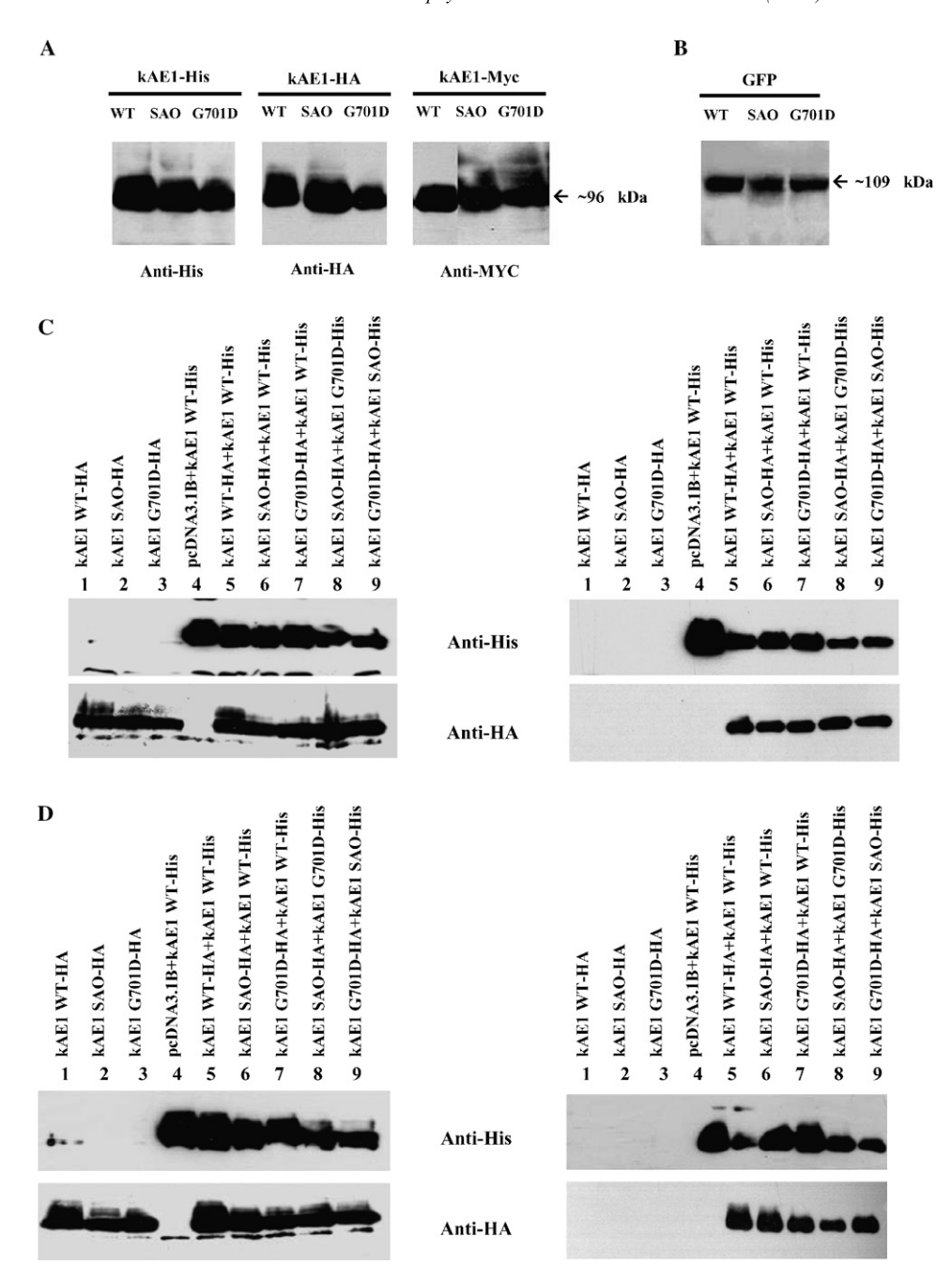


Fig. 1. Expression of wild-type and mutant kAE1 fusion proteins in HEK 293 cells analyzed by Western blot method (A and B), and interaction of wild-type and mutant kAE1 fusion proteins in HEK 293 cells analyzed by affinity co-purification (C) and co-immunoprecipitation (D).

either 6×His or HA epitope could be differentiated by anti-His (Figs. 1C and D, upper panels) and anti-HA (Figs. 1C and D, lower panels) antibodies. kAE1 WT-HA, kAE1 SAO-HA, and kAE1 G701D-HA were expressed and detected in the cell lysates by anti-HA (Figs. 1C and D, left, lower panels, lanes 1–3). Since kAE1 WT-His was not co-expressed in the same cells in this set of transfections, it was not detected in these three lysates (Figs. 1C and D, left, upper panels, lanes 1–3). kAE1 WT-His (in the presence of pcDNA3.1B) was expressed and detected by only anti-His antibody (Figs. 1C and D, left, upper panels, lane 4) but not by anti-HA antibody (Figs. 1C and D, left, lower pan-

els, lane 4). In the cell lysates of co-expressions between wild-type or mutant kAE1-His and wild-type or mutant kAE1-HA, both kAE1 fusion proteins were expressed and detected by the two antibodies (Figs. 1C and D, left, upper and lower panels, lanes 5–9).

The cell lysates containing only kAE1 WT-HA, kAE1 SAO-HA, or kAE1 G701D-HA without kAE1 His could not be detected in the samples after affinity co-purification and co-immunoprecipitation using anti-His and anti-HA antibodies (Figs. 1C and D, right, upper and lower panels, lanes 1–3) while the cell lysate containing kAE1 WT-His alone could be detected after in the affinity co-purification

and co-immunoprecipitation using anti-His (but undetectable by anti-HA antibody) (Figs. 1C and D, right, upper and lower panels, lane 4).

kAE1 WT-His co-expressed with either kAE1 WT-HA, kAE1 SAO-HA, or kAE1 G701D-HA could be detected in the samples after affinity co-purification and co-immuno-precipitation using both anti-His and anti-HA antibodies (Figs. 1C and D, right, upper and lower panels, lanes 5–7), indicating that heterodimers between kAE1 WT-His and either kAE1 WT-HA, kAE1 SAO-HA, or kAE1 G701D-HA could be formed.

Interestingly, the affinity co-purification and co-immunoprecipitation could detect both mutant proteins in the co-expressions between kAE1 G701D-His and kAE1 SAO-HA, and between kAE1 SAO-His and kAE1 G701D-HA by using both anti-His and anti-HA antibodies (Figs. 1C and D, right, upper and lower panels, lanes 8–9). This indicates that the heterodimers between kAE1 G701D-His and kAE1 SAO-HA, or between kAE1 SAO-His and kAE1 G701D-HA did occur. Thus, these two

mutations do not affect the structural folding involving in the interaction or dimerization property of kAE1 protein.

Cellular localization of wild-type and mutant kAE1 fusion proteins in HEK 293 cells

Cellular localization of wild-type and mutant kAE1 fusion proteins was examined by using immunofluorescence or protein fluorescence and confocal microscopy. The representative transfected HEK 293 cells expressing either kAE1 WT-Myc or kAE1 WT-HA show their predominant expressions at the cell surface (Fig. 2A: A–B and C–D). These results confirmed those that have previously been reported [16,21,22]. In contrast, the HEK 293 cells expressing either kAE1 SAO-Myc or kAE1 SAO-HA showed intracellular retention of the proteins (Fig. 2A: E–F and G–H) and similar finding was observed with the HEK 293 cells expressing either kAE1 G701D-Myc or kAE1 G701D-HA (Fig. 2A: I–J and K–L). The average percentages (means ± SD) of relative cell-surface

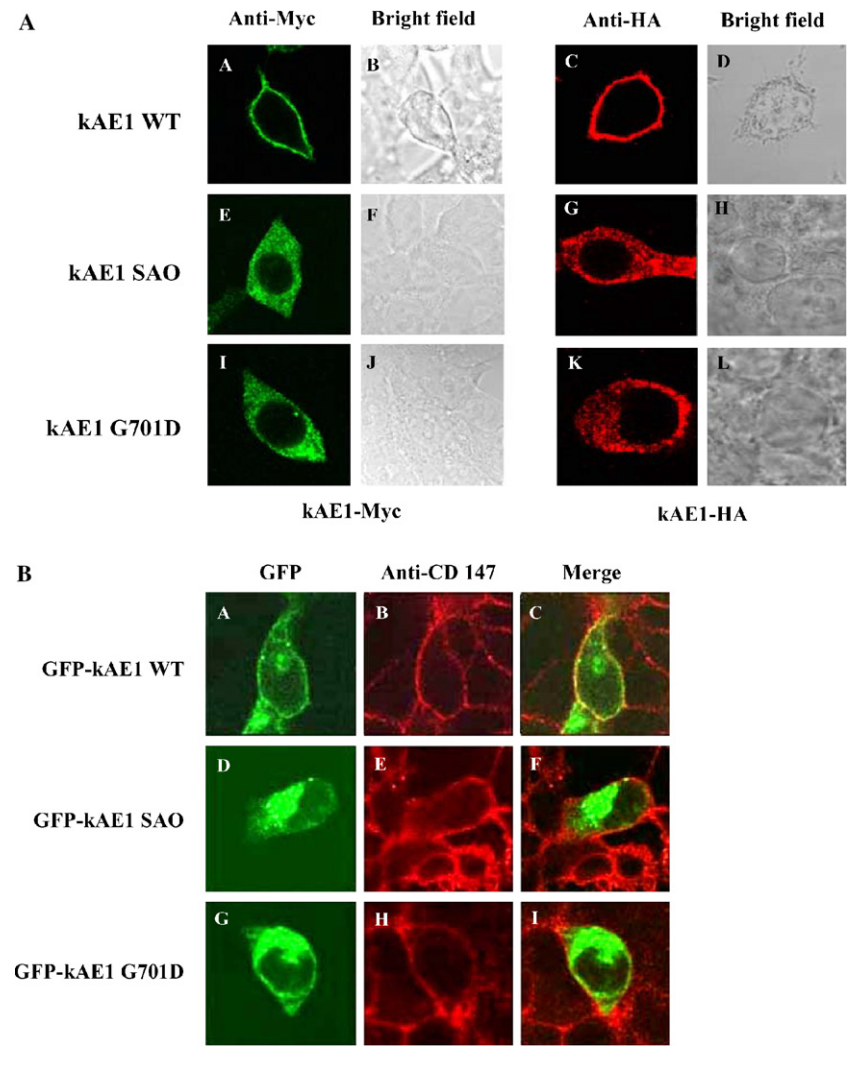


Fig. 2. Cellular localization of wild-type and mutant kAE1 fusion proteins tagged with Myc or HA (A), and GFP (B) in HEK 293 cells.

expressions of kAE1 WT-Myc were  $74.9 \pm 9.6\%$  (n=10), kAE1 SAO-Myc  $0.9 \pm 0.4\%$  (n=10, p < 0.0001), and kAE1 G701D-Myc  $1.2 \pm 0.6\%$  (n=10, p < 0.0001). A similar results were obtained for cell-surface expressions of kAE1 WT-HA ( $78.3 \pm 5.6\%$ , n=3), kAE1 SAO-HA ( $1.5 \pm 0.4\%$ , n=3, p < 0.0001), and kAE1 G701D-HA ( $1.4 \pm 0.2\%$ , n=3, p < 0.0001). These results indicate that in contrast to kAE1 WT that expressed on the cell surface, kAE1 SAO and kAE1 G701D retained within intracellular compartment and fail to traffic to locate on the cell membrane.

Green fluorescent signal generated from GFP fused to the wild-type and mutant kAE1 proteins could directly be examined without an immunological staining by a confocal microscope (Fig. 2B). To better locate the surface of HEK 293 cells, a cell surface marker-CD147 (β-subunit of Na<sup>+</sup>/K<sup>+</sup>-ATPase) was also stained by the immunofluorescence method using mouse anti-CD147 antibody. The GFP-kAE1 fusion protein was predominantly expressed at the cell surface and co-localized with the surface marker-CD147 (Fig. 2B: A-C). In contrast, the GFP-kAE1 SAO and GFP-kAE1 G701D fusion proteins showed predominantly intracellular localization with very little cellsurface expression (Fig. 2B: D-F and G-I). The average percentages (mean  $\pm$  SD) of relative cell surface expressions of GFP-kAE1 were  $53.5 \pm 2.5$  (n = 3), GFP-kAE1 SAO  $4.6 \pm 1.5$  (n = 3, p < 0.0005), and GFP-kAE1 G701D  $6.9 \pm 7.6$  (n = 3, p < 0.0001). These confirmed the results as demonstrated above that while kAE1 WT prominently located at the plasma membrane of HEK 293 cells, kAE1 SAO and kAE1 G701D showed greatly decreased or no cell surface expression.

Co-expression and cellular localization of wild-type and mutant kAE1 fusion proteins in HEK 293 cells

To study the effect of mutant kAE1 on the wild-type kAE1 and vice versa, and the effect on each other of the two mutant kAE1 (kAE1 SAO and kAE1 G701D), kAE1-WT co-expressed with either kAE1 SAO or kAE1 G701D, and kAE1 SAO co-expressed with kAE1 G701D were examined in HEK 293 cells. The co-expression of kAE1 WT-Myc with kAE1 WT-HA showed cell surface expression and co-localization of both kAE1 proteins (Figs. 3A-C) with an estimated average percentage of relative cell surface expression of  $48.5 \pm 6.6\%$  (n = 10). Co-expressions of kAE1 WT-Myc with kAE1 SAO-HA or kAE1 WT-Myc with kAE1 G701D-HA showed obvious cell surface expression and co-localization of both wild-type and mutant kAE1 proteins (Figs. 3D-F and G-I) with estimated average percentages of relative cell surface expression of  $43.3 \pm 7.8\%$  (n = 10) and  $48.1 \pm 11.2\%$  (n = 10), respectively. There were no significant differences (p > 0.05) of the estimated average percentages of cell surface expression among these three co-expressions. These results indicate that kAE1 WT could rescue both kAE1 SAO and kAE1 G701D from the intracellular retention (Fig. 2A) to locate

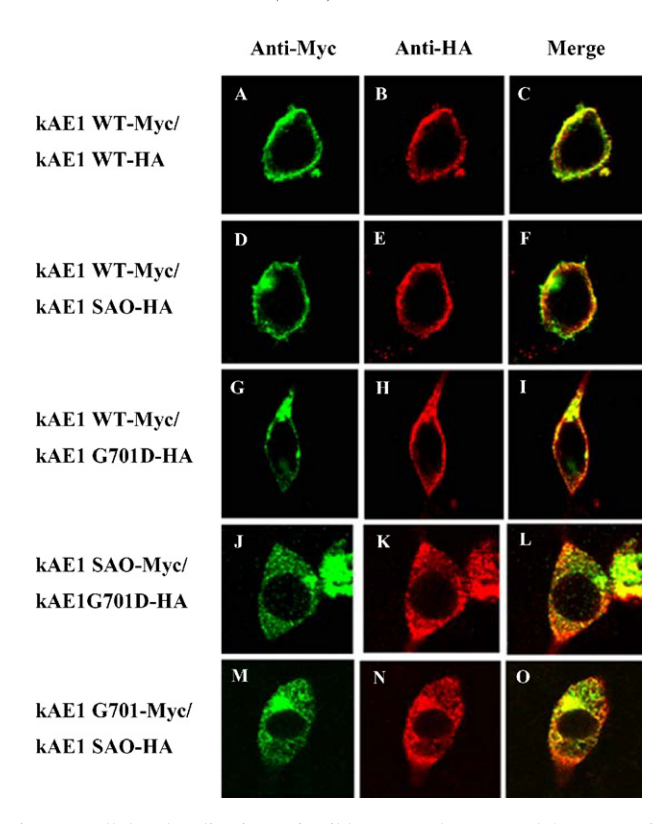


Fig. 3. Cellular localization of wild-type and mutant kAE1 proteins tagged with Myc and HA co-expressed in HEK 293 cells detected by immunofluorescence staining using anti-Myc (green) and anti-HA (red) antibodies. (For interpretation of the references to color in this figure legend, the reader is referred to the web version of this paper.)

at the cell membrane. These would explain the nature of recessive characteristic of these two mutations and also explain the normal phenotype in individuals who carry heterozygous AE1 SAO or G701D mutation.

To mimic kAE1 SAO/G701D compound heterozygous condition, kAE1 SAO-Myc and kAE1 G701D-HA, and kAE1 G701D-Myc and kAE1 SAO-HA were co-expressed in HEK 293 cells. The results of these co-expressions showed predominant retention of both kAE1 mutant fusion proteins in cytoplasm with very little or no cell surface expression in HEK 293 cells expressing kAE1 SAO-Myc and kAE1 G701D-HA (Figs. 3J–L), and kAE1 G701D-Myc and kAE1 SAO-HA (Figs. 3M–O), with estimated average percentages of relative cell surface expression of  $2.0 \pm 1.0\%$  (n = 10) and  $2.4 \pm 1.6\%$  (n = 10), respectively. There were highly significant differences (p < 0.0001) when they were compared with the results of the above three co-expression experiments.

Similar results were obtained when GFP-kAE1 WT was co-expressed with kAE1 WT-HA (Figs. 4A–C), and when kAE1 WT-HA was co-expressed with either GFP-kAE1 G701D (Figs. 4D–F) or GFP-kAE1 SAO (Figs. 4G–I) in HEK 293 cells that the two kAE1 fusion proteins (in each case) were expressed and co-localized on the cell membrane, but when GFP-kAE1 G701D was co-expressed with kAE1 SAO-HA, the two mutant

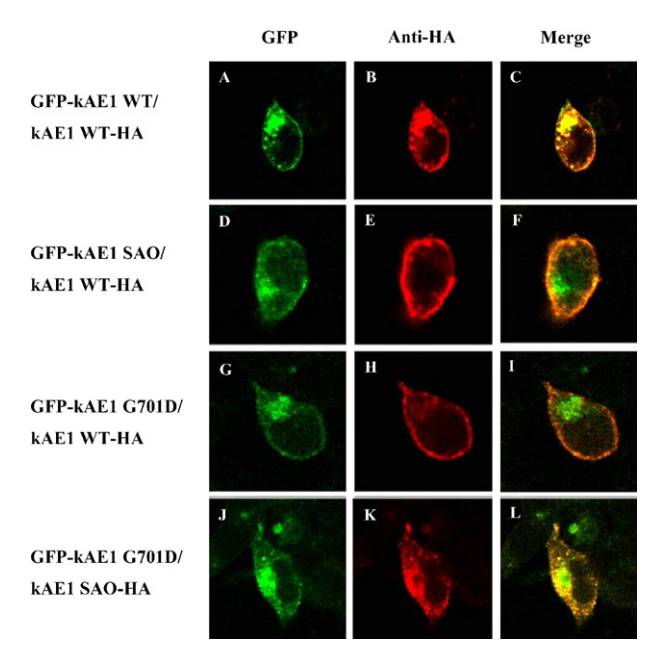


Fig. 4. Cellular localization of wild-type and mutant kAE1 tagged with GFP (green) and HA stained by anti-HA antibody (red) co-expressed in HEK 293 cells. (For interpretation of the references to color in this figure legend, the reader is referred to the web version of this paper.)

kAE1 fusion proteins were mainly co-expressed in the cytoplasm (Figs. 4J–L).

Thus, while kAE1 WT could rescue kAE1 SAO and kAE1 G701D to locate at the cell surface, kAE1 SAO and kAE1 G701D fail to rescue each other to the cell surface, resulting in their intracellular retention. These results would explain the molecular pathogenesis of dRTA caused by the compound heterozygous AE1 SAO/G701D mutations which was first demonstrated in the present study.

Analysis of cell surface expression of kAE1 fusion proteins by flow cytometry

The Myc epitope was inserted at the third extracellular loop at the position 557 of kAE1, allowing the detection of its cell surface expression on HEK 293 cells by immunofluorescence staining method and flow cytometry (see details in Supplementary text and Fig. 5). The relative cell surface expressions of kAE1 SAO-Myc (1.49  $\pm$  0.11%) and kAE1 G701D-Myc (0.89  $\pm$  0.22%) were significantly lower than that of KAE1 WT-Myc (42.90  $\pm$  12.86%, p < 0.005). kAE1 WT-Myc could partially rescue kAE1 SAO-HA or kAE1 G701D-HA to express at the cell surface. The relative cell surface expressions of kAE1 SAO-Myc co-expressed with kAE1 G701D-HA, and of kAE1 G701D-Myc co-expressed with kAE1 SAO-HA were very low (0.57  $\pm$  0.22% and  $0.71 \pm 0.36\%$ , respectively) and significantly different  $(p \le 0.005)$  when compared with that of kAE1 WT-Myc co-expressed with kAE1 WT-HA (Supplementary Fig. 5A).

The results of relative fluorescence intensities in different expression conditions (Supplementary Fig. 5B) were corresponding well to the percentages of relative cell surface expressions present (Supplementary Fig. 5A). Very low values were observed when kAE1 SAO-Myc was co-expressed with kAE1 G701D-HA ( $0.02\pm0.04$ ) and of kAE1 G701D-Myc co-expressed with kAE1 SAO-HA ( $0.03\pm0.05$ ). The results of cell surface expression analyzed by flow cytometry also indicated that kAE1 SAO and kAE1 G701D have impaired trafficking and fail to rescue each other and were unable to traffic the cell surface.

Taken together, the results of this study have showed that kAE1 SAO and kAE1 G701D could form heterodimers with kAE1 WT and could also form heterodimer between each other when they were co-expressed in cultured mammalian (HEK 293) cells. Trafficking of these two mutant kAE1 proteins to cell membrane when they were individually expressed was impaired; therefore, they could not locate at the cell surface. However, their trafficking impairment could be corrected and their cell surface expression could be rescued by co-expression of wild-type kAE1 protein [21,22,29], the so-called 'dominant positive effect' of the wild-type kAE1 on the mutant kAE1 proteins [8]. This would explain the absence of dRTA phenotype in individuals with heterozygous AEI G701D or SAO mutation. The co-expression of kAE1 SAO with kAE1 G701D in the cultured mammalian cells to mimic the compound heterozygous AEI SAO/G701D mutations observed in many patients with this condition demonstrated that the two mutant kAE1 proteins were intracellularly retained. The hetero-dimerization of kAE1 SAO and kAE1 G701D failed to rescue each other to express at the cell surface. This would therefore explain the molecular pathogenesis of the compound heterozygous AEI SAO/G701D mutations as it would cause the loss of kAE1 at basolateral membrane of the α-intercalated cells to function in anion (chloride/bicarbonate) exchange in the kidney of the patients with dRTA and SAO.

#### Acknowledgments

This work was supported by the Thailand National Center for Genetic Engineering and Biotechnology (BIOTEC, Grant No. BT-B-07-MG-B4-4501) and Thailand Research Fund (TRF, Grant No. BRG4880007). The authors thank Professor Reinhart A. Reithmeier (University of Toronto), and Professor Joseph R. Casey (University of Alberta), Canada, for providing plasmid constructs, and Associate Professor Watchara Kasinrerk (Chiangmai University), Thailand for giving anti-CD147 antibody. Dr. Prida Malasit, the Senior Research Scholar of Thailand Research Fund (TRF) and the Directors of Division of Medical Molecular Biology, and BIOTEC-Medical Biotechnology Unit, is grateful for his support.

#### Appendix A. Supplementary data

Supplementary data associated with this article can be found, in the online version, at doi:10.1016/j.bbrc. 2006.09.113.

#### References

- [1] L.C. Showe, M. Ballantine, K. Huebner, Localization of the gene for the erythroid anion exchange protein, band 3 (EMPB3), to human chromosome 17, Genomics 1 (1987) 71–76.
- [2] F.C. Brosius 3rd, S.L. Alper, A.M. Garcia, H.F. Lodish, The major kidney band 3 gene transcript predicts an amino-terminal truncated band 3 polypeptide, J. Biol. Chem. 264 (1989) 7784–7787.
- [3] A. Kollert-Jons, S. Wagner, S. Hubner, H. Appelhans, D. Drenckhahn, Anion exchanger 1 in human kidney and oncocytoma differs from erythroid AE1 in its NH2 terminus, Am. J. Physiol. 265 (1993) F813–F821.
- [4] M.L. Jennings, Oligomeric structure and the anion transport function of human erythrocyte band 3 protein, J. Membr. Biol. 80 (1984) 105– 117
- [5] H.M. Van Dort, R. Moriyama, P.S. Low, Effect of band 3 subunit equilibrium on the kinetics and affinity of ankyrin binding to erythrocyte membrane vesicles, J. Biol. Chem. 273 (1998) 14819– 14826.
- [6] Z.I. Cabantchik, Erythrocyte membrane transport, Novartis Found Symp. 226 (1999) 6–16, discussion 16–19.
- [7] S.L. Alper, J. Natale, S. Gluck, H.F. Lodish, D. Brown, Subtypes of intercalated cells in rat kidney collecting duct defined by antibodies against erythroid band 3 and renal vacuolar H+-ATPase, Proc. Natl. Acad. Sci. USA 86 (1989) 5429–5433.
- [8] P.T. Yenchitsomanus, S. Kittanakom, N. Rungroj, E. Cordat, R.A. Reithmeier, Molecular mechanisms of autosomal dominant and recessive distal renal tubular acidosis caused by SLC4A1 (AE1) mutations, J. Mol. Gen. Med. 1 (2005) 49–62.
- [9] C. Shayakul, S.L. Alper, Inherited renal tubular acidosis, Curr. Opin. Nephrol. Hypertens 9 (2000) 541–546.
- [10] L.J. Bruce, D.L. Cope, G.K. Jones, A.E. Schofield, M. Burley, S. Povey, R.J. Unwin, O. Wrong, M.J. Tanner, Familial distal renal tubular acidosis is associated with mutations in the red cell anion exchanger (Band 3, AE1) gene, J. Clin. Invest. 100 (1997) 1693–1707.
- [11] P. Jarolim, C. Shayakul, D. Prabakaran, L. Jiang, A. Stuart-Tilley, H.L. Rubin, S. Simova, J. Zavadil, J.T. Herrin, J. Brouillette, M.J. Somers, E. Seemanova, C. Brugnara, L.M. Guay-Woodford, S.L. Alper, Autosomal dominant distal renal tubular acidosis is associated in three families with heterozygosity for the R589H mutation in the AE1 (band 3) Cl-/HCO3-exchanger, J. Biol. Chem. 273 (1998) 6380– 6388
- [12] F.E. Karet, F.J. Gainza, A.Z. Gyory, R.J. Unwin, O. Wrong, M.J. Tanner, A. Nayir, H. Alpay, F. Santos, S.A. Hulton, A. Bakkaloglu, S. Ozen, M.J. Cunningham, A. di Pietro, W.G. Walker, R.P. Lifton, Mutations in the chloride-bicarbonate exchanger gene AE1 cause autosomal dominant but not autosomal recessive distal renal tubular acidosis, Proc. Natl. Acad. Sci. USA 95 (1998) 6337–6342.
- [13] S. Weber, M. Soergel, N. Jeck, M. Konrad, Atypical distal renal tubular acidosis confirmed by mutation analysis, Pediatr. Nephrol. 15 (2000) 201–204.
- [14] S. Sritippayawan, S. Kirdpon, S. Vasuvattakul, S. Wasanawatana, W. Susaengrat, W. Waiyawuth, S. Nimmannit, P. Malasit, P.T. Yenchitsomanus, A de novo R589C mutation of anion exchanger 1 causing distal renal tubular acidosis, Pediatr. Nephrol. 18 (2003) 644–648.
- [15] J.A. Quilty, E. Cordat, R.A. Reithmeier, Impaired trafficking of human kidney anion exchanger (kAE1) caused by hetero-oligomer formation with a truncated mutant associated with distal renal tubular acidosis, Biochem. J. 368 (2002) 895–903.
- [16] J.A. Quilty, J. Li, R.A. Reithmeier, Impaired trafficking of distal renal tubular acidosis mutants of the human kidney anion exchanger kAE1, Am. J. Physiol. Renal Physiol. 282 (2002) F810–F820.

- [17] A.M. Toye, L.J. Bruce, R.J. Unwin, O. Wrong, M.J. Tanner, Band 3 Walton, a C-terminal deletion associated with distal renal tubular acidosis, is expressed in the red cell membrane but retained internally in kidney cells, Blood 99 (2002) 342–347.
- [18] M.A. Devonald, A.N. Smith, J.P. Poon, G. Ihrke, F.E. Karet, Non-polarized targeting of AE1 causes autosomal dominant distal renal tubular acidosis, Nat. Genet. 33 (2003) 125–127.
- [19] N. Rungroj, M.A. Devonald, A.W. Cuthbert, F. Reimann, V. Akkarapatumwong, P.T. Yenchitsomanus, W.M. Bennett, F.E. Karet, A novel missense mutation in AE1 causing autosomal dominant distal renal tubular acidosis retains normal transport function but is mistargeted in polarized epithelial cells, J. Biol. Chem. 279 (2004) 13833–13838.
- [20] V.S. Tanphaichitr, A. Sumboonnanonda, H. Ideguchi, C. Shayakul, C. Brugnara, M. Takao, G. Veerakul, S.L. Alper, Novel AE1 mutations in recessive distal renal tubular acidosis. Loss-of-function is rescued by glycophorin A, J. Clin. Invest. 102 (1998) 2173–2179.
- [21] S. Kittanakom, E. Cordat, V. Akkarapatumwong, P.T. Yenchitsomanus, R.A. Reithmeier, Trafficking defects of a novel autosomal recessive distal renal tubular acidosis mutant (S773P) of the human kidney anion exchanger (kAE1), J. Biol. Chem. 279 (2004) 40960– 40971
- [22] E. Cordat, S. Kittanakom, P.T. Yenchitsomanus, J. Li, K. Du, G.L. Lukacs, R.A. Reithmeier, Dominant and recessive distal renal tubular acidosis mutations of kidney anion exchanger 1 induce distinct trafficking defects in MDCK cells, Traffic 7 (2006) 117–128
- [23] S. Vasuvattakul, P.T. Yenchitsomanus, P. Vachuanichsanong, P. Thuwajit, C. Kaitwatcharachai, V. Laosombat, P. Malasit, P. Wilairat, S. Nimmannit, Autosomal recessive distal renal tubular acidosis associated with Southeast Asian ovalocytosis, Kidney Int. 56 (1999) 1674–1682.
- [24] P.T. Yenchitsomanus, N. Sawasdee, A. Paemanee, T. Keskanokwong, S. Vasuvattakul, S. Bejrachandra, W. Kunachiwa, S. Fucharoen, P. Jittphakdee, W. Yindee, C. Promwong, Anion exchanger 1 mutations associated with distal renal tubular acidosis in the Thai population, J. Hum. Genet. 48 (2003) 451–456.
- [25] L.J. Bruce, O. Wrong, A.M. Toye, M.T. Young, G. Ogle, Z. Ismail, A.K. Sinha, P. McMaster, I. Hwaihwanje, G.B. Nash, S. Hart, E. Lavu, R. Palmer, A. Othman, R.J. Unwin, M.J. Tanner, Band 3 mutations, renal tubular acidosis and South-East Asian ovalocytosis in Malaysia and Papua New Guinea: loss of up to 95% band 3 transport in red cells, Biochem. J. 350 (Pt 1) (2000) 41–51.
- [26] K.E. Choo, T.K. Nicoli, L.J. Bruce, M.J. Tanner, A. Ruiz-Linares, O.M. Wrong, Recessive distal renal tubular acidosis in Sarawak caused by AE1 mutations, Pediatr. Nephrol. 21 (2006) 212–217.
- [27] A.E. Schofield, D.M. Reardon, M.J. Tanner, Defective anion transport activity of the abnormal band 3 in hereditary ovalocytic red blood cells, Nature 355 (1992) 836–838.
- [28] J.D. Groves, S.M. Ring, A.E. Schofield, M.J. Tanner, The expression of the abnormal human red cell anion transporter from South-East Asian ovalocytes (band 3 SAO) in Xenopus oocytes, FEBS Lett. 330 (1993) 186–190.
- [29] J.C. Cheung, E. Cordat, R.A. Reithmeier, Trafficking defects of the Southeast Asian ovalocytosis deletion mutant of anion exchanger 1 membrane proteins, Biochem. J. 392 (2005) 425–434.
- [30] M.A. Lopata, D.W. Cleveland, B. Sollner-Webb, High level transient expression of a chloramphenicol acetyl transferase gene by DEAEdextran mediated DNA transfection coupled with a dimethyl sulfoxide or glycerol shock treatment, Nucleic Acids Res. 12 (1984) 5707– 5717.



## Proteomic Identification of Altered Proteins in Skeletal Muscle During Chronic Potassium Depletion: Implications for Hypokalemic Myopathy

Visith Thongboonkerd,\*,† Rattiyaporn Kanlaya,†,‡ Supachok Sinchaikul,§ Paisal Parichatikanond,∥ Shui-Tein Chen,§,⊥ and Prida Malasit†,#

Medical Molecular Biology Unit, Office for Research and Development, Faculty of Medicine Siriraj Hospital, Mahidol University, Bangkok, Thailand, Department of Immunology, Faculty of Medicine Siriraj Hospital, Mahidol University, Bangkok, Thailand, Institute of Biological Chemistry and Genomic Research Center, Academia Sinica, Taipei, Taiwan, Department of Pathology, Faculty of Medicine Siriraj Hospital, Mahidol University, Bangkok, Thailand, Institute of Biochemical Sciences, College of Life Science, National Taiwan University, Taipei, Taiwan, and Medical Biotechnology Unit, National Center for Genetic Engineering and Biotechnology, National Science and Technology Development Agency, Bangkok, Thailand

#### Received April 2, 2006

Prolonged potassium depletion is a well-known cause of myopathy. The pathophysiology of hypokalemic myopathy, however, remains unclear. We performed a gel-based, differential proteomics study to define altered proteins in skeletal muscles during chronic potassium depletion. BALB/c mice were fed with normal chow (0.36%  $K^+$ ) or  $K^+$ -depleted (KD) diet (<0.001%  $K^+$ ) for 8 weeks (n = 5 in each group). Left gastrocnemius muscles were surgically removed from each animal. Histopathological examination showed mild-degree infiltration of polymornuclear and mononuclear cells at the interstitium of the KD muscles. Extracted proteins were resolved with two-dimensional electrophoresis (2-DE), and visualized with Coomassie Brilliant Blue R-250 stain. Quantitative intensity analysis revealed 16 up-regulated protein spots in the KD muscles, as compared to the controls. These differentially expressed proteins were subsequently identified by peptide mass fingerprinting and by quadrupole time-of-flight tandem mass spectrometry (Q-TOF MS/MS). Most of the altered proteins induced by chronic potassium depletion were muscle enzymes that play significant roles in several various metabolic pathways. Other upregulated proteins included myosin-binding protein H, alpha-B Crystallin, and translationally controlled tumor protein (TCTP). These findings may lead to a new roadmap for research on hypokalemic myopathy, to better understanding of the pathophysiology of this medical disease, and to biomarker discovery.

Keywords: potassium • hypokalemia • myopathy • muscle • enzymes • proteomics • proteome

#### Introduction

Hypokalemia, which is generally defined as a serum K<sup>+</sup> of less than 3.5 mmol/L, is one of the most common electrolyte disorders encountered in clinical practice and found in more than 20% of hospitalized patients.<sup>1</sup> It is also common in outpatients who take thiazide diuretics for treatment of hypertension, with an incidence of up to 48%.<sup>2</sup> Hypokalemia may

\* To whom correspondence should be addressed. Visith Thongboonkerd, MD, FRCPT, Medical Molecular Biology Unit, Office for Research and Development, 12th Floor Adulyadej Vikrom Building, 2 Prannok Road, Siriraj Hospital, Bangkoknoi, Bangkok 10700, Thailand; Phone/Fax: +66-2-4184793; E-mail: thongboonkerd@dr.com (or) vthongbo@yahoo.com.

be asymptomatic if the deficit is temporary and the degree of the deficit is modest to mild (3.0–3.5 mmol/L), but it can be a cause of death when the degree of the deficit is severe (<3.0 mmol/L) and the dysregulation is left untreated. Prolonged  $K^+$  deficiency can affect several organ systems, particularly cardiovascular, gastrointestinal, renal, and musculoskeletal systems.  $^{3-5}$  Muscular defects from chronic  $K^+$  depletion have been defined as "hypokalemic myopathy", a disease known for quite some time, but the molecular mechanisms or the links between  $K^+$  deficiency and muscle injury remain unclear.  $^{6-10}$ 

Previously, several studies had evaluated physiological changes in skeletal muscles during  $K^+$  depletion. These reports, however, focused only on roles of sodium pumps and the balance of cellular cations. None of these studies had explored the global alterations in muscle proteins during prolonged  $K^+$  depletion, the information of which may imply the pathogenic mechanisms of hypokalemic myopathy. In the postgenomic era, proteomic technologies are widely available and have been

 $<sup>^\</sup>dagger$  Office for Research and Development, Faculty of Medicine Siriraj Hospital.

<sup>&</sup>lt;sup>‡</sup> Department of Immunology, Faculty of Medicine Siriraj Hospital.

<sup>§</sup> Institute of Biological Chemistry and Genomic Research Center.

Department of Pathology, Faculty of Medicine Siriraj Hospital.

<sup>&</sup>lt;sup>⊥</sup> National Taiwan University.

<sup>\*</sup> National Science and Technology Development Agency.

proven to be useful to unravel the pathophysiology of human diseases. 14-16 There are several studies that have applied proteomics to examining skeletal muscle proteome. 17-20 However, none of these available references has adopted proteomics to hypokalemic myopathy.

The present study has utilized proteomic methodology to identify changes in protein expression in skeletal muscles of mice exposed to prolonged  $K^+$  depletion. Hypokalemia was induced by giving ad libertum  $K^+$ -depleted (KD) diet to BALB/c mice for 8 weeks, whereas the control mice received normal-  $K^+$  chow. A gel-based, differential proteomics study of left gastrocnemius muscles revealed alterations in the expression of 16 muscle proteins in the KD mice. Among these altered proteins, 15 were identified by quadrupole time-of-flight (Q-TOF) mass spectrometry (MS) and tandem mass spectrometry (MS/MS). Functional significance and potential roles of these identified proteins in hypokalemic myopathy are discussed.

#### **Materials and Methods**

**Animals and Diets.** Young male BALB/c mice (n = 5 in each group; total n = 10) with comparable initial body weights (35.06)  $\pm$  1.12 vs 35.82  $\pm$  0.68 g; p = 0.823) were used in the present study. They were fed with ad libertum normal-K<sup>+</sup> (0.36% K<sup>+</sup>; #TD97214; Harland Teklad, Madison, WI) or KD (<0.001% K+; #TD88239) chow for 8 weeks. All other elements in the diet (including protein, casein, D,L-methionine, sucrose, corn starch, corn oil, cellulose, mixed vitamin, ethoxyquin, calcium phosphate, calcium carbonate, sodium chloride, magnesium oxide, magnesium sulfate, ferric citrate, manganous carbonate, zinc carbonate, cupric carbonate, sodium iodate, and sodium selenite) were identical between the two types of diets. After 8 weeks of differential diets, the mice were sacrificed and the left gastrocnemius muscles were surgically removed for further proteomic analysis. All studies of animals were in accordance with the Institutional Animal Care and Use Committee and The Guide for the Care and Use of Laboratory Animals.

Protein Extraction for Proteomic Analysis. Muscle was excised into several thin slices and the contaminated blood was washed with ice-cold PBS. The tissue was then briskly frozen in liquid nitrogen, ground to powder, resuspended in a buffer containing 7 M urea, 2 M thiourea, 4% 3-[(3-cholamidopropyl)dimethylamino]-1-propanesulfonate (CHAPS), 2% (v/v) ampholytes (pH 3-10), 120 mM dithiothreitol (DTT), and 40 mM Tris-base, and incubated at 4 °C for 30 min. After low-speed centrifugation (12 000 g for 5 min), the supernatant was saved and the protein concentration was measured by spectrophotometry using Bio-Rad Protein Assay (Bio-Rad Laboratories, Hercules, CA) based on Bradford's method. Because urea, thiourea, CHAPS, and other compositions in the sample/lysis buffer can interfere with the protein estimation, we generated the standard curve using bovine serum albumin at the concentrations of 0, 2, 5, 7, and  $10 \mu g/\mu L$  in the same sample/lysis buffer to make sure that the standards and the samples had the same background that might occur due to chemical interference. Muscle proteins extracted from each animal were further resolved in individual 2-D gels; n = 5 gels (from 5 animals) for each group; total n = 10 gels.

**Two-Dimensional Electrophoresis (2-DE) and Staining.** Immobiline DryStrip, linear pH 3-10, 7-cm long (Amersham Biosciences, Uppsala, Sweden), was rehydrated overnight with 200  $\mu$ g total protein (equal loading for each sample) that was premixed with rehydration buffer containing 7 M urea, 2 M thiourea, 2% CHAPS, 2% (v/v) ampholytes (pH 3-10), 120 mM

DTT, 40 mM Tris-base, and bromophenol blue (to make the final volume of 150  $\mu$ L per strip). The first dimensional separation (IEF) was performed in Ettan IPGphor II IEF System (Amersham Biosciences) at 20 °C, using stepwise mode to reach 9 000 V·h. After completion of the IEF, proteins on the strip were equilibrated in a buffer containing 6 M urea, 130 mM DTT, 30% glycerol, 112 mM Tris base, 4% sodium dodecyl sulfate (SDS), and 0.002% bromophenol blue for 10 min, and then with another buffer containing 6 M urea, 135 mM iodoacetamide, 30% glycerol, 112 mM Tris base, 4% SDS, and 0.002% bromophenol blue for 10 min. The IPG strip was then transferred onto 12% acrylamide slab gel (8  $\times$  9.5 cm), and the second dimensional separation was performed in SE260 Mini-Vertical Electrophoresis Unit (Amersham Biosciences) with the current  $20 \,\mu\text{A/gel}$  for 1.5 h. Separated protein spots were then visualized using Coomassie Brilliant Blue R-250 stain (Fluka Chemica AG, Buchs, Switzerland).

Spot Analysis and Matching. Image Master 2D Platinum (Amersham Biosciences) software was used for matching and analysis of protein spots on 2-D gels. Parameters used for spot detection were (i) minimal area = 10 pixels, (ii) smooth factor = 2.0, and (iii) saliency = 2.0. A reference gel was created from an artificial gel combining all of the spots presenting in different gels into one image. The reference gel was then used for matching of corresponding protein spots between gels. Background subtraction was performed and the intensity volume of individual spot was normalized with total intensity volume (summation of the intensity volumes obtained from all spots in the same 2-D gel). Variability of 2-D spot pattern was evaluated by determining the coefficient of variation (CV) of the normalized intensity of corresponding spot across different gels (%CV = standard deviation/mean  $\times$  100%). Comparisons between groups were performed using unpaired t test. P values less than 0.05 were considered statistically significant.

In-Gel Tryptic Protein Digestion. Differentially expressed protein spots were excised from the 2-D gels and the gel pieces were washed with 200  $\mu$ L of 50% acetonitrile (ACN)/25 mM NH<sub>4</sub>HCO<sub>3</sub> buffer (pH 8.0) for 15 min twice. The gel pieces were then washed once with 200  $\mu$ L of 100% ACN and dried using a Speed Vac concentrator (Savant, Holbrook, NY). Dried gel pieces were swollen with 10 µL of 1% (w/v) trypsin (Promega, Madison WI) in 25 mM NH<sub>4</sub>HCO<sub>3</sub>. The gel pieces were then crushed with siliconized blue stick and incubated at 37 °C for at least 16 h. Peptides were subsequently extracted twice with  $50 \,\mu\text{L}$  of 50% ACN/5% trifluoroacetic acid (TFA); the extracted solutions were then combined and dried with the Speed Vac concentrator. The peptide pellets were then resuspended in  $10 \,\mu\text{L}$  of 0.1% TFA and the resuspended solutions were purified using ZipTip<sub>C18</sub> (Millipore, Bedford, MA). Ten microliters of sample was drawn up and down in the ZipTip for 10 times and then washed with 10  $\mu$ L of 0.1% formic acid by drawing up and expelling the washing solution for 3 times. The peptides were finally eluted with 5  $\mu$ L of 75% ACN/0.1% formic acid.

Protein Identification by Q-TOF MS and MS/MS. The proteolytic samples were premixed 1:1 with the matrix solution (5 mg/mL  $\alpha$ -cyano-4-hydroxycinnamic acid (CHCA) in 50% ACN, 0.1% v/v TFA and 2% w/v ammonium citrate) and spotted onto the 96-well MALDI (matrix-assisted laser desorption/ionization) sample stage. The samples were analyzed by the Q-TOF Ultima MALDI instrument (Micromass, Manchester, UK), which was fully automated with predefined probe motion pattern and the peak intensity threshold for switching over from MS survey scanning to MS/MS, and from one MS/MS to

research articles Thongboonkerd et al.

another. Within each sample well, parent ions that met the predefined criteria (any peak within the m/z 800–3000 range with intensity above 10 count  $\pm$  include/exclude list) were selected for CID MS/MS using argon as the collision gas and a mass dependent  $\pm 5$  V rolling collision energy until the end of the probe pattern was reached (all details are available at http://proteome.sinica.edu.tw).

For peptide mass fingerprinting, both MASCOT (http:// www.matrixscience.com) and ProFound (http://129.85.19.192/ profound\_bin/WebProFound.exe) search engines were used. Proteins were identified based on the assumptions that peptides were monoisotopic, oxidized at methionine residues and carbamidomethylated at cysteine residues. The search was performed using the mammalian protein database of the NCBI (National Center for Biotechnology Information). A mass tolerance of 50 ppm was used and up to 1 missed trypsin cleavage was allowed. Identities with probability-based MOWSE (molecular weight search) scores > 69 (for MASCOT) and/or Z scores > 1.65 (for ProFound) were considered as "significant hits". For MS/MS peptide sequence identification, the MASCOT search engine was employed. Search parameters allowed were similar to those for PMF. Peptides with ions scores >37 were considered as "significant hits". Only significant hits from peptide mass fingerprinting and/or MS/MS peptide ion search were reported in the Results.

**2-D Western Blotting.** After the completion of 2-DE as described above, proteins were transferred onto a nitrocellulose membrane and nonspecific bindings were blocked with 5% milk in PBS for 1 h. The membrane was then incubated with rabbit polyclonal anti- $\beta$ -enolase antibody (1:200 in 5% milk in PBS) (Santa Cruz Biotechnology, Inc., Santa Cruz, CA) at room temperature for 1 h. After washing, the membrane was further incubated with swine anti-rabbit IgG conjugated with horse-radish peroxidase (1:1000 in 5% milk in PBS) (Dako, Glostrup, Denmark) at room temperature for 1 h. Reactive protein spots were then visualized with SuperSignal West Pico chemiluminescence substrate (Pierce Biotechnology, Inc., Rockford, IL).

Measurement of Serum Creatine Kinase Levels. Total CK level was measured using a standard Oliver-Rosalki assay, as described previously.<sup>21,22</sup> CK-MM was examined by Western blot analysis. Details of the blotting procedures were the same as described above, except only for the antibody, which was goat anti-CK-MM conjugated with horseradish peroxidase (Biocheck, Inc., Foster City, CA). CK-MB level was measured using a CK-MB Enzyme Immunoassay Kit (Biocheck, Inc.). Positive control was the CK-MB standards containing 0, 7.5, 15, 50, 100, and 200 ng/mL CK-MB. Color intensity was measured spectrophotometrically at λ450 nm.

#### **Results and Discussion**

Clinical Data and Histopathological Findings. The mice in both groups had comparable amounts of dietary intake (Figure 1). After 8 weeks of differential diets, the mice were sacrificed and the left gastrocnemius muscles were surgically removed for histopathological examination and proteomic analysis. Plasma K<sup>+</sup> levels on sacrificed date were  $4.46 \pm 0.23$  and  $1.51 \pm 0.21$  mmol/L for control and KD mice, respectively (p < 0.0001). In addition to severe hypokalemia, the KD mice also developed metabolic alkalosis. Plasma  $\text{HCO}_3^-$  levels were 25.67  $\pm$  0.38 and 31.90  $\pm$  2.11 mmol/L for control and KD mice, respectively (p < 0.005). Histopathological examination using Hematoxylin-Eosin stain showed only mild-degree infiltration of polymorphonuclear and mononuclear cells at some areas

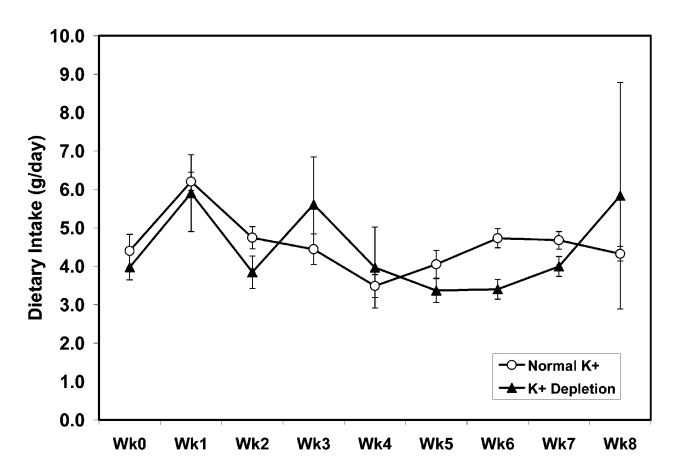


**Figure 1.** Dietary intake. The animals in both groups had comparable amounts of food intake throughout the study (except at week 2 and 6, when the KD mice had slightly less amounts of diet).

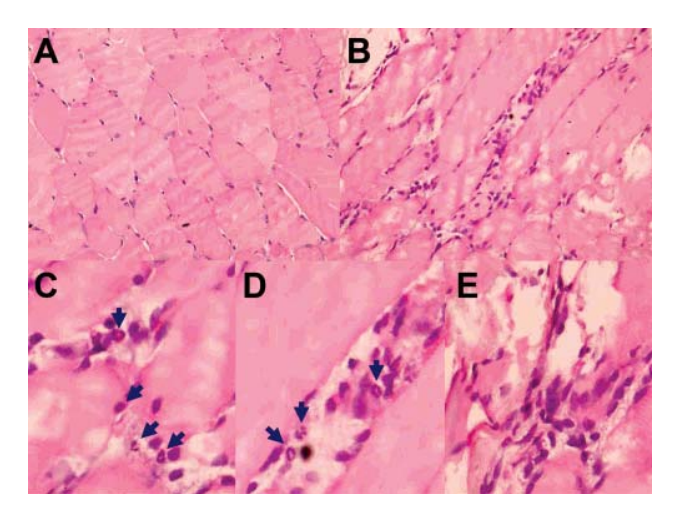
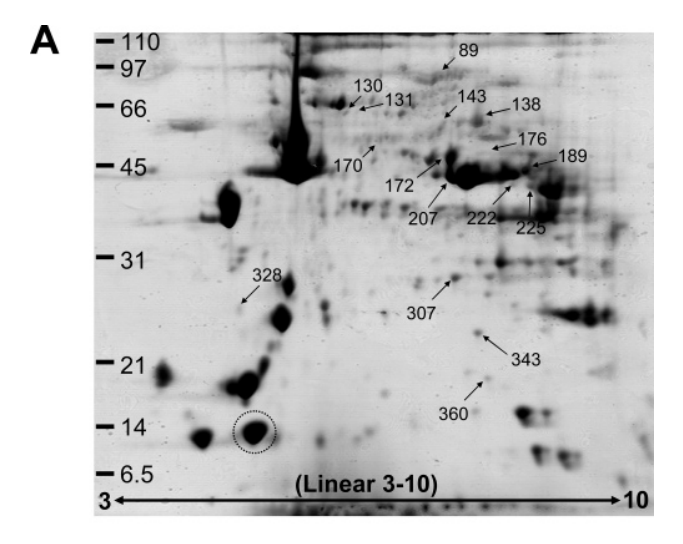


Figure 2. Histopathological findings. Sections of left gastrocnemius muscles were stained with hematoxylin-eosin. (A) Representative section of the normal murine muscles. (B) Representative section of the KD murine muscles that shows mild-degree infiltration of polymorphonuclear and mononuclear cells at some areas of the interstitium. The mentioned abnormal finding was found only in a few areas per section, whereas the remaining areas appeared normal. There was no vacuolization or inclusion body observed. (C–E) Polymorphonuclear (indicated with arrow heads) and mononuclear cells. Original magnification powers were 200× in (A) and (B) and 400× in (C–E).

of the interstitium of the KD muscles (Figure 2). The mentioned abnormal finding was found only in a few areas per section, whereas the remaining areas appeared normal. Neither vacuolization nor inclusion body was observed. The absence of vacuolization in our murine model of hypokalemic myopathy was not surprising as vacuolization was not found in all cases of human hypokalemic myopathy. In addition, degree and duration of potassium depletion might be the important factors for the characteristic vacuolization.

**Altered Proteome in K** $^+$ -**Depleted Muscles.** The muscles were ground and resuspended in a lysis buffer (detailed in Materials and Methods section). Muscle proteins extracted from each animal were resolved in individual 2-D gel (n = 5 gels for 5 animals in each group) using board-range (p*I* 3-10, linear) IPG strips. The separated proteins were then visualized with



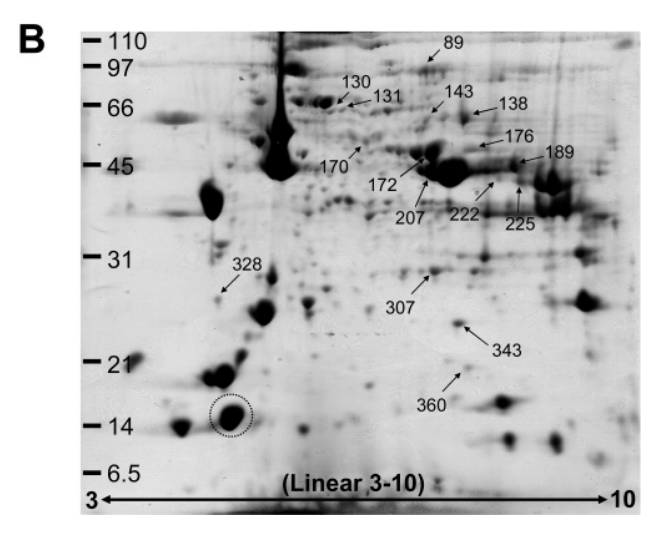


Figure 3. Proteome map of differentially expressed proteins between normal and KD mice. (A) Representative 2-D gel of the normal murine muscle proteome. (B) Representative 2-D image for muscle proteome of the KD mice. Equal amount of 200  $\mu$ g total protein extracted from left gastrocnemius muscles was loaded in individual IPG strip and resolved by 2-DE (n=5 gels from 5 different animals in each group). Separated proteins were then visualized by Coomassie Blue R-250 stain. Quantitative intensity analysis was performed and only significant differences between the two groups were subjected to identification, using MS peptide mass fingerprinting and MS/MS peptide sequencing, and are labeled. Numbers of protein spots correspond to those reported in Tables 1 and 2. The spot in the circled area and spot #307 were selected for further analysis of the variability (see

Coomassie Brilliant Blue R-250 stain. Using 2-D analysis software and highly stringent criteria for spot detection (described in details in Materials and Methods section), approximately 260 protein spots were visualized in each 2-D gel. Figure 3A illustrates a representative 2-D gel of the normal controls, whereas Figure 3B shows a representative 2-D gel of the KD muscles.

Quantitative intensity analysis revealed significantly differential expression of 16 protein spots between the two groups (Figure 3 and Table 1). Interestingly, the intensity levels of all differentially expressed spots were increased in the KD muscles. The degree of the up-regulation ranged from 1.21- to 8.27-fold.

Using MALDI-MS, 13 of these altered proteins were successfully identified (Table 1). The identities of 13 proteins obtained from peptide mass fingerprinting were confirmed by Q-TOF MS/MS sequencing (Table 2). Q-TOF MS/MS analyses not only provided consistent results with those obtained from peptide mass fingerprinting but also identified 2 additional proteins that were not able to be identified by peptide mass fingerprinting (spots # 343 and 360). Sequences of the peptides identified by Q-TOF MS/MS are provided in Table 2.

To confirm our proteomic data, 2-D Western blot analysis of  $\beta$ -enolase was performed. Figure 4 clearly illustrates that expression levels of at least two forms of  $\beta$ -enolase were obviously increased in the KD muscles. This finding was consistent with the proteomic data, in which two forms of  $\beta$ -enolase were detected to be up-regulated in the KD muscles.

Brief Descriptions and Functional Significance of the Altered Muscle Proteins. Of the 15 spots representing 14 unique proteins that were identified by either MS peptide mass fingerprinting or MS/MS sequencing, most of them were muscle enzymes, except only for myosin-binding protein H (#131), translationally controlled tumor protein, translationally controlled 1 (#328), and alpha-B Crystallin (#343). Using the Pathway Tools (http://bioinformatics.ai.sri.com/ptools/),<sup>23–25</sup> more details of these enzymes including their descriptions and metabolic pathways could be obtained and are provided in Table 3. Because these metabolic pathways (totally 25 pathways) are crucial for cellular function and bioenergetics, the up-regulation of several enzymes involving in these multiple pathways during prolonged K<sup>+</sup> deprivation might be associated with the pathogenic mechanisms of hypokalemic myopathy. Further functional studies are required to address roles or functional significance of these altered muscle enzymes in hypokalemia-induced muscle injury.

On the other hand, the up-regulation of muscle enzymes may be the result of muscle damage, and elevated muscle enzymes can be used as the biomarkers. Creatine kinase (CK) reversibly catalyzes the transfer of phosphate between ATP and various phosphogens (e.g., creatine phosphate). CK isoenzymes also play a central role in energy transduction in tissues with large, fluctuating energy demands, such as skeletal muscle, heart, brain and spermatozoa.<sup>26</sup> In clinical practice, the increase in serum CK level in the absence of cardiac or brain infarction indicates significant muscle damage and is generally used as the diagnostic marker for rhabdomyolysis and/or muscle injury.10 In the present study, we identified the increase in muscle isoform of CK in murine skeletal muscles. Additional findings were severe hypokalemia and metabolic alkalosis. These data therefore strengthen our model of hypokalemic myopathy.

Alpha-B Crystallin belongs to the small heat shock protein (HSP) family.<sup>27</sup> This protein was initially found in eye lens to serve the function for transparency and refractive index of the lens. However, its expression is not limited only to eye lens.<sup>28</sup> It is generally known that various HSPs are expressed in skeletal muscles, including small HSPs (i.e., ubiquitin, alpha-B Crystallin, HSP20, and HSP27), HSP60, HSP70, and HSP90. There is evidence suggesting that HSP expression in muscle fiber is type-specific.<sup>29</sup> Like other chaperones, alpha-B Crystallin prevents stress-induced protein denaturation and precipitation by binding to unfolded or denatured proteins, thereby suppressing irreversible protein aggregation and consecutive cell damage.<sup>30</sup> We therefore propose that the increase in muscle alpha-B

research articles Thongboonkerd et al.

Table 1. Differentially Expressed Muscle Proteins in Normal vs K<sup>+</sup>-depleted (KD) Mice

	•												
spot no.	protein	NCBI IDa	accession	MS MOWSE Score	MS Z Score	MS/MS Ion Score	%coverage (MS, MS/MS)	theoretical p <i>I</i> /MW (kDa)	$\begin{array}{c} \text{estimated} \\ pI/\text{MW} \\ \text{(kDa)} \end{array}$	$\begin{array}{c} \text{intensity} \\ \text{(Normal)} \\ \text{(Mean} \pm \text{SEM)} \end{array}$	intensity (KD) (Mean ± SEM)	ratio (KD /Normal)	P values
88	muscle glycogen phosphorylase Mus musculus	gi 15277968	AAH12961	54	2.43	126	15, 4	6.7/98	7.3/91	$0.0376 \pm 0.0198$	$0.2236 \pm 0.0625$	5.95	0.022
130	dihydrolipoamide S-acetyltransferase precursor [Mus musculus]	gi 16580128	AAL02400	72	2.43	39	29, 3	5.7/59	6.2/66	$0.0054 \pm 0.0054$	$0.0445 \pm 0.0048$	8.27	0.001
131	myosin-binding protein H (MyBP-H) (H-protein)	gi 6093458	P70402	124	2.43	105	44, 8	5.7/53	6.3/67	$0.0054 \pm 0.0035$	$0.0321 \pm 0.0081$	5.97	0.017
138	pyruvate kinase M [Mus musculus]	gi 551295	BAA07457	153	2.43	128	37, 13	7.6/58	7.8/63	$0.2506 \pm 0.0372$	$0.3606 \pm 0.0329$	1.44	0.049
143	dihydrolipoamide dehydrogenase [Mus musculus]	gi 2078522	AAC53170	92	2.43	80	23, 8	8.0/55	7.4/62	$0.0406 \pm 0.0175$	$0.0891 \pm 0.0093$	2.19	0.040
170	unidentified	$NA^b$	$\mathrm{NA}^{b}$	$NA^{b}$	$NA^{b}$	$NA^b$	NA, NA $^b$	$NA/NA^b$	6.6/53	$0.0426 \pm 0.0112$	$0.0848 \pm 0.0142$	1.99	0.048
172	enolase 3, beta muscle [Mus musculus]	gi 15488630	AAH13460	257	2.43	261	56, 12	6.7/47	7.4/49	$0.8635 \pm 0.0413$	$1.1278 \pm 0.0595$	1.31	0.006
176	enolase 3, beta muscle [Mus musculus]	gi 15488630	AAH13460	193	2.43	114	50, 6	6.7/47	7.9/50	$0.0209 \pm 0.0209$	$0.1392 \pm 0.0169$	6.65	0.002
189	phosphoglycerate kinase (EC 2.7.2.3) - mouse	gi 91176	A25567	92	2.43	142	29, 7	7.5/45	8.4/44	$0.2036 \pm 0.1260$	$0.6682 \pm 0.0162$	3.28	9000
207	creatine kinase, muscle [Mus musculus]	gi 6671762	NP_031736	209	2.43	286	56, 20	6.6/43	7.4/43	$0.8461 \pm 0.0278$	$1.0394 \pm 0.0536$	1.23	0.013
222	NAD(P) dependent steroid dehydrogenase-like [Mus musculus]	gi 18043286	AAH19945	$\mathrm{NA}^{b}$	2.43	$\mathrm{NA}^{b}$	$21$ , NA $^b$	8.4/41	8.2/42	$0.0292 \pm 0.0185$	$0.0828 \pm 0.0108$	2.83	0.037
225	aldolase 1, A isoform [Mus musculus]	gi 42490830	AAH66218	88	2.43	149	36, 16	8.5/40	8.5/42	$0.1010 \pm 0.0441$	$0.2631 \pm 0.0249$	2.61	0.013
307	triosephosphate isomerase 1 [Mus musculus]	gi 6678413	NP_033441	158	2.43	346	53, 24	6.9/27	7.4/29	$0.1678 \pm 0.0101$	$0.2035 \pm 0.0075$	1.21	0.022
328	tumor protein, translationally controlled 1 [Mus musculus]	gi 6678437	NP_033455	51	2.43	261	25, 22	4.8/20	4.8/26	$0.0223 \pm 0.0092$	$0.0565 \pm 0.0081$	2.53	0.024
343	crystallin, alpha B [Mus musculus]	gi 6753530	$NP_034094$	$NA^{b}$	$NA^{b}$	22	NA, 9	6.8/20	7.7/24	$0.0530 \pm 0.0073$	$0.1005 \pm 0.0180$	1.90	0.040
360	nucleoside- diphosphate kinase 1 [Mus musculus]	gi 13542867	AAH05629	$\mathrm{NA}^{b}$	$\mathrm{NA}^b$	47	NA, 7	6.8/17	7.9/20	$0.0576 \pm 0.0062$	$0.0821 \pm 0.0077$	1.43	0.037

 $^a$  NCBI = National Center for Biotechnology Information  $\,^b$  NA = Not available

Table 2. Sequencing of Differentially Expressed Proteins Using Q-TOF MS/MS

		ion	coverage		_
spot no.	protein	scores	(%)	identified peptides	residues
89	muscle glycogen phosphorylase [Mus musculus]	126	4	ARPEFTLPVHFYGR	193-206
				VLYPNDNFFEGKELR	279 - 293
				HLQIIYEINQR	400 - 410
130	dihydrolipoamide S-acetyltransferase precursor [Mus musculus]	39	3	VAPAPAGVFTDIPISNIR	324-341
131	myosin-binding protein H (MyBP-H) (H-protein)	105	8	NLALGDKFFLR	140 - 150
				ASIDILVIEKPGPPSSIK	268 - 280
				TGQWFTVLER	316 - 325
138	pyruvate kinase M [Mus musculus]	128	13	LNFSHGTHEYHAETIK	74 - 89
				EATESFASDPILYRPVAVALDTK	93-115
				FGVEQDVDMVFASFIR	231-246
1.40	19 1 1 2 21 11 1 04 1 1	0.0	0	RFDEILEASDGIMVAR	279-294
143	dihydrolipoamide dehydrogenase [Mus musculus]	80	8	ALLNNSHYYHMAHGKDFASR	90-109
				IGKFPFAANSR	418-428
172	enolase 3, beta muscle [Mus musculus]	261	10	VCHAHPTLSEAFR	483-495 184-197
172	enotase 5, beta muscle [Mus musculus]	201	12	IGAEVYHHLKGVIK TAIQAAGYPDKVVIGMDVAASEFYR	229-253
				IEEALGDKAVFAGR	413-426
176	enolase 3, beta muscle [Mus musculus]	114	6	IGAEVYHHLK	184-193
170	enotase 3, beta muscle [was musculus]	114	Ü	IGAEVYHHLKGVIK	184-197
				IEEALGDKAVFAGR	413-426
189	phosphoglycerate kinase (EC 2.7.2.3) - mouse	142	7	LGDVYVNDAFGTAHR	157-171
100	phosphogrycerate kinase (20 2.7.2.6) inouse	112	•	ALESPERPFLAILGGAK	200-216
207	creatine kinase, muscle [Mus musculus]	286	20	GYTLPPHCSR	139-148
				SFLVWVNEEDHLR	224-236
				AGHPFMWNEHLGYVLTCPSNLGTGLR	267-292
				HPKFEEILTR	305-314
				GTGGVDTAAVGAVFDISNADR	321-341
225	aldolase 1, A isoform [Mus musculus]	149	16	PHPYPALTPEQK	2-13
				ADDGRPFPQVIK	88 - 99
				IGEHTPSALAIMENANVLAR	154 - 173
				CPLLKPWALTFSYGR	290 - 304
307	triosephosphate isomerase 1 [Mus musculus]	346	24	DLGATWVVLGHSER	86 - 99
				RHVFGESDELIGQK	100 - 113
				HVFGESDELIGQK	101 - 113
				VSHALAEGLGVIACIGEK	114-131
				VVLAYEPVWAIGTGK	161-175
328	tumor protein, translationally-controlled 1 [Mus musculus]	261	22	DLISHDELFSDIYK	6-19
				DLISHDELFSDIYKIR	6-21
				IREIADGLCLEVEGK	20 - 34
				GKLEEQKPER	101 - 110
343	crystallin, alpha B [Mus musculus]	55	9	TIPITREEKPAVAAAPK	158-174
360	nucleoside-diphosphate kinase 1 [Mus musculus]	47	7	TFIAIKPDGVQR	7-18

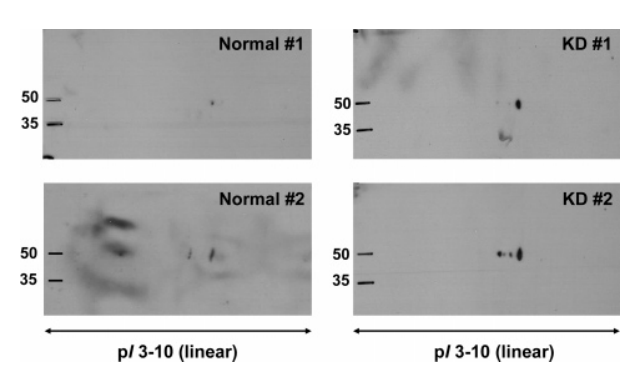


**Figure 4.** 2-D Western blot analysis of  $\beta$ -enolase. Muscle proteins resolved with 2-DE (totally 50  $\mu$ g per gel) were transferred onto a nitrocellulose membrane and probed with rabbit polyclonal anti- $\beta$ -enolase antibody (1:200 in 5% milk in PBS) and subsequently with swine anti-rabbit IgG conjugated with horseradish peroxidase (1:1000 in 5% milk in PBS). Reactive protein spots were then visualized with a chemiluminescence substrate. N=2 individual animals in each group.

Crystallin in our model may be the regulatory mechanism for muscle injury and damage during hypokalemic stress.

Translationally controlled tumor protein (TCTP) belongs to the TCTP family that is involved in calcium binding and microtubule stabilization.31,32 TCTP was originally identified as a serum-inducible 23-kDa protein that undergoes an early and prominent increase upon serum stimulation in cultured cells.33 It was recently shown to be a tubulin-binding protein that interacts with microtubules during the cell cycle.34 Recently, several reports highlighted the importance of TCTP for cell cycle progression and malignant transformation.<sup>35</sup> In addition, TCTP was shown to display an extracellular function as a histaminereleasing factor and to have anti-apoptotic activity.36,37 These findings led to the other names or synonyms for this protein, including histamine-releasing factor (HRF)<sup>36</sup> and fortilin.<sup>37</sup> With a board range of cellular function, its role in hypokalemic myopathy, however, remains unknown and deserves further investigation.

**Murine versus Rat Muscle Proteomes.** In the present study, we identified a total of 15 protein spots representing 14 unique proteins that were regulated during chronic K<sup>+</sup> depletion in "BALB/c mice". Recently, Yan and colleagues<sup>17</sup> performed proteomic analysis and established initial 2-D reference maps of skeletal muscles from a "Wistar rat". Proteins derived from

 Table 3. Brief Descriptions of Muscle Enzymes That Were Significantly Altered During Chronic Potassium Depletion

enzyme ( <i>component of</i> )	synonyms	pathways
aldolase 1, A isoform	fructose-1,6-bisphosphate aldolase	Calvin cycle
(EC reaction -lyases)  creatine kinase, muscle (EC reaction - transferases)	fructose-1,6-bisphosphate triosephosphate-lyase fructose-bisphosphate aldolase	formaldehyde assimilation II (RuMP cycle) fructose degradation to pyruvate and lactate (anaerobic) gluconeogenesis glycolysis I glycolysis II glycolysis IV mannitol degradation I sorbitol degradation sorbitol fermentation to lactate, formate, ethanol and acetate sucrose degradation to ethanol and lactate (anaerobic) xylulose-monophosphate cycle interconversion of creatine and creatine phosphate
•	To.	
dihydrolipoamide S-acetyltransferase precursor ( <i>Pyruvate dehydrogenase multienzyme complexes</i> )	E2	pyruvate degradation II
dihydrolipoamide dehydrogenase (EC reaction - oxidoreductases)	lipoate acetyltransferase pyruvate dehydrogenase complex E2 components thioltransacetylase A diaphorase dihydrolipoyl dehydrogenase E3 component of alpha-ketoacid dehydrogenase complexes lipoamide reductase	interconversion of dihydrolipoamide and lipoamide
enolase 3, beta muscle	lipoyl dehydrogenase 2,3-diphospho-p-glycerate,	gluconeogenesis
(degradosome)	2-phospho-D-glycerate phosphotransferase 2-phospho-D-glycerate hydrolyase 2-phosphoglycerate dehydratase	glycolysis I respiration (anaerobic)
muscle glycogen phosphorylase (glycogen phosphorylase/glycogen-maltotetraose phosphorylase)	phosphopyruvate hydratase 1,4-alpha-D-glucan:orthophosphate alpha-D-glucosyltransferase	glycogen degradation
nucleoside-diphosphate kinase 1 (nucleoside diphosphate kinase/ UDP kinase/ CDP kinase/ dUDP kinase/ dCDP kinase/ dTDP kinase/ dADP kinase/ dGDP kinase)	amylophosphorylase polyglucose phosphorylase polyphosphorylase ATP-nucleoside diphosphate phosphotransferase  NDK, NDP kinase	<ul><li>de novo biosynthesis of pyrimidine ribonucleotides</li><li>de novo biosynthesis of</li></ul>
phosphoglycerate kinase (EC 2.7.2.3)	nucleoside 5'-diphosphate phosphotransferase nudiki phosphoglycerate phosphorylase	pyrimidine deoxyribonucleotides purine nucleotides <i>de novo</i> biosynthesis I salvage pathway of pyrimidine nucleotides 2-dehydro-D-gluconate degradation
(EC reaction - transferases)		Calvin cycle fructose degradation to pyruvate and lactate (anaerobic) gluconeogenesis glucose fermentation to lactate II glucose heterofermentation to lactate I glyceraldehyde—3-phosphate degradation glycolysis I glycolysis IV sorbitol fermentation to lactate, formate, ethanol and acetate sucrose degradation to ethanol and lactate (anaerobic)
pyruvate kinase M (pyruvate kinase subunit)	ATP:pyruvate 2-O-phosphotransferase	glycolysis I
triosephosphate isomerase 1 (EC reaction - isomerases)	phosphoenol transphosphorylase phosphoenolpyruvate kinase phosphotriose isomerase triose phosphate isomerase	Calvin cycle fructose degradation to pyruvate
	triose phosphoisomerase triosephosphate mutase	and lactate (anaerobic) glycolysis I glycolysis II glycolysis IV sorbitol fermentation to lactate, formate, ethanol and acetate sucrose degradation to ethanol and lactate (anaerobic)

"abdominal" skeletal muscles were resolved using two ranges of IPG strips, with pI 3-10 (nonlinear) and pI 4-7 (linear). A total of 652 and 697 protein spots, respectively, were detected by silver stain, and a total of 74 proteins were identified. Of these identified proteins, pyruvate kinase M,  $\beta$ -enolase, creatine kinase M, aldolase, triosephosphate isomerase 1, and alpha-B Crystallin were also identified in our murine model of hypokalemic myopathy. However, muscle glycogen phosphorylase, dihydrolipoamide S-acetyltransferase precursor, dihydrolipoamidedehydrogenase, myosin-bindingprotein H, phosphoglycerate kinase, NAD(P)-dependent steroid dehydrogenase-like protein, TCTP, and nucleoside-diphosphate kinase 1 that were identified from "gastrocnemius" muscles in our present study were not identified in their study. These differences might simply imply the differential expression of muscle proteins in different species of rodents. However, some technical issues should be taken into account for these differences. We analyzed "gastrocnemius" muscles, whereas they identified proteins from skeletal muscles at "abdominal wall". Moreover, both of these studies have not identified all of the visualized protein spots. We selectively identified only the regulated proteins affected by chronic K<sup>+</sup> depletion, whereas they selectively analyzed only 100 spots from >1000 spots visualized. Thus, a lot of proteins remain unidentified in both studies.

Serum Levels of Creatine Kinase (CK) and  $\beta$ -Enolase. To assess whether levels of some of the up-regulated muscle enzymes were also increased in the serum, we measured total CK (using Oliver-Rosalki assay21,22), CK-MM (using Western blot analysis), and CK-MB (using an ELISA) levels in sera of all 10 animals. The results indicated that serum total CK, CK-MM, and CK-MB levels were all negative (or under the detectable limits of their respective methods) in all the samples (both in normal and KD groups). Moreover, Western blot analysis of  $\beta$ -enolase, while provided a promising data on muscles as shown in Figure 4, showed the negative result in the sera of both normal and KD groups. Considering these data together with the histopathological findings, they might implicate that hypokalemic myopathy in our murine model was not as severe as rhabdomyolysis in humans. However, as we performed all the experiments and histopathological examination at the time-point of 8 weeks of K<sup>+</sup> depletion, serial analyses including the earlier and later time-points should be performed to address whether rhabdomyolysis has not occurred in our murine model or it might occur at the very early time-point but was finally recovered; thus, negative findings were obtained for serum markers.

Technical Concerns. (i) One of the most critical issues for gel-based, proteomic analysis is the reproducibility and comparability of 2-D spot pattern in different 2-D gels. To address this issue in our present study, we evaluated the coefficient of variation (CV) of a selected protein spot (circled in Figure 3) across 10 different gels. %CV was calculated by dividing the standard deviation by mean of intensity volume of the corresponding spot and multiplying by 100. Figure 5A shows the zoom-in, cropped images of the selected spot in all gels. Intragroup %CVs of this spot were 14.45% and 11.42% for the normal and KD mice, respectively. %CV of this spot for both groups was only 12.33% when the intensities of this spot in all 10 gels were considered. As this selected spot was quite intense and might be saturated, we also evaluated the CV of another spot (#307 in Figure 3) with much less intensity. Figure 5B shows the consistent results and demonstrates that intragroup %CVs of spot #307 were 13.50% and 8.19% for the normal and

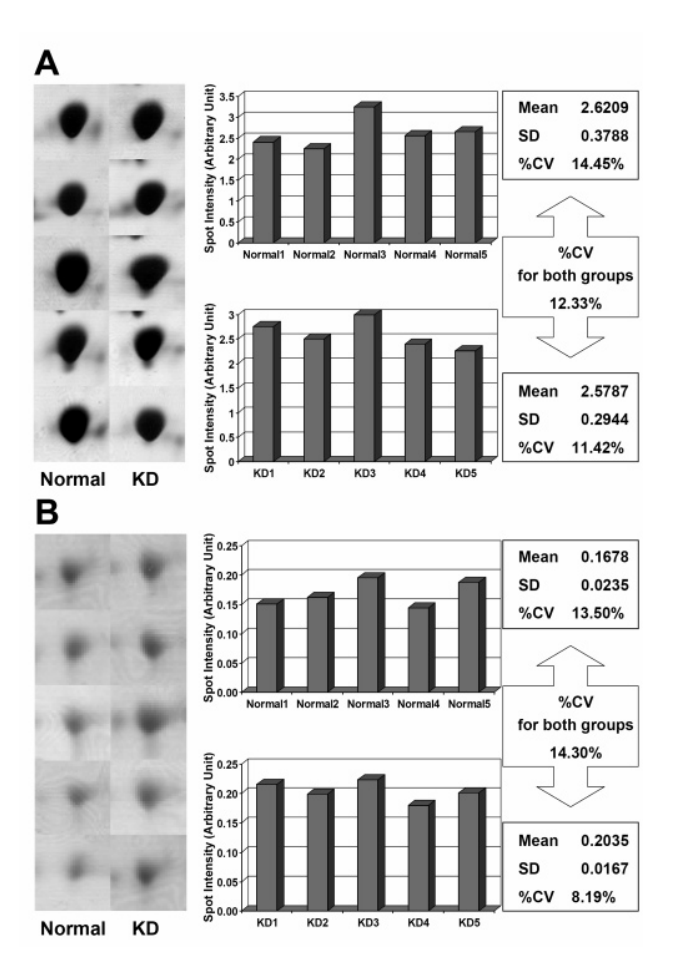


**Figure 5.** Variability. Zoom-in images of the selected spots from individual 2-D gels (n = 5 for each group). (A) Spot that is circled in Figure 3. (B) Spot #307. Coefficient of variation (CV) was then calculated (%CV = (standard deviation/mean)  $\times$  100%).

KD mice, respectively. %CV of this spot for both groups was only 14.30% when the intensities of this spot in all 10 gels were used for the calculation.

Considering all spots presented in each gel together, overall %CVs (%CV $_{\rm total}$ ) were 13.35, 11.37, and 11.84% for normal, KD, and both groups, respectively. In previous gel-based, proteome studies of human tissues, cell lines, and body fluids, up to 25% of CV was observed and acceptable for the reproducibility of 2-DE.  $^{38-40}$  Hence, our results were justified for the standard quantitative differential proteomics. We also demonstrated that normalization of spot intensity in our present study was justified for the comparability of intensity volume of each protein spot across different gels, as the summation of normalized intensity volumes of all spots in each 2-D gel was comparable between groups (76.36  $\pm$  4.56 and 79.42  $\pm$  4.04 arbitrary units for normal and KD mice, respectively; p value was 0.629).

(ii) As discussed above, we have been very concerned for the inter-individual variability among different animals within or between groups. We performed the proteomic analysis using only one gel per animal and, thus, did not address an issue of intraindividual or interassay variability in the present study because several recent articles, by our<sup>41</sup> and other groups,<sup>42</sup> have readily demonstrated that the 2-D spot pattern is highly reproducible when the identical protocols and standardized parameters are used for different assays of the same sample.

research articles Thongboonkerd et al.

However, to demonstrate that our present study was standardized and justified, we also performed 2-DE of a set of triplicates, which were resolved separately in different experiments. The data clearly confirmed that the 2-D spot pattern was essentially identical among the three gels that were run on different occasions (see Figure S1 in the Supporting Information).

(iii) The total number of protein spots visualized in the present study was relatively small for the muscle proteome. This could be explained by some technical limitations. First, we used a small format 2-D gel in the present study that has considerable limitations in protein separation; much more spots should have been resolved using a large format (using 18 to 24-cm-long IPG strip). Second, Coomassie Brillaiant Blue R-250 stain was employed in our present study. Much more spots would be expected to be detectable with the more sensitive stains; i.e., silver, fluorescence dyes, and colloidal Coomassie. Finally, we used the highly stringent criteria or parameters for detection of "true protein spots" (see Materials and Methods section). The total number of detected spots would be greater if the lower stringent criteria or parameters were used.

(iv) It should be noted that all the animals in the present study had metabolic alkalosis. Changes in blood pH might be one of the factors contributing to altered proteome in the KD muscles and should be taken into account for the interpretation of our data. Finally, we have not performed the experiment comparing changes due to hypokalemic myopathy to those caused by other forms of myopathy. It would be interesting to determine whether the findings in our present study are specific for hypokalemic myopathy and to evaluate whether these abnormal findings can be recovered after treatment with  $\rm K^+$  repletion.

#### **Conclusions**

We have demonstrated that prolonged  $K^+$  depletion caused alterations in several muscle proteins in mice. Most of these altered proteins were enzymes that are involved in several various metabolic pathways and are crucial for cellular function and bioenergetics. These data may lead to a new roadmap for research on hypokalemic myopathy and to biomarker discovery. Our findings also underscore the potential use of proteomics to unravel the pathogenic mechanisms and pathophysiology of human diseases.

**Abbreviations:** ACN, acetonitrile; CHAPS, 3-[(3-cholamidopropyl)dimethylamino]-1-propanesulfonate; CHCA,  $\alpha$ -cyano-4-hydroxycinnamic acid; CK, creatine kinase; CV, coefficient of variation; DTT, dithiothreitol; HRF, histamine-releasing factor; HSP, heat shock protein; KD, K<sup>+</sup>-depleted; MALDI, matrix-assisted laser desorption/ionization; MOWSE, molecular weight search; MS, mass spectrometry; MS/MS, tandem mass spectrometry; Q-TOF, quadrupole time-of-flight; SDS, sodium dodecyl sulfate; TFA, trifluoroacetic acid; TCTP, translationally controlled tumor protein

**Acknowledgment.** We thank Somchai Chutipongtanate, Wipawanee Kasemworaphoom, Napat Songtawee, Theptida Semangoen, and Lt. Col. Duangporn Phulsuksombati for their technical assistance and Drs. Sumalee Nimmannit, Yasushi Nakagawa, Somkiat Vasuvattakul, Pa-thai Yenchitsomanus, and Suchai Sritippayawan for their advice. This study was supported by the Thailand Research Fund to P. Malasit (Senior Research Scholar Program; Grant #RTA4680017) and by Vejdusit Foundation to V.T.

**Supporting Information Available:** A set of triplicates of 2-D gels derived from the same muscle sample that were run separately in different experiments (Figure S1). The data show the essentially identical pattern of 2-D spots among different gels. This material is available free of charge via the Internet at http://pubs.acs.org.

#### References

- (1) Cohn, J. N.; Kowey, P. R.; Whelton, P. K.; Prisant, L. M. New guidelines for potassium replacement in clinical practice: a contemporary review by the National Council on Potassium in Clinical Practice. *Arch. Intern. Med.* **2000**, *160*, 2429–2436.
- (2) Mount, D. B.; Zandi-Nejad, K. Disorders of potassium balance. In *Brenner & Rector's The Kidney*, 7th ed.; Brenner, B. M., Ed.; W. B. Saunders: Philadelphia, 2004; pp 997–1040.
- (3) Gennari, F. J. Hypokalemia. *N. Engl. J. Med.* **1998**, 339, 451–458.
- (4) Gennari, F. J. Disorders of potassium homeostasis. Hypokalemia and hyperkalemia. Crit. Care Clin. 2002, 18, 273–88., vi.
- (5) Antes, L. M.; Kujubu, D. A.; Fernandez, P. C. Hypokalemia and the pathology of ion transport molecules. *Semin. Nephrol.* 1998, 18, 31–45.
- (6) Tang, N. L.; Hui, J.; To, K. F.; Ng, H. K.; Hjelm, N. M.; Fok, T. F. Severe hypokalemic myopathy in Gitelman's syndrome. *Muscle Nerve* 1999, 22, 545–547.
- (7) Satoh, J.; Kuroda, Y.; Nawata, H.; Yanase, T. Molecular basis of hypokalemic myopathy caused by 17alpha-hydroxylase/17,20lyase deficiency. *Neurology* 1998, 51, 1748–1751.
- (8) Finsterer, J.; Hess, B.; Jarius, C.; Stollberger, C.; Budka, H.; Mamoli, B. Malnutrition-induced hypokalemic myopathy in chronic alcoholism. J. Toxicol. Clin. Toxicol. 1998, 36, 369–373.
- (9) Allison, R. C.; Bedsole, D. L. The other medical causes of rhabdomyolysis. *Am. J. Med. Sci.* **2003**, *326*, 79–88.
- (10) Warren, J. D.; Blumbergs, P. C.; Thompson, P. D. Rhabdomyolysis: a review. *Muscle Nerve* 2002, 25, 332–347.
- (11) Ng, Y. C. Hypokalemia downregulates cardiac alpha 1 and skeletal muscle alpha 2 isoforms of Na+,K(+)-ATPase in ferrets. *Biochem. Biophys. Res. Commun.* **1993**, *196*, 39–46.
- (12) McDonough, A. A.; Thompson, C. B. Role of skeletal muscle sodium pumps in the adaptation to potassium deprivation. *Acta Physiol. Scand.* **1996**, *156*, 295–304.
- (13) Thompson, C. B.; Choi, C.; Youn, J. H.; McDonough, A. A. Temporal responses of oxidative vs. glycolytic skeletal muscles to K+ deprivation: Na+ pumps and cell cations. *Am. J. Physiol.* 1999, 276, C1411–C1419.
- (14) Thongboonkerd, V. Proteomic analysis of renal diseases: Unraveling the pathophysiology and biomarker discovery. Expert Rev. Proteomics 2005, 2, 349–366.
- (15) Marko-Varga, G.; Fehniger, T. E. Proteomics and disease—the challenges for technology and discovery. J. Proteome Res. 2004, 3, 167–178.
- (16) Petricoin, E.; Wulfkuhle, J.; Espina, V.; Liotta, L. A. Clinical proteomics: revolutionizing disease detection and patient tailoring therapy. *J. Proteome Res.* 2004, 3, 209–217.
- (17) Yan, J. X.; Harry, R. A.; Wait, R.; Welson, S. Y.; Emery, P. W.; Preedy, V. R.; Dunn, M. J. Separation and identification of rat skeletal muscle proteins using two-dimensional gel electrophoresis and mass spectrometry. *Proteomics* 2001, 1, 424–434.
- (18) van den Heuvel, L. P.; Farhoud, M. H.; Wevers, R. A.; van Engelen, B. G.; Smeitink, J. A. Proteomics and neuromuscular diseases: theoretical concept and first results. *Ann. Clin. Biochem.* 2003, 40, 9-15
- (19) Shishkin, S. S.; Kovalyov, L. I.; Kovalyova, M. A. Proteomic studies of human and other vertebrate muscle proteins. *Biochemistry* (*Mosc.*) 2004, 69, 1283–1298.
- (20) Cagney, G.; Park, S.; Chung, C.; Tong, B.; O'Dushlaine, C.; Shields, D. C.; Emili, A. Human tissue profiling with multidimensional protein identification technology. *J. Proteome Res.* 2005, 4, 1757–1767.
- (21) Miyada, D. S.; Dinovo, E. C.; Nakamura, R. M. Creatine kinase reactivation by thiol compounds. *Clin. Chim. Acta* **1975**, *58*, 97–99.
- (22) Nealon, D. A.; Henderson, A. R. The apparent Arrhenius relationships of the human creatine kinase isoenzymes using the Oliver-Rosalki assay. *Clin. Chim. Acta* **1976**, *66*, 131–136.
- (23) Karp, P. D.; Paley, S.; Romero, P. The Pathway Tools software. *Bioinformatics* **2002**, *18* (Suppl 1), S225–S232.
- (24) Karp, P. D.; Krummenacker, M.; Paley, S.; Wagg, J. Integrated pathway-genome databases and their role in drug discovery. *Trends Biotechnol.* **1999**, *17*, 275–281.

- (25) Karp, P. D.; Paley, S. Integrated access to metabolic and genomic data. J. Comput. Biol. 1996, 3, 191–212.
- Trask, R. V.; Strauss, A. W.; Billadello, J. J. Developmental regulation and tissue-specific expression of the human muscle creatine kinase gene. J. Biol. Chem. 1988, 263, 17142-17149.
- (27) Frederikse, P. H.; Dubin, R. A.; Haynes, J. I.; Piatigorsky, J. Structure and alternate tissue-preferred transcription initiation of the mouse alpha B-crystallin/small heat shock protein gene. Nucleic Acids Res. 1994, 22, 5686-5694.
- (28) Dubin, R. A.; Wawrousek, E. F.; Piatigorsky, J. Expression of the murine alpha B-crystallin gene is not restricted to the lens. Mol. Cell Biol. 1989, 9, 1083-1091.
- (29) Liu, Y.; Steinacker, J. M. Changes in skeletal muscle heat shock proteins: pathological significance. Front Biosci. 2001, 6, D12-
- (30) Ganea, E. Chaperone-like activity of alpha-crystallin and other small heat shock proteins. Curr. Protein Pept. Sci. 2001, 2, 205–
- (31) Gross, B.; Gaestel, M.; Bohm, H.; Bielka, H. cDNA sequence coding for a translationally controlled human tumor protein. Nucleic Acids Res. 1989, 17, 8367.
- (32) Yarm, F. R. Plk phosphorylation regulates the microtubulestabilizing protein TCTP. Mol. Cell Biol. 2002, 22, 6209-6221.
- (33) Benndorf, R.; Nurnberg, P.; Bielka, H. Growth phase-dependent proteins of the Ehrlich ascites tumor analyzed by one- and two-dimensional electrophoresis. Exp. Cell Res. 1988, 174, 130-
- (34) Gachet, Y.; Tournier, S.; Lee, M.; Lazaris-Karatzas, A.; Poulton, T.; Bommer, U. A. The growth-related, translationally controlled protein P23 has properties of a tubulin binding protein and

- associates transiently with microtubules during the cell cycle. J. Cell Sci. 1999, 112 (Pt 8), 1257-1271.
- (35) Bommer, U. A.; Thiele, B. J. The translationally controlled tumour protein (TCTP). Int. J. Biochem. Cell Biol. 2004, 36, 379-385.
- MacDonald, S. M.; Rafnar, T.; Langdon, J.; Lichtenstein, L. M. Molecular identification of an IgE-dependent histamine-releasing factor. Science 1995, 269, 688-690.
- (37) Li, F.; Zhang, D.; Fujise, K. Characterization of fortilin, a novel antiapoptotic protein. J. Biol. Chem. 2001, 276, 47542-47549.
- (38) Hunt, S. M.; Thomas, M. R.; Sebastian, L. T.; Pedersen, S. K.; Harcourt, R. L.; Sloane, A. J.; Wilkins, M. R. Optimal replication and the importance of experimental design for gel-based quantitative proteomics. J. Proteome Res. 2005, 4, 809-819.
- (39) Terry, D. E.; Desiderio, D. M. Between-gel reproducibility of the human cerebrospinal fluid proteome. Proteomics 2003, 3, 1962-
- (40) Molloy, M. P.; Brzezinski, E. E.; Hang, J.; McDowell, M. T.; VanBogelen, R. A. Overcoming technical variation and biological variation in quantitative proteomics. Proteomics 2003, 3, 1912-
- (41) Klein, E.; Klein, J. B.; Thongboonkerd, V. Two-dimensional gel electrophoresis: a fundamental tool for expression proteomics studies. Contrib. Nephrol. 2004, 141, 25–39.
- (42) Witzmann, F. A.; Li, J. Cutting-edge technology. II. Proteomics: core technologies and applications in physiology. Am. J. Physiol. Gastrointest. Liver Physiol. 2002, 282, G735-G741.

PR060136H

#### A NEW DENSOVIRUS ISOLATED FROM THE MOSQUITO TOXORHYNCHITES SPLENDENS (WIEDEMANN) (DIPTERA:CULICIDAE)

Sa-nga Pattanakitsakul<sup>1,4</sup>, Kobporn Boonnak<sup>1,2</sup>, Kusuma Auethavornanan<sup>1,2</sup>, Aroonroong Jairungsri<sup>1</sup>, Thaneeya Duangjinda<sup>4</sup>, Punjaporn Puttatesk<sup>1</sup>, Supatra Thongrungkiat<sup>3</sup> and Prida Malasit<sup>1,4</sup>

<sup>1</sup>Division of Medical Molecular Biology, Office for Research and Development, <sup>2</sup>Department of Immunology and Immunology Graduate Program, Faculty of Medicine Siriraj Hospital, Mahidol University, Bangkok, Thailand; <sup>3</sup>Department of Medical Entomology, Faculty of Tropical Medicine, Mahidol University, Bangkok, Thailand; <sup>4</sup>Medical Biotechnology Unit, National Center for Genetic Engineering and Biotechnology (BIOTEC), National Science and Technology Development Agency (NSTDA), Pathum Thani, Thailand

Abstract. A new densovirus was isolated and characterized in laboratory strains of *Toxorhynchites splendens*. The virus was detected by polymerase chain reaction (PCR) from mosquitoes reared in our laboratory. PCR fragments from each mosquito were compared by single strand conformation polymorphism (SSCP) assay and found to be indistinguishable. Thus, it is likely the densoviruses from these mosquitoes contain homologous nucleotide sequences. The PCR fragment corresponding to a 451 bp densovirus structural gene segment from each of 5 mosquitoes had 100% identical nucleotide sequences. Phylogenetic analysis of the structural gene sequence suggests the newly isolated densovirus is more closely related to *Aedes aegypti* densovirus (*Aae*DNV) than to *Aedes albopictus* densovirus (*Aal*DNV). Analysis of offspring and predated larvae suggests that vertical and horizontal transmission are responsible for chronic infections in this laboratory strain of *Toxorhynchites splendens*. The virion DNA is 4.2 kb in size, is closely related to, but distinct from, known densoviruses in the genera *Brevidensovirus* and *Contravirus*. The virus is tentatively named *Toxorhynchites splendens* densovirus (*Ts*DNV).

#### INTRODUCTION

Densoviruses (DNV) are small non-enveloped, single-stranded DNA viruses that belong to the family Parvoviridae (Kurstak, 1972; Bachmann *et al.*, 1975; Tijssen *et al.*, 1976;

Correspondence: Dr Sa-nga Pattanakitsakul, Division of Medical Molecular Biology, 12<sup>th</sup> Fl Adulyadej Vikrom Building, Faculty of Medicine Siriraj Hospital, Mahidol University, Prannok Road, Bangkok Noi, Bangkok 10700, Thailand.

Tel/Fax: 66 (0) 2418-4793

E-mail: sispn@mahidol.ac.th or sipml@mahidol.ac.th The GenBank accession number of the sequence reported in this paper is AF395903

Siegl et al, 1985). This family is currently subdivided into two subfamilies, the Parvovirinae and the Densovirinae. Viruses in the former subfamily infect vertebrates while the latter infects invertebrates (mainly insects). All densoviruses have narrow host ranges, infecting only closely related insects and causing fatal disease in their host larvae. Within the Densovirinae, three genera are known: Densovirus (infecting cockroaches), Iteravirus (infecting silk worms) and Brevidensovirus or Contravirus (infecting mosquitoes). The members of the genus Densovirus, Junonia coenia densovirus (JcDNV) and Galleria mellonella densovirus (GmDNV), have a genome size of

6 kb, while a member of the genus *Iteravirus*, *Bombyx mori* densovirus (*Bm*DNV), possesses a genome of 5.2 kb (Jourdan *et al*, 1990; Bando *et al*, 1992,1995; Dumas *et al*, 1992).

The genomes of the members of both Densovirus and Iteravirus genera contain inverted terminal repeats and can separately encapsidate (equally) plus or minus a singlestranded DNA in their virions (Jourdan et al, 1990; Bando et al, 1990,1995; Dumas et al, 1992). The genus Brevidensovirus or Contravirus contains Aedes aegypti densovirus (AeDNV or Aae DNV) and Aedes albopictus parvovirus or Aedes albopictus densovirus (AaPV or AalDNV). Aedes aegypti densovirus was originally isolated from a laboratory colony of Ae. aegypti larvae (Lebedeva et al, 1973). This virus is infectious to mosquito larvae of the genera Aedes, Culex and Culiseta when it is introduced into the water in which they are reared. The virus can infect all stages, including larvae, pupae and adults of both sexes. Ae. albopictus densovirus was isolated from an Ae. albopictus cell line (C6/36) and was discovered during experiments designed to determine the pathogenicity of the Mosquito African Virus (MAV) for Ae. aegypti larvae (Jousset et al, 1993). The genomes of both viruses have been cloned and sequenced (Lebedeva et al, 1973; Afanasiev et al, 1991; Jousset et al, 1993; Boublik et al, 1994a). Both are small icosahedral, non-enveloped viral particles of 18-20 nm in diameter containing a single-stranded linear DNA of 4 kb and mostly minus polarity (Afanasiev et al, 1991; Jousset et al, 1993; Boublik et al, 1994a,b; Chen et al. 2004). These two densoviruses share about 77.3% similarity in nucleotide sequences over the whole genome (Boublik et al, 1994a). Both have palindromic structures that can form stable hairpin structures at both termini. These structures are believed to be involved in DNA replication, excision from plasmids and integration into host cell DNA (Afanasiev et al, 1991, 1994; Boublik et al,

1994a). Most of their genome is encoded in 3 open reading frames (ORF) on the plus strand with the left and mid ORFs coding for non-structural (NS) proteins and the right ORF coding for structural proteins (Boublik *et al*, 1994a). In AaeDNV, there is one extra ORF encoded on the minus strand, but it codes for a polypeptide of no known function (Afanasiev *et al*, 1991).

Apart from these two well characterized densoviruses, several densoviruses have also been demonstrated in cell lines of several mosquito species, including *Culex theileri*, *Haemagogus equinus* and *Toxorhynchites amboinensis* (O'Neill *et al*, 1995; Paterson *et al*, 2005), indigenous *Ae. aegypti* mosquitoes (Kittayapong *et al*, 1999) and a laboratory strain of *Cx. pipiens* larvae (Jousset *et al*, 2000). We describe here a novel densovirus from laboratory strains of the mosquito *Tx. splendens*. This mosquito was used routinely in the laboratory for dengue virus isolation by intrathoracic injection from patient's serum.

#### MATERIALS AND METHODS

#### Mosquitoes

Tx. splendens mosquitoes were field-collected from rural Thai locations and identified according to the pictorial key described by Huang (1977). They were maintained in the laboratory for serveral generations at a temperature of 28°C. They were fed daily with larvae of Ae. aegypti and Cx. quinquefasciatus. Adults were kept in large mesh cages (60 x 60 x 60 cm) and given 10% sugar solution and 10% multivitamin syrup soaked in cotton pads as food. No blood meals were required. Mating took place while in flight, with the pairs usually falling downward during copulation. Oviposition began approximately one week after emergence.

#### Aedes albopictus densovirus (AalDNV)

Ae. albopictus densovirus was kindly provided by Dr Pattamaporn Kittayapong, Depart-

ment of Biology, Faculty of Science, Mahidol University (Burivong et al, 2004). This virus was maintained by culturing in densovirus-free C6/36 cells in 5 ml Leibovitz's medium (L-15) containing 10% FBS in T-25 tissue culture flasks for 7 days at 28°C. Culture supernatants were collected in aliquots for isolation of DNA and used as positive control DNA templates for PCR reactions.

DNA isolation for polymerase chain reaction (PCR)

Adult mosquitoes. DNA from Tx. splendens mosquitoes was isolated using DNAzol reagent (GibcoBRL, New York, USA). Briefly, a mosquito was homogenized with a hand held glass homogenizer in a 1.5-ml microcentrifuge tube containing 300 µl of Leibovitz's medium (L-15) and 1% fetal bovine serum (FBS). Then the homogenate was centrifuged at 11,600g for 20 minutes at 4°C. One hundred microliters of supernatant was added to 250 µl of DNAzol solution followed by gentle mixing, then allowed to stand at room temperature for 5 minutes before further centrifugation again at 11,600g for 20 minutes at 4°C. The DNA was precipitated by adding 125 µl of cold absolute ethanol and mixing thoroughly, then allowed to stand at room temperature for 5 minutes. The DNA pellet was then collected by centrifugation at 11,600g for 20 minutes at 4°C and washed twice with 500 µl of 70% ethanol before being dried and dissolved in 10 µl of distilled water for use as a template for PCR reactions.

Larvae. DNA from a pool of 5 larvae of Ae. aegypti or Cx. quinquefasciatus, and a larva of Tx. splendens, was isolated using DNAzol reagent (GibcoBRL, New York, USA) as described above. Finally, 5 µl of undiluted or 1:10 diluted DNA was used as a template for PCR.

Aa/DNV culture supernatant. One hundred microliters of Aa/DNV culture supernatant was added to 250 µl of DNAzol solution and the DNA was purified as described in the proto-

col above. Finally the DNA was dissolved in 10  $\mu$ l of distilled water and 5  $\mu$ l was used for PCR.

#### Amplification of densovirus DNA using PCR

Primer design. The primers used for amplification were the forward primer (5' AAC AAG ACA GAG ACT GCT AAC 3', or residues 2968 to 2988) and the reverse primer (5' GCA TTC TTG GAT ATG ATG TTC T 3', or residues 3422 to 3401). This primer pair was selected from conserved sequences of the structural gene of both the *AaI*DNV and *Aae*DNV genomes and was expected to be specific for PCR amplification of a densovirus DNA fragment. The nucleotide positions cited corresponded to the sequence of *Aae*DNV (GenBank Accession No. M37899). All primers were synthesized by the Bioservice Unit, National Science and Technology Development Agency, Thailand.

DNA amplification. PCR was performed in 25 µl of reaction mixture containing 10 mM Tris-HCl (pH 9.0), 50 mM KCl, 0.1% Triton X-100, 1.5 mM MgCl<sub>2</sub>, 10 pmol of primers, 0.2 mM dNTPs, 1 unit of Taq DNA polymerase (Promega, Madison, USA) and 5 µl of purified DNA extracted from mosquito samples. The reaction mixture was initially denatured at 94°C for 5 minutes and subjected to 30 cycles with the cycling profile of denaturation at 94°C for 1 minute, annealing at 55°C for 1 minute and extension at 72°C for 1 minute. Finally, the PCR products were detected by electrophoresis of 5 ml reaction mixture in 2% agarose gel (FMC Bioproducts, Rockland, USA) and examination of the ethidium bromide-stained gel under a UV transilluminator. In the case of larvae, reamplification was performed by adding 1 µl of primary PCR product into 24 µl of freshly prepared reaction mixture. Then the tubes were taken to the thermal cycler and the same procedure was followed as used for the primary PCR.

Single strand conformation polymorphism (SSCP)

A slightly modified SSCP analysis (Orita

et al, 1989; Bannai et al, 1994) was performed to analyze the heterogeneity of densovirus isolated from the mosquitoes. Specifically, 1 µl of amplified PCR product was mixed with 7 µl of denaturing solution containing 95% formamide, 20 mM EDTA, 0.05% bromophenol blue and 0.05% xylene cyanol FF. The mixtures were denatured at 95°C for 5 minutes and immediately cooled on ice before 1-5 µl of the mixture was applied on 10% polyacrylamide gel (acrylamide:bisacrylamide = 49:1) containing 5% glycerol in 45 mM Tris-borate (pH 8.0)/ 1 mM EDTA buffer at 4°C or room temperature. The electrophoresis was performed at 20 mA for 4-6 hours in a minigel electrophoresis apparatus with a constant temperature control system (AE-6410, ATTO, Tokyo, Japan). Single-strand DNA fragments in the gel were visualized by silver staining (Daiichi Pure Chemicals, Tokyo, Japan).

#### Nucleotide sequencing

Nucleotide sequencing was performed using a BigDye<sup>TM</sup> Terminator Cycle Sequencing kit (PE-Applied Biosystems, CA, USA) according to the supplier's protocol with an ABI PRISM 310 Genetic Analyzer. Briefly, the PCR fragments were first purified using a QIAquick Gel Extraction kit (QIAGEN, Hilden, Germany) and 40 ng of purified fragments were used as the template for cycle sequencing using Ampli Taq DNA polymerase. The sequencing was performed on both strands of DNA fragments.

### Phylogenetic analysis of densovirus genomic fragments

To characterize the genome of the densovirus from *Tx. splendens* mosquitoes, nucleotide sequences derived from PCR fragments were used for analysis. The resulting sequences were then aligned with other densovirus sequences deposited in the GenBank database, reported by O'Neill *et al* (1995) and assessed by employing PHYLIP package version 3.57c. Maximum likelihood analysis was used to calculate genetic dis-

tances using the DNADIST program. Phylogenetic trees were constructed using UPGMA algorithms available in the NEIGHBOUR program. The reliability of different phylogenetic groupings was evaluated by using bootstrap analysis (1000 bootstrap replications) using SEQBOOT and CONSENSE programs.

#### Cultivation of densovirus in mosquito cell lines

A source mosquito was homogenized in 1 ml of Leibovitz's medium (L-15) containing 1% fetal bovine serum (FBS) and 10% tryptose phosphate broth (TPB). The homogenate was filtered through a 0.2 μ Millipore membrane and then applied to a culture of densovirus-free C6/36 cells and a culture of *Tx. splendens* (TRA284) cells in T-25 tissue culture flasks at room temperature overnight before further cultivaiton in 5 ml L-15 containing 10% FBS for another 6 days at 28°C. Culture supernatants were collected in aliquots for further virus identification and analysis.

## Isolation of viral DNA from mosquitoes and AalDNV culture supernatant

Isolation of viral DNA was performed according to Molitor et al (1984) with some modification. Pools of 60 mosquitoes were homogenized in 30 ml of Leibovitz's medium (L-15) containing 1% fetal bovine serum (FBS) and centrifuged at 10,600g for 10 minutes. The supernatant was collected and then centrifuged at 114,000g using a 60 Ti rotor (Beckman, USA) for 4 hours at 4°C. Viral pellets were resuspended in 50 mM Tris-HCl, pH 8.0, 25 mM EDTA and 20 µg/ml RNase A and incubated at 37°C for 30 minutes. After incubation, suspensions were mixed with 0.5% SDS, 0.4 mg/ml proteinase K and incubated further at 65°C for 2 hours. After protein digestion, suspensions were extracted twice by vortexing for 5 minutes in the presence of 0.15 M NaCl and 1 volume of saturated phenol. The virion DNA was precipitated twice with the addition of 2 volumes of absolute ethanol and kept at -70°C for 20 minutes before centrifugation at 11,290g for 20 minutes. Virion DNA was resuspended in 50  $\mu$ l of sterile distilled water and stored at -70°C until used. Three microliters of DNA was applied for agarose gel electrophoresis to determine the size of the DNA. In the case of purification of AalDNV DNA, 400 ml of infected culture supernatant was clarified at 10,600g for 10 minutes using a JA 14 rotor (Beckman, USA) to remove cell debris before further processing as described earlier. Finally the DNA was dissolved in 50  $\mu$ l of distilled water and 1  $\mu$ l of DNA was also applied in the same agarose gel electrophoresis.

#### RESULTS

Detection of densovirus in mosquitoes and larvae

Two pools of Tx. splendens mosquitoes randomly collected from pools of mosquitoes reared in our laboratory were studied for the presence of densoviruses. The two pools were collected 2 years apart. Mosquitoes from the first pool (n=27) and from the second pool (n=20) were individually analysed by PCR. All mosquitoes gave a similar amplicon of 451 bp although the electrophoresis band intensity differed (Fig 1). Amplicon size was the same as that of the positive control DNA template isolated from Aa/DNV. No amplicons were detected in the negative controls. By SSCP analysis, only a single pattern of singlestranded DNA was obtained from Tx. splendens mosquitoes in non-denaturing polyacrylamide gel electrophoresis (Fig 2). The pattern was quite different from that of the AalDNV samples. To examine the possibility of densovirus transmission in Tx. splendens mosquitoes, 20 pools of 5 Ae. aegypti or Cx. quinquefasciatus larvae and 50 Tx. splendens larvae were collected and analysed by PCR. A positive PCR was observed in 15 pools of Ae. aegypti, 10 pools of Cx. guinguefasciatus and 50 Tx. splendens larvae after reamplification. All the PCR products proved to

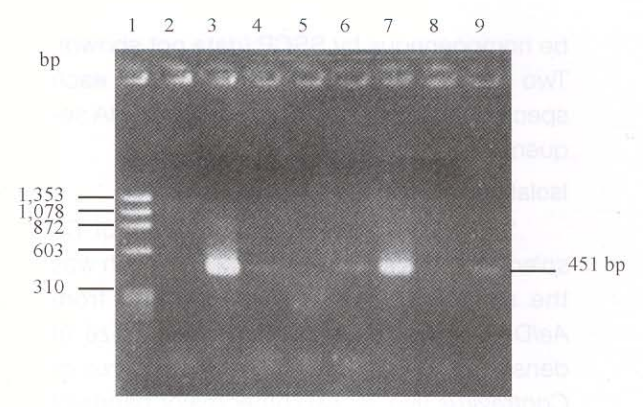


Fig 1–PCR amplification of a densovirus specific amplicon using DNA template isolated from *Toxorhynchites splendens* mosquitoes. The expected amplified product was approximately 451 bp. Lane 1: *Hae* III digested ØX174 DNA marker. Lanes 2 and 3 are a negative reagent blank and *AaI*DNV DNA positive control, respectively. Lanes 4-9: PCR product from mosquito template DNA. The results shown are representative examples from 27 mosquitoes that showed similar PCR products.

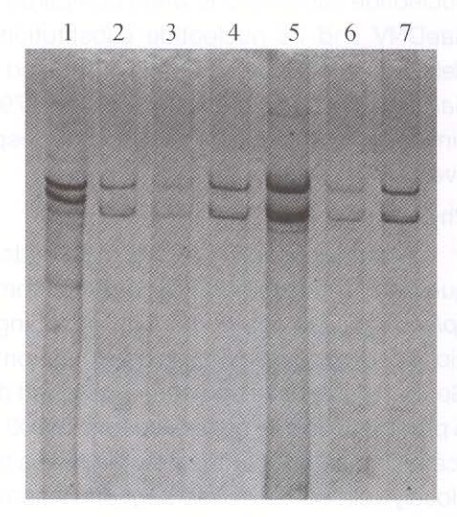


Fig 2–Single strand conformation polymorphism (SSCP) analysis of amplified PCR products from *Toxorhynchites splendens* mosquitoes. Lane 1 is PCR-SSCP from *AaI*DNV DNA is shown in lane 3 in Fig 1. Lanes 2-7 are PCR-SSCP from related mosquito specimens shown in lanes 4-9 in Fig 1. These again serve as representatives for the samples from 27 mosquitoes.

be homogeneous by SSCP (data not shown). Two representative PCR products from each species were shown to have identical DNA sequences.

#### Isolation of virion DNA from mosquitoes

Virion DNA isolated from the pool of *Tx. splendens* was shown to be 4.2 kb, which was the same size as the DNA isolated from *Aal*DNV. This closely resembled the size of densoviruses in the genus *Brevidensovirus* or *Contravirus* (Fig 3). Two other major bands of very small size (less than 500 bp) were also observed.

## Nucleotide sequencing of the PCR fragment from *Tx. splendens*

The nucleotide sequence of 412 bp from the central region of the PCR product (excluding the primer sequences at each end of the 451 bp amplicon) were aligned with the mosquito densovirus sequences obtained from the GenBank database (Fig 4). There were 53 nucleotide substitutions when compared with AaeDNV and 78 nucleotide substitutions, 4 deletions and 1 insertion when compared with AaIDNV. This translates as 87.1% and 79.9% similarity in nucleotide sequences, respectively.

#### Phylogenetic analysis

A 301-bp portion of the nucleotide sequence of the amplified PCR product from *Tx. splendens* was compared with matching regions of other densoviruses obtained from the GenBank database and other published data. A phylogenetic tree generated from 1,000 replicates indicated that the new virus was more closely related to *Aedes aegypti* densovirus (*Aae*DNV) than to other insect densoviruses observed in cultured cell lines (Fig 5).

#### Cultivation of densovirus in cell lines

Attempted culture of the densovirus in mosquito cell lines using inoculum prepared from *Tx. splendens* homogenates was performed in both *Ae. albopictus* (C6/36) cells and *Tx. amboinensis* (TRA284) cells. Serial

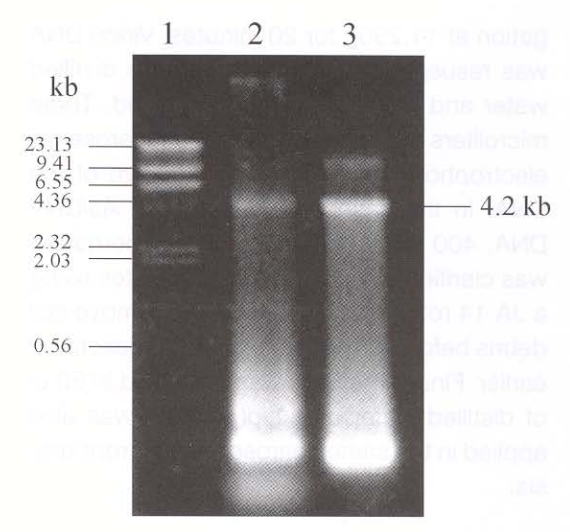


Fig 3-Agarose gel electrophoresis of densovirus DNA isolated from Toxorhynchites splendens mosquitoes. Viral DNA was isolated from a pool of 60 Toxorhynchites splendens mosquitoes and 3 µl of the DNA solution was subjected to 1% agarose gel electrophoresis. Lane 1: Hind III digested λ DNA marker. Lane 2 shows the 4.2 kb DNA band from the pooled mosquito extract. Lane 3 is the 4.2 kb DNA band from AalDNV-infected culture supernatant which served as a size reference for DNA isolated from viruses of the genus Brevidensovirus or Contravirus. The 2 bands of small DNA fragments at around 500 bp have not yet been identified but may be residual host DNA remaining in the viral DNA preparation.

passage was confirmed by PCR using extracts from culture supernatant as the template. The PCR results were positive for only the first 4 passages of cultivation and negative thereafter (data not shown).

#### DISCUSSION

Densoviruses have been identified and isolated from mosquito larvae and cell lines for many years (Lebedeva et al, 1973; Buchatsky, 1989; Boublik et al, 1994b; O'Neill et al, 1995; Burivong et al, 2004; Chen et al, 2004; Paterson et al, 2005). Some densovi-